

The mechanics of submerged granular flows

Elena Nucci

$$p^g = p^g \frac{I_{so}}{I_{so} + I_s} + \rho_s f_1 \theta$$



UNIVERSITÀ DEGLI STUDI DI TRENTO

Dipartimento di Ingegneria Civile
e Ambientale

2015

Doctoral thesis in **Environmental Engineering, 27 cycle**

Department of Civil, Environmental and Mechanical Engineering, **University of Trento**

Academic year 2013/2014

Supervisor: **Prof. Ing. Aronne Armanini, DICAM**

University of Trento

Trento, Italy

28 aprile 2015

Acknowledgements

I wish to express my esteem and my gratitude to my supervisor, Professor Armanini, for his guidance during the development of the theories presented and for the great breadth of knowledge that he taught me.

I wish to thank professor Larcher and professor Dumbser, co-authors of my publications, for their contributions.

A special thanks to Sabrina Meninno, PhD coursemate, for long debates on granular matter.

Finally, I thank the technicians of the Hydraulics laboratory and Roberto Mancabelli, MS student, for the collaborations in the experimental analysis presented in Chapter 3.

Contents

List of Symbols	vii
List of Figures	xxi
Summary	xxiii
Overview of the thesis	xxvii
1 Introduction	1
1.1 Debris Flows	1
1.2 Granular Flows	4
1.3 A two phase approach	6
1.3.1 Favre average and ensemble average	7
1.4 Literature relevant to the thesis	10
1.4.1 Bagnold's dispersive pressure theory	10
1.4.1.1 Limits of Bagnold's theory	12
1.4.2 The kinetic theory of dense gases	13
1.4.2.1 Different formulations of the functions f_i	17
1.4.3 The generation of granular temperature	19
1.4.4 A model for chains of particles	19
1.4.5 Granular flow regimes over fixed and mobile bed	22
1.4.6 The coexistence of the collisional and the frictional regimes	23
1.4.7 The coefficient of restitution of submerged granular flows	24
1.4.8 The two phase approach	25
1.4.8.1 The interphase force	25

2	The rheology of the granular phase	29
2.1	Granular phase	29
2.1.1	A heuristic rheological model for the frictional regime	30
2.2	Steady state flow	34
2.3	Numerical method	36
2.4	Experimental investigation	38
2.4.1	The internal stresses of the liquid phase	40
2.5	Results	41
2.6	The kinetic energy balance	44
2.7	The total energy balance of the granular phase	45
2.8	The core region	47
2.9	The kinetic energy balance in the core region	49
2.10	The influence of the sidewall	51
3	Further investigations on the interphase forces	53
3.1	Introduction	53
3.2	Voidage function	55
3.3	The drag force fluctuations	58
3.4	Experimental investigations	61
3.4.1	The measurement of the concentration	62
3.4.2	Flow in the column	64
3.4.2.1	Experimental results	66
3.4.2.2	The velocity of the liquid phase	70
3.4.2.3	The pressure of the liquid phase	71
3.4.3	Free fall flow	72
3.4.4	Preliminary results	72
3.5	The fluctuations of the drag in the kinetic energy balance	74
4	Further investigations on the diluted flow conditions	79
4.1	Introduction	79
4.2	Literature review	80

4.3	Stresses tensor of the liquid phase	82
4.3.1	Dynamic viscosity of interstitial fluid	83
4.3.2	Closure models for the Reynolds stresses in granular flows	84
4.3.2.1	Mixing length models in granular flows	84
4.3.2.2	$k - \epsilon$ models in granular flows	86
4.4	Preliminary results	87
5	The extension to the 2D model	91
5.1	Introduction	91
5.2	The numerical model for PDE equations	93
5.3	The equation of state of the liquid phase	94
5.4	The equation of state of the granular phase	95
5.4.1	The numerical formulation	98
5.4.1.1	Modifications of the numerical model	101
5.4.2	Geometry and Boundary Conditions	102
5.5	Preliminary results	104
6	Conclusions	107
A	Equations of the flow in the column	119
A.1	Equations of the solid phase	120
A.2	Equations of the liquid phase	122
B	Decomposition of the drag force	125
B.1	Drag 1-Reynolds decomposition and average	126
B.2	Drag 2-Reynolds decomposition and average	128
B.3	Drag 3-Reynolds decompositions and average	129
C	Equations of the diluted two phase flow in uniform flow con- ditions	133

List of Symbols

Constants

δ_{ij}	Kronecker's delta	[−]
κ	Von Karman constant	[−]
μ_w	Dynamic viscosity of water	$[ML^{-1}T^{-1}]$
ν_w	Cinematic viscosity of water	$[L^2T^{-1}]$
k_B	Boltzman constant	$[MLT^{-1}\Theta^{-1}]$

Dimensionless Groups

Re	Reynolds number	[−]
Re_d	Reynolds number of the particles	[−]
Ba	Bagnold number	[−]
I	Inertial parameter	[−]
I_s	Savage number	[−]
St	Stokes number	[−]

Functions

C_D	Drag coefficient	[–]
μ^{g-coll}	Dynamic viscosity of the kinetic theory	$[ML^{-1}T^{-1}]$
μ_f	Dynamic viscosity of the liquid phase	$[ML^{-1}T^{-1}]$
$f(c)$	Voidage function	[–]
$f^{(1)}(u, r, t)$	Single-particle velocity distribution function of the kinetic theory	[–]
f_1	Function in the equation of state of the kinetic theory [55]	[–]
f_2	Function in collisional dynamic viscosity of the kinetic theory [55]	[–]
$f_2(c)$	Function in the relation of the shear stresses of the liquid phase	[–]
f_4	Function in the collisional coefficient of diffusion of the kinetic theory [55]	[–]
f_5	Function in the dissipation rate of the kinetic theory [55]	[–]
f_c	Filter function of the intermittency [10]	[–]
f_{i-JS}	Functions of the kinetic theory according to [48]	[–]
g_o	Radial distribution function	[–]
k_{Θ}	Diffusion coefficient of the kinetic theory	$[ML^{-1}T^{-1}]$

Matrixes

\mathbf{K}_{kl}	Stiffness matrix	[–]
\mathbf{M}_{kl}	Mass matrix	[–]

Parameters

m	Exponent of the voidage function	$[-]$
α_2	Shape factor of particles	$[-]$
α_3	Shape factor of particles	$[-]$
Δ	Relative density	$[-]$
δ	Angle of projection	$[\circ]$
η_{Lou}	Ratio between the frictional and the total stresses of the granular phase	$[-]$
γ	Parameter of EOS	$[-]$
Ω	Domain of the PDE system	$[-]$
$\rho_{\beta o}$	Reference density of EOS	$[-]$
ξ	Coefficient of calibration of the relation between the different type of concentration	$[-]$
a, b	Constants of the different relation for the mixing length of turbulence proposed	$[-]$
c^*	Maximum packing concentration of the solid phase	$[-]$
c_μ	Parameter of the $k - \epsilon$	$[-]$
e_o	Elastic coefficient of restitution in the normal direction	$[-]$
I_o	Parameter of the $\mu(I) - model$	$[-]$
I_{so}	Parameter of the <i>heuristic model</i>	$[-]$
K	Hydraulic conductivity of the mixture	$[LT^{-1}]$

k	Permeability of the mixture	$[L^2]$
k_β	Constant of compressibility of the EOS	$[-]$
n	Exponent of the weighted voidage function proposed	$[-]$

Subscripts

β	Subscript for the phases	$[-]$
f	Subscript for the liquid phase	$[-]$
g	Subscript for the granular phase	$[-]$
i	Subscript for the direction of the vector	$[-]$
j	Subscript for the direction of the vector	$[-]$
s	Subscript for the solid phase	$[-]$
w	Subscript for water	$[-]$

Superscripts

β	Superscript for the phases	$[-]$
f	Superscript for the liquid phase	$[-]$
g	Superscript for the granular phase	$[-]$
s	Superscript for the solid phase	$[-]$
w	Superscript for water	$[-]$

Tensors

D_{ij}	Strain rate tensor	$[-]$
----------	--------------------	-------

T_{ij}^β	Tensor of the internal stresses	$[ML^{-1}T^{-2}]$
T_{ij}^{coll}	Collisional component of the tensor of the internal stresses of the granular phase	$[ML^{-1}T^{-2}]$
T_{ij}^{fric}	Frictional component of the tensor of the internal stresses of the granular phase	$[ML^{-1}T^{-2}]$

Variables

$\langle \psi \rangle$	Averaged value of any properties of the particles of the kinetic theory	$[-]$
α	Slope of the flow in uniform condition	$[^\circ]$
β	tangential coefficient of restitution of the solid particles	$[-]$
χ_i	Coefficients of the residual drag force	$[-]$
$\dot{\gamma}$	Shear rate	$[T^{-1}]$
ϵ	Fluid-phase turbulent dissipation rate	$[L^2T^{-3}]$
η	non dimensional normal coordinate	$[-]$
λ	Linear concentration	$[-]$
λ_a	Surface concentration	$[-]$
$\hat{\mathbf{Q}}_t$	unknown coefficients of the numerical solution of DAEs	$[-]$
μ	Friction coefficient [34]	$[-]$
μ_2	Friction coefficient of the collisional regime [34]	$[-]$
μ_e	Effective viscosity in presence of particles	$[ML^{-1}T^{-1}]$
μ_s	Static friction angle [34]	$[-]$

ν_t	Eddy viscosity in presence of particles	$[L^2T^{-1}]$
Ω	Intermittency function [10]	$[-]$
ω	Angular momentum of the solid particles	$[T^{-1}]$
\bar{c}	Ensemble concentration	$[-]$
\bar{D}	Average drag force	$[ML^{-2}T^{-2}]$
$\overline{u_\beta^\beta}$	Ensemble velocity	$[L^1T^{-1}]$
∂V	Border of the surface between the two phases in the control volume	$[L]$
ϕ_k	Test functions of the numerical model for PDE's	$[-]$
ψ	Any properties of the particles of the kinetic theory	$[-]$
ρ_β	Density	$[ML^{-3}]$
τ^β	Shear stresses	$[ML^{-1}T^{-2}]$
τ^{g-coll}	Collisional shear stress of the granular phase	$[ML^{-1}T^{-2}]$
τ^{g-fric}	Frictional shear stress of the granular phase	$[ML^{-1}T^{-2}]$
τ_{12-Ba}	Shear stress of the granular phase [13]	$[ML^{-1}T^{-2}]$
τ_{r3}^f	Shear stress normal to the section of the column in the vertical direction	$[ML^{-1}T^{-2}]$
Θ	Granular temperature	$[L^2T^{-2}]$
θ_2	Friction angle of collisional regime [34]	$[^\circ]$
θ_k	Test functions of the numerical model for PDE's	$[-]$

$\theta_k(t)$	piecewise polynomial basis functions of classical Galerkin approach	[–]
$\theta_l(t)$	piecewise polynomial basis functions of maximum degree N	[–]
θ_s	Friction angle [34]	[°]
φ	Friction angle of the granular material	[°]
\widehat{D}	Dimensionless drag force	[–]
$\widetilde{\Theta}$	Granular temperature of the spin	[L^2T^{-2}]
$\widetilde{u}_\beta^\beta$	Favre averaged velocity	[L^1T^{-1}]
A	Surface of the section of the column	[L^2]
A_b	Surface of the base of the pyramid of the configuration of the particles	[L^2]
A_{bv}	Projection of the surface of the base of the pyramid of the configuration of the particles	[L^2]
c	Instantaneous value of the concentration of the solid phase	[–]
c'	Fluctuating value of the concentration of the solid phase	[–]
d	Diameter of the particles	[L]
$D(\bar{c}, \bar{U})$	Drag force calculated with the average value	[$ML^{-2}T^{-2}$]
D_i^β	Drag force	[$ML^{-2}T^{-2}$]
D_R	Residual drag	[$ML^{-2}T^{-2}$]
$D_{i+\frac{1}{2}}(q_h^-, q_h^+)$	Fluxes of the interfaces of the numerical model for PDE's	[–]
D_{sp-i}	Drag force of the single sphere	[$ML^{-2}T^{-2}$]

e	Elastic coefficient of restitution in the normal direction	$[-]$
h	Water depth	$[L]$
h^*	Hydraulic load	$[L]$
I	Inertial momentum of the solid particles	$[ML^2]$
k	Fluid-phase turbulent kinetic energy	$[L^2T^{-2}]$
K_s	Oscillatory component of the solid phase [40]	$[L^2T^{-2}]$
k_s	Large-scale sediment velocity fluctuations [40]	$[L^2T^{-2}]$
l	Mixing length of the closure model for turbulence	$[L]$
m	Mass of the phase	$[M]$
N	Degree of the piecewise polynomial	$[-]$
N	Numbers of solid particles inside the control volume	$[-]$
n	Uniform number density of particles	$[-]$
p^β	Pressure	$[ML^{-1}T^{-2}]$
p^{g-coll}	Collisional component of the granular pressure	$[ML^{-1}T^{-2}]$
p^{g-com}	Compressible component of the granular pressure	$[ML^{-1}T^{-2}]$
p^{g-fric}	Frictional component of the granular pressure	$[ML^{-1}T^{-2}]$
p_{-Ba}	Dispersive pressure of the granular phase [13]	$[ML^{-1}T^{-2}]$
q_n^h	Predictor solutions of the numerical model for PDE's	$[-]$
Q_l	Liquid discharge	$[L^3T^{-1}]$
Q_s	Solid discharge	$[L^3T^{-1}]$

R_h	Hydraulic radius	$[ML^{-1}T^{-2}]$
S	Surface between the two phases in the control volume	$[L^2]$
s	Distance between two particles	$[L]$
s	Spin of the solid particles	$[LT^{-1}]$
S_i	Stencils of the numerical model for PDE's	$[-]$
T	Ordinary temperature	$[\Theta]$
T	Period of integration	$[T]$
t	Variable for the time	$[T]$
t^n	Current time level of the numerical model for PDE's	$[T]$
t^{n+1}	New time level of the numerical model for PDE's	$[T]$
T_i	Elements of the triangles of the numerical model for PDE's	$[-]$
$u_\beta^{l\beta}$	Fluctuating value of the velocity	$[L^1T^{-1}]$
u_n^h	Numerical solutions of the numerical model for PDE's	$[-]$
u_β^β	Instantaneous value of the velocity	$[L^1T^{-1}]$
u_i^{fil}	Velocity in porous media flow	$[LT^{-1}]$
U_{r-i}	Relative velocity between the liquid and the solid phase	$[LT^{-1}]$
V	Control volume	$[L^3]$
V_s	Solid fraction of the control volume	$[L^3]$
w_n^h	Approximative solutions of the numerical model for PDE's	$[-]$
x_i	Spatial coordinates	$[L]$

z	Vertical coordinate	$[L]$
Vectors		
\mathbf{e}_i	Unit vector of the Cartesian tern	$[-]$
\mathbf{E}	Vector of differential terms of DAEs	$[-]$
\mathbf{F}_x	Vector of fluxes in the longitudinal direction of the numerical model for PDE's	$[-]$
\mathbf{F}_y	Vector of fluxes in the normal direction of the numerical model for PDE's	$[-]$
\mathbf{F}	Vector of known terms of DAEs	$[-]$
\mathbf{F}^β	Vector of the interaction force	$[ML^{-2}T^{-2}]$
\mathbf{G}_x	Vector of viscous fluxes in the longitudinal direction of the numerical model for PDE's	$[-]$
\mathbf{G}_y	Vector of viscous fluxes in the normal direction of the numerical model for PDE's	$[-]$
\mathbf{g}^β	Vector of the gravity accelaration	$[LT^{-2}]$
\mathbf{NC}_x	Vector of non conservative fluxes in the longitudinal direction of the numerical model for PDE's	$[-]$
\mathbf{NC}_y	Vector of non conservative fluxes in the normal direction of the numerical model for PDE's	$[-]$
$\mathbf{Q}(t)$	Vector of unknown of DAEs	$[-]$
\mathbf{S}	Vector of source terms of the numerical model for PDE's	$[-]$
\mathbf{u}^β	Vector of the velocities	$[LT^{-1}]$
\mathbf{W}	Vector of conservative variables of the numerical model for PDE's	$[-]$

List of Figures

1.1	Different slopes of granular clusters [43].	6
1.2	Linear concentration scheme.	10
1.3	Sketch of the flow and notation.	19
1.5	Distribution along the flow depth (η is the dimensionless vertical coordinate) of the intermittency function proposed by Armanini et al. [10]	24
2.1	Distribution along the flow depth of measured values of the apparent friction angle, i.e. the inverse tangent of the ratio between shear stress and pressure in a uniform flow of spheres and water.	33
2.2	Representation of the glass-walled open channel used for the experimental analysis. This figure belongs to [8].	39
2.3	Distribution along the flow depth of the experimental: (a) velocity; (b) internal shear stresses of the granular and the liquid phases calculated from the momentum balance in the longitudinal direction assuming that the drag is totally balanced by the weight of the fluid phase.	41
2.4	Comparison between results of the numerical simulation (line) and experimental data (symbols) of: (a) particle concentration profile; (b) granular temperature profile.	42

2.5	Comparison between results of the numerical simulation (line) and experimental data (symbols) of: (a) granular velocity profile; (b) granular velocity gradient profile.	43
2.6	Comparison between computed (lines) and observed (symbols) of: (a) granular pressure profile; (b) granular shear stresses profile.	43
2.7	Collisional and frictional component of (a) pressure and of (b) shear stress. Comparison between computed (lines) and observed (symbols) values.	44
2.8	Distribution along the depth of the (dimensionless) terms of the kinetic energy balance of the collisional component eq.(2.18). Experimental data (symbols) and predictions of the model (lines)	45
2.9	Distribution along the depth of the dimensionless terms of the total energy balance eq.(2.29). Each terms of eq.(2.29) is divided by $\rho_s g^{1.5} h^{0.5}$. Comparison between experimental data (symbols) and results of the model (lines).	46
2.10	Comparison between computed (solid line) and observed (circles) values of the ratio of frictional to total stresses plotted versus volume concentration.	47
2.11	Distribution along the transversal direction x_3 of the non-dimensional longitudinal velocity of the granular phase u^g/\sqrt{gd} observed at the free surface in the experiment described in section 3. W denotes the width of the channel.	51
3.1	The dot line represents the voidage function according to the theoretical relation derived eq.(3.7) while the red line represents the voidage function according to eq.(3.5). In dashed line the maximum value of the concentration is reported.	57
3.2	Magnitude of each coefficient of the fluctuating components of the drag force as a function of the concentration.	60

3.3	Section of the column in the x_1, x_2 plane. This figure belongs to [56].	61
3.4	Column sets up in the hydraulic laboratory with the two cameras for videos. This figure belongs to [56].	61
3.5	Hypothetical disposition of particles	62
3.6	Scheme of the forces involved in the momentum balances.	64
3.7	Distribution across the flow depth of concentration.	67
3.8	Distribution along the flow depth of the average value of the velocity (a) in the vertical direction x_3 ; (b) the average value of the velocity in the horizontal plane x_1, x_2	67
3.9	Distribution along the flow depth of the fluctuations of the velocities: (a) in the vertical direction x_3 ; (b) in the horizontal plane x_1, x_2 . In blue the measurement of the granular phase and in red of the liquid phase.	68
3.10	Distribution along the flow depth of the dimensionless correlations of the fluctuations of the velocities and the concentration: (a) in the vertical direction x_3 ; (b) in the horizontal plane x_1, x_2 . In blue the measurement of the granular phase and in red of the liquid phase.	68
3.11	Distribution along the flow depth of the correlations of the dimensionless fluctuations of the velocities and concentration: (a) in the vertical direction x_3 ; (b) in the horizontal plane x_1, x_2 . In blue the measurement of the granular phase and in red of the liquid phase.	69
3.12	Distribution of the drag vs concentration. Measurements of the flow in the column.	70
3.13	Different terms of the correlations of the fluctuations of the momentum balance for different runs: with a liquid discharge of 160 [l/min]	71
3.14	Measurements of the fluid pressure for different discharges.	72

3.15	Distribution of the average drag vs concentration. Measurements of the free fall flow.	73
3.16	Distribution of the average drag vs concentration. Summary of the measured data.	73
3.17	The voidage function calculated from the experimental data is shown in blue dot. The red line represents the voidage function according to eq.(3.5), while the green line is the voidage function according to eq.(3.9)	74
3.18	Comparison between the dissipation rate in the kinetic energy balance, obtained according to different formulations. The stars represent the dissipation rate due to the drag fluctuations, obtained following Armanini <i>et al.</i> (2014), eq.(3.39). The crosses represent the dissipation rate of the drag fluctuations obtained according to the diffusive hypothesis by Hsu <i>et al.</i> (2004), eq.(3.40). The circles represent the kinetic energy dissipation rate due to the inelastic collisions, eq.(3.38). The experimental data are presented in Armanini <i>et al.</i> (2009). . .	76
4.1	Comparison among the expression of the stresses of the liquid phase following different relations of the mixing length of a two phase flow. Furthermore, the red dot represents the stresses according to relation (4.11).	85
4.2	Comparison between results of the numerical simulation (solid line) and experimental data (circles) of: (a) particle concentration profile; (b) granular temperature profile.	88
4.3	Comparison between results of the numerical simulation (solid line) and experimental data (circles) of: (a) velocity of the liquid phase; (b) velocity of the granular phase.	89
4.4	Collisional and frictional component of (a) pressure and of (b) shear stress. Comparison between computed (solid line) and observed (circles) values.	89

4.5	Terms of the momentum equation in x_1 of the liquid phase . . .	89
4.6	Terms of the momentum equation in x_1 of the solid phase. . .	90
5.1	Geometry in Gambit.	102
5.2	Comparison between results of the numerical simulation DAE (solid line) and results of the numerical simulation PDE (circles) of: (a) particle concentration profile; (b) granular temperature profile.	104
5.3	Comparison between results of the numerical simulation DAE (solid line) and results of the numerical simulation PDE (circles) of: (a) granular velocity profile; (b) liquid velocity gradient profile.	105
5.4	Comparison between results of the numerical simulation DAE (solid line) and results of the numerical simulation PDE (circles) of: (a) granular pressure profile; (b) granular shear stresses profile.	105

Summary

The thesis tackles the mechanics of submerged granular flows driven by gravity, focusing on the rheological formulations and on the numerical solutions of the equations that govern this type of flow. In particular, a two-phase approach is assumed. The liquid phase, usually water, is described with a Newtonian rheology. The rheology of the granular phase depends on the type of contacts among the particles. Two opposite conditions are identified: if the contacts among particles are instantaneous the regime is named collisional, while, when the contacts become long lasting and involved more particles at the same time the regime is called frictional. In the thesis a proper model for the rheology of the granular phase, able to account for both the regimes, is presented. This model is based on the fundamental evidence that the granular phase is characterized by the coexistence of the collisional regime, which dominates near the free surface, and of the frictional regime, which becomes relevant approaching the loose static bed Armanini et al. [5]. The kinetic theories of dense gases Jenkins and Savage [48] are adopted to describe the collisional regime, while for the frictional regime a new rheological formulation, dependent on the Savage number, which comes from the analysis of the force involved, is given. In addition, the model, named heuristic model [11], introduces a specific equation of state also for the frictional regime. The model is based only on a single parameter, which presumably depends on the properties of the contact forces of the material. A numerical code able to integrate the equations of the mass, momentum

and energy of the two-phase, in uniform flow conditions, was developed by Armanini et al. [6] and the results are compared with the experimental data. In the applications to hyperconcentrated channel flows the effect of the side walls and of the internal stresses of the liquid phase are neglected in the momentum balance equations, therefore the drag force is balanced by the weight of the liquid phase. The heuristic model is able to predict in a satisfactory way the distributions across the flow depth of the velocity, concentration, granular temperature and stresses and in particular, it allows to discriminate between the collisional and the frictional components of the shear and of the normal stresses.

Another important issue addressed in the thesis concerns the balances of the energy of the granular phase. The model is able to describe the mechanisms of production, diffusion and dissipation of energy, relevant to both the mean component of the flow and the fluctuating component (i.e., the collisional component). In uniform flow conditions, near the static loose bed, the model predicts that the flux of the diffused fluctuating energy exceeds an order of magnitude the locally dissipated flux of fluctuating energy. This suggests that the motion of the grains, even at concentrations close to that of packing, is always accompanied by a certain degree of granular temperature as already observed by Armanini et al. [10].

Furthermore, the description of the mechanisms of exchange among the terms of the total energy balance and of the kinetic energy balance, and between the two energy balances is given. In the thesis, the role of the interaction between the liquid and the solid phase in the kinetic energy balance is analysed [59]. A specific experimental investigation to understand the difference between the drag averaged over time and the drag calculated with respect the average velocities and concentration is carried out. This difference between the two drags represents the contribution to the drag due to the correlations between the fluctuating components of the concentration and of the velocities. By integrating the heuristic model across the flow depth, it is

possible, in principle, to derive a set of shallow water equations that are able to describe the behaviour of debris flows and wet avalanches.

Overview of the thesis

The thesis is organized in five chapters.

- Chapter 1 contains an overview of the significance of the topic of the thesis and a review of the literature relevant to the formulation of the theories developed.
- In Chapter 2 a heuristic model for the rheology of the granular phase is presented. This is the main original contribution of the thesis and the results are published in Armanini et al. [11]. The set of equations of hyperconcentrated granular flow, in stationary and uniform conditions, under the hypothesis that the stresses of the liquid phase are negligible in the momentum balances, is numerically solved and the results are compared with experimental data. The numerical method was presented in Armanini et al. [6]. The chapter also contains considerations on the total energy balance of the granular phase and on the kinetic energy balance. The concept of core region and the effect of the sidewall are discussed.
- In Chapter 3 the definition of the drag force for a hyperconcentrated granular flow is tackled, underlining its role in the momentum balances and in the energy balances. The definition of the average drag is discussed. Experimental investigations of the flow in the column and of the free fall flow are carried out in order to better understand these

concepts. A part of this chapter is published in Nucci et al. [59] and the whole content is going to be submitted to a scientific journal.

- In Chapter 4 a review of the literature regarding the definition of the closure relation of the stresses of the liquid phase of submerged granular flows is developed. Some relations are proposed. The set of equations solved in Chapter 2 is written adding the equations of the liquid phase. Preliminary numerical results are compared with experimental data.
- Chapter 5 tackles the extension of the complete system of equations of Chapter 4 to the non-uniform and non-stationary 2D case. The set of equations are implemented in a numerical model proposed by Dumbser [27]. A description of the numerical model, the geometry and the boundary conditions are presented. A set of adaptations of the numerical model for the application to granular flows are presented. The chapter concludes with some preliminary results.
- Chapter 6 contains the conclusions that are carried out thank to the theories developed.

Chapter 1

Introduction

Chapter 1 contains an overview of the significance of the topic of the thesis and a review of the literature relevant to the formulation of the theories developed.

1.1 Debris Flows

Flows of highly concentrated mixtures of water and sediments driven by gravity characterize many geomorphological phenomena. Among these are debris flows, which frequently affect urbanized mountainous areas, causing loss of lives and property damage. Debris and mud flows are statistically rare but these phenomena show a great destructive power. Substantially, they are a non-stationary phenomena, which occur in a very short time. From a hydrological point of view the most frequently cause is a long rainfall, which saturates the ground, followed by an intense rainfall that triggers the collapse. Furthermore, from a morphological point of view, there must be the presence of an amount of repository material, placed on a slope such that the gravity force, relevant to the submerged weight, governs the collapse. Usually the availability of material is due to disaggregation of rocks caused by chemical actions of water, alternation of freezing and thawing, vegetation,

or to the leaching of moraine clusters, which become permeable and unstable. Obviously, a debris flow moves away the material available, and a very long process of accumulation is necessary for material to build up again. For these reasons, the return period between two dangerous events is usually 50 – 100 years. Other different mechanisms can be ascribed to the category of debris flows, such as a landslide that flows along in a river bed, or damage to a weir or to a natural dam. The event of 1966 in the Jiang Jia Ravine, where there was a $600.000m^3$ casting of the sediment due to the collapse of a dam caused by an earthquake, is a significant example. In particular, three possible mechanisms of initiation of a casting due to the presence of a weir/dam are recognized:

- the erosion due to the passage of water above the body of the bridge
- the filtration within the weir body
- the occurrence of a progressive failure mechanism

The three cases reported refer to the diagram by Takahashi [66] (page. 77).

Moreover, while the ordinary mass transport phenomena in river, bed and suspended load are due to the drag of the streaming, the active forces of debris flows are the gravity force and the interactions among particles. In fact, debris flows are such hyperconcentrated that flow resistance is caused by the contacts.

Debris flows are phenomena which have been known for a long time, but only a few decades ago did engineers and geologists start to adopt conceptual tools able to tackle these phenomena with minor empiricism. The first approaches were more or less descriptions and classifications without any physical basis. Takahashi [66] distinguishes between four types of debris flows, assigning to each its own rheology, but the range of validity of each type of flow must unfortunately be known *a priori*. From this point of view, a conceptual simplification able to reduce the subjectivity of the classifications appears urgent.

From a physical point of view, a simplified approach to the modelization of debris flows or wet snow avalanches, is to treat them as a hyperconcentrated flows of two fluids: the interstitial fluid, which behaviour follows the fluid mechanics and it is treated with a proper rheology, and the solid phase that is the granular flows, with a specific rheology too. With respect to the liquid phase usually it is water, at constant temperature, so a Newtonian fluid which obeys to Navier-Stokes equations. However, usually the particles with minor dimension (less than $30\mu\text{m}$) are considered to be scattered in the liquid phase, because is too fine to deposit, and this mixture is treated as an homogeneous fluid taking into account for the presence of cohesive material. The solid phase is composed by major particles, whose dimensions are comparable to those of sand, and it is treated as a *granular flows*. Under the hypothesis that the number of the particles inside the controlled volume is sufficiently big, that is the dimension of the particles is small enough with respect to the infinitesimal controlled volume, continuum mechanics can be applied to the ensemble of particles, with a proper rheology, to describe the interactions among particles. It is evident that this approach fails for big sediments, that is with dimensions comparable to the dimensions of the boundaries of the flow.

In particular, the two-phase approach allows the description of the behaviour of debris flows in all their phases: from their formation, which typically occurs in the highest part of the basin, to the arrest phase, which often occurs in the alluvial fans.

Since the geometry of the sections and the slope change along the path, the same debris flow presents kinematic and dynamic characteristics that change in space and time while flowing downstream. The concentration of the solid phase is one of the flow quantities with the largest spatial variation. In fact it reaches high values in the upper part of the basin, and tends gradually to reduce, especially in the arrest area, due to the progressive deposition of the sediment.

To assess the consequences of these events on structures and infrastructures, one usually adopts depth integrated models. These models, however, require closure equations, i.e. the relationships between some global quantities, such as depth integrated quantities. Usually, these consist in the flow resistance (stress at the bed) and in the transport capacity of the solid phase, expressed as a function of local depth integrated parameters such as the average velocity, the total flow depth and some physical properties of the solid and liquid phase (density, particle size, etc.). More details on these aspects are provided in [66, 9, 42, 8, 4].

In analogy to what is done for rivers, closure relationships for debris flows are derived under steady and uniform flow conditions, but are assumed to be locally valid in unsteady and nonuniform conditions. The closure relationships can be derived experimentally, but it is always necessary to keep as reference a conceptual model that allows the reliability of the simplified and empirical schemes and the completeness of the experimental analysis to be checked.

In particular, the thesis aims to become an instrument for the modelization of debris flows.

1.2 Granular Flows

It is to point out that throughout the following discussion the presence of cohesive sediments is neglected, in order to focus on the rheology of incoherent debris flows. In this case the material of the solid phase consists of particles with sizes ranging from a few centimetres up to a few meters, transported downstream along with water.

Granular materials are an agglomerate of macroscopic particles which show peculiar behaviours with respect to the standard states of matter. In this respect, in fact, the granular material can be considered as a further state of matter [43].

The granular state of matter as a gas

The particles of the granular material interact with instantaneous collision similar to the molecules of gases. However, there are two main differences between an ideal gas and a granular gas:

- there are no effects due to the thermodynamic temperature;
- the interactions among grains are dissipative, either due to the friction among particles and to the inelastic type of collision.

The particles of an ideal gas are perfectly smooth and elastic. The energy scale is due to the product of the $k_B T$, Boltzman constant ($1.4 \cdot 10^{-23} JK^{-1}$) and T the thermodynamic temperature, while, in granular flows, the particles have a mass m and a diameter D , much greater than the dimension of molecules, such that the potential energy mgd , where g is the gravity acceleration, results, in standard conditions, 10^{12} times $k_B T$.

The granular state of matter as a liquid

Granular matter can flow like a liquid. However experimental evidence shows peculiar behavior of the granular flows, such that it seems that the entropy of the system globally reduces, violating the laws of the mixing of fluids [64, 37]. Instead, the ordinary entropy of these processes is negligible compared to the dynamic effects of these types of flows.

The granular state of matter as a solid

The static behaviour of a cluster behaves like a solid, but, the analogy is allowed only for a slope less than the repose angle of the material. In fact, as it is shown in figure 1.1(a) and 1.1(b), for slopes higher than the friction angle of the material, the particles of the cluster begin to flow like a liquid. Also in this case there is a specific behaviour: the particles, which are near the free surface, start running, while the under particles are stop and form a loose static bed. The velocity and the velocity gradient are normal to the bed and decrease asymptotically to zero approaching the lower layer.

The granular flows are characterized by the coexistence of solid particles and

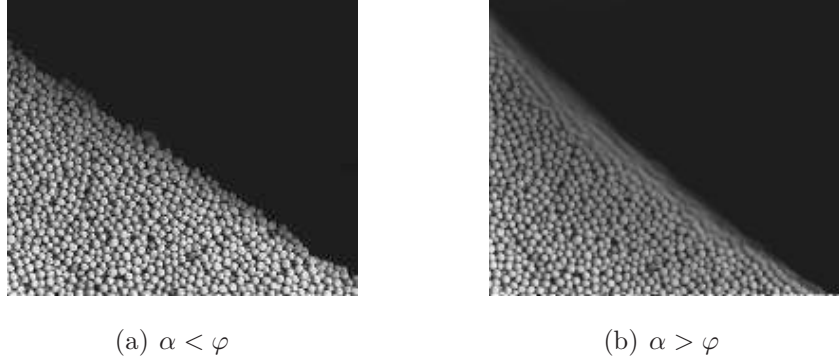


Figure 1.1: Different slopes of granular clusters [43].

of a fluid that fills the voids. Usually the interstitial fluids are water or air or both. In order to describe the mechanics of granular flows, at least a two phase approach is needed.

1.3 A two phase approach

If the two-phase are treated as two fluids without any mass exchange between them, their dynamics is described by the same mass and momentum conservation equations (Cauchy equations) [67, 41]:

$$\left\{ \begin{array}{l} \frac{\partial \rho^\beta}{\partial t} + \frac{\partial (\rho^\beta u_i^\beta)}{\partial x_i} = 0 \\ \frac{\partial \rho^\beta u_i^\beta}{\partial t} + \frac{\partial (\rho^\beta u_i^\beta u_j^\beta)}{\partial x_j} = \rho^\beta g_i^\beta + \frac{\partial T_{ij}^\beta}{\partial x_j} + F_i^\beta \end{array} \right. \quad (1.1)$$

Throughout the thesis, the interstitial fluid is water. The notations of eqs.(1.1) represent: the superscript $\beta = g$ is for the granular fluid phase while $\beta = f$ is for interstitial fluid. $\rho^g = c\rho_s$ and $\rho^f = (1 - c)\rho_w$ are the density of the granular and of the liquid phase, where c is the volume concentration; ρ_s is the material density of the grains and ρ_w is the water density; u_i^β is the

generic component of the velocity vector; T_{ij}^β is the tensor of the internal stresses and F_i^β is the vector of the interaction forces between the two-phase. Because of the principle of reciprocity $F_i^g = -F_i^f$. g_i^β is the component of the mass force (per unit volume) acting on each phase, which in the present case is the vector of the gravity acceleration g , i.e. $g_i^\beta = -g\partial z/\partial x_i$, where z represents the vertical rising direction. These are the notations generally adopted in the thesis.

The rheology of the liquid phase depends on the properties of the fluid. The fluid pressure of the two-phase approach corresponds to the *pore pressure* of the geotechnical approach.

The rheology of the granular phase is characterized by two different mechanisms of interaction among particles: almost instantaneous collisional contacts and long lasting contacts. A distinction between the characteristic time scales of these two types of contact is provided by da Cruz et al. [22]. These two kinds of interaction identify two regimes, which are known respectively as the *collisional regime* and the *frictional regime* [48, 16, 36]. In the literature of the kinetic theory the frictional regime is also named dense flow [44]. In general, it is possible to assume that the stresses corresponding to the two regimes, \mathbf{T}^{coll} for the instantaneous contacts and \mathbf{T}^{fric} for the long lasting contacts, can be added [48], namely $T_{ij}^g = T_{ij}^{coll} + T_{ij}^{fric}$. Even though in almost all applications it is *de facto* assumed that these two regimes are stratified and physically separated [48, 49, 57], recent experimental investigations [10] have shown that they alternate in space and time through an intermittent mechanism, similar to that existing between the viscous and the turbulent sub-layers in the turbulent boundary layer of a smooth wall.

1.3.1 Favre average and ensemble average

In order to apply the properties of continuum mechanics, the equations of the two phase approach are expressed in terms of average variables, under the necessary condition that the control volume is sufficiently large with respect

to the dimension of the particles, but sufficiently small with respect to the dimension of the flow field. In the framework of granular flows, two different type of averages are proposed: the *ensemble average* and the *Favre average*.

The ensemble average is usually adopted in the framework of the kinetic theory, and is the average used in the thesis. According to Jenkins and Savage [48], the ensemble value of any property $\psi(u)$ of the flow is found:

$$\langle \psi \rangle = \frac{1}{n} \int \psi(u) f^{(1)}(u, r, t) du \quad (1.2)$$

where $f^{(1)}(u, r, t)$ is a single-particle velocity distribution function, such that $f^{(1)}(u, r, t) du$ represents the probable number of particles per unit volume at time t and position r with velocities u in the element du . The brackets $\langle \rangle$ represent the average of all the particles, which, at each instant, are inside a control volume. In contrast, Drew [26] proposes weighting the equations of the two-phase on the concentration, that is, the *Favre average*. The Favre average is based on the definition of the average concentration of the ensemble, given as:

$$\bar{c} = \lim_{N \rightarrow \infty} \frac{1}{N} \Sigma c \quad (1.3)$$

and the other average quantities, identified by the over line, can be derived with respect to the average concentration. The main advantage of the Favre average is that averaging the instantaneous equations of the mass and of the momentum conservation, the terms due to the correlations of the fluctuations are avoided.

The Favre average is now applied, for example, to the mass conservation balance of the granular phase, that reads as:

$$\frac{\partial}{\partial t} \rho_s c + \frac{\partial}{\partial x_i} \rho_s c u_i^g = 0 \quad (1.4)$$

In terms of mean values and instantaneous variables ($c = \bar{c} + c'$ and $u_i =$

$\bar{u}_i + u_i'$), eq. (1.4) is:

$$\frac{\partial}{\partial t} \rho_s \bar{c} + \frac{\partial}{\partial t} \rho_s c' + \frac{\partial}{\partial x_i} \rho_s \bar{c} u_i^g + \frac{\partial}{\partial x_i} \rho_s \bar{c} u_i^{g'} + \frac{\partial}{\partial x_i} \rho_s c' u_i^g + \frac{\partial}{\partial x_i} \rho_s c' u_i^{g'} = 0 \quad (1.5)$$

Then, averaging in time, eq.(1.5) becomes:

$$\frac{\partial}{\partial t} \rho_s \bar{c} + \frac{\partial}{\partial t} \rho_s \bar{c}' + \frac{\partial}{\partial x_i} \rho_s \overline{\bar{c} u_i^g} + \frac{\partial}{\partial x_i} \rho_s \overline{\bar{c} u_i^{g'}} + \frac{\partial}{\partial x_i} \rho_s \overline{c' u_i^g} + \frac{\partial}{\partial x_i} \rho_s \overline{c' u_i^{g'}} = 0 \quad (1.6)$$

The average value of the fluctuating terms of the first order are equal to zero, so eq. (1.6) reduces to:

$$\frac{\partial}{\partial t} \rho_s \bar{c} + \frac{\partial}{\partial x_i} \rho_s \overline{c u_i^g} + \frac{\partial}{\partial x_i} \rho_s \overline{c' u_i^{g'}} = 0 \quad (1.7)$$

The average velocity of the ensemble is defined as:

$$\bar{u}_i^g = \frac{\langle \rho_s c u_i^g \rangle}{\langle \rho_s c \rangle} \quad (1.8)$$

where the brackets represent the average of all the particles in the control volume. The Favre average velocity is related to the average velocity of the ensemble by $\tilde{u}_i^g = \bar{u}_i^g + u_i^{g''}$, where $u_i^{g''} = \overline{c' u_i^g} / \bar{c}$, and by multiplying the Favre average velocity, on both sides, by the average concentration \bar{c} , it results that:

$$\bar{c} \tilde{u}_i^g = \bar{c} \bar{u}_i^g + \bar{c} u_i^{g''} = \bar{c} \bar{u}_i^g + \frac{\overline{c' u_i^g} \bar{c}}{\bar{c}} = \bar{c} \bar{u}_i^g + \overline{c' u_i^g} \quad (1.9)$$

such that eq.(1.7) reduces to:

$$\frac{\partial}{\partial t} \rho_s \bar{c} + \frac{\partial}{\partial x_i} \rho_s \bar{c} \tilde{u}_i^g = 0 \quad (1.10)$$

so the term due to the correlation of the fluctuation of the concentration and the velocity disappears.

The main advantage is that the final system of equations average with

the Favre procedure shows fewer unknowns.

1.4 Literature relevant to the thesis

1.4.1 Bagnold's dispersive pressure theory

The pioneer of the constitutive relations of granular flows is Bagnold, thanks to his studies on the dispersion of solid spherical grains, with constant diameter and with the same density as the liquid phase, sheared in a Newtonian fluids of varying viscosity, in a coaxial cylinder rheometer. According to Bagnold the collision among particles occurs to develop a dispersive pressure in the flow field, which substantially depends on the mean distance among the grains. For spherical particles, it is possible to express this distance, called linear concentration λ , as the ratio between d , the diameter of the particles, and s the mean distance between two grains: $\lambda = d/s$ (figure 1.2). In case of spheres, the linear concentration is related to the volume concentration, c , through the following relation:

$$\lambda = \frac{c^{1/3}}{c^*^{1/3} - c^{1/3}} \quad (1.11)$$

where c^* is the maximum value of the concentration, *packing concentration*, which, for spheres, results in the so called *cannonballs* configuration, 0.74. The experimental data collected allows Bagnold to assume that, for a sufficiently high value of the shear velocity, the dispersive pressure depends on the square of the shear rate, that is, in a uniform flow in the longitudinal

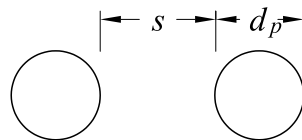


Figure 1.2: Linear concentration scheme.

direction x_1 and normal direction x_2 :

$$p_{-Ba} = a \cos \varphi \rho_s \left(\lambda d \frac{\partial u_1^g}{\partial x_2} \right)^2 \quad (1.12)$$

φ is the dynamic friction angle, which Bagnold assumes to be constant in the *grain inertial regime*, and a is an experimental constant (Bagnold proposes $a = 0.042$). The expression of the dispersive pressure, eq.(1.12), can be derived from the momentum exchange that occurs due to the collisions of the particles. Furthermore the dispersive pressure is induced by a dispersive shear stress, that is:

$$\tau_{12-Ba} = a \sin \varphi \rho_s \left(\lambda d \frac{\partial u_1^g}{\partial x_2} \right)^2 \quad (1.13)$$

In the model proposed by Bagnold, the relation between the shear stresses and the normal stresses is Coulombian:

$$\frac{\tau_{12-Ba}}{p_{-Ba}} = \tan \varphi \quad (1.14)$$

Bagnold found a parameter Ba (called in subsequent works the Bagnold number [38]) that distinguishes between the *grain inertia regime*, where the stresses depend on the square of the shear rate, and the *macro viscous regime*, where the stresses are linearly dependent on the shear rate.

In particular, Ba is the ratio between collisional and viscous stresses:

$$Ba = \frac{\rho_f \lambda^{1/2} \dot{\gamma} d^2}{\mu_f} \quad (1.15)$$

where d represents the grain diameter, $\dot{\gamma}$ the shear rate and ρ_f and μ_f are the density and the viscosity of the interstitial fluid respectively. Bagnold's theory shows its limit when applied to the grain inertia region in uniform flow condition because, from the integral of the stresses, it appears that the

concentration can only be constant.

1.4.1.1 Limits of Bagnold's theory

Armanini et al. [8] demonstrate that applying Bagnold's theory to submerged granular flows driven by gravity, in uniform flow conditions, the profile of the concentration across the flow depth is constant. In fact, in these conditions, the shear and the normal stresses of the dispersive pressure theory are balanced by the corresponding components of the gravitational forces:

$$\tau_{12-Ba} = \int_{x_2}^h (1+c)\Delta g \sin \alpha dy \quad (1.16)$$

$$p_{-Ba} = \int_{x_2}^h c\Delta g \cos \alpha dy \quad (1.17)$$

such that the ratio of eq.(1.16) and eq.(1.17) is:

$$\frac{\tau_{12-Ba}}{p_{-Ba}} = \frac{\int_{x_2}^h (1+c)\Delta g dy}{\int_{x_2}^h c\Delta g dy} \tan \alpha \quad (1.18)$$

From the previous discussion, the stresses of Bagnold's theory are Coulombian, such that the ratio is equal to $\tan \varphi$ eq.(1.14) for each value of φ , which is a property of the material, and the concentration is constant across the flow depth. On the other hand, experimental evidence shows that the concentration assumes its maximum value approaching the mobile bed, c^* , and becomes zero approaching the free surface [5]. Moreover, the forces between particles or the impulsive forces in collisions result from the fluctuations of the particle velocity about the mean. These fluctuations are an inevitable result of the collisions between particles being swept together by the mean flow. Bagnold does not consider these fluctuations except to assume that they were random and that the production of mean kinetic energy associated with them is balanced by dissipation into heat in collisions.

1.4.2 The kinetic theory of dense gases

The limits of Bagnold's theory were overcome in the 1980's with the introduction of the kinetic theory of dense gases for an idealized granular material comprised of identical, smooth, imperfectly elastic, spherical particles which is flowing at such a density and is being deformed at such a rate that particles interact only through binary collisions with their neighbors, incorporating the important difference that collisions between the grains inevitably dissipate energy [48]; [46]; [47]; [54]; [45]. The assumptions are:

- the kinetic theory of gases describes a gas as a large number of small particles (atoms or molecules), all of which are in constant, random motion.
- the particles constantly collide with each other and with the walls of the container.
- the kinetic theory explains macroscopic properties of gases, such as pressure, temperature, and volume, by considering their molecular composition and motion.
- essentially, the theory assumes that pressure is due to collisions between particles moving at different velocities through Brownian motion.

The fundamental idea of the theory is that the collisions between particles are *binary* and that the velocities of a pair of colliding particles are *independent*. The normal component of the instantaneous velocities of a particle before and after a collision are related through the *coefficient of restitution* e , which is a constant between 0 and 1. If the particles are rough, there is also a loss of energy associated with the component of the relative velocity of the contact points along the line of contact. In this case, the tangential components of the instantaneous velocities of a particle before and after a collision are related through the *alternating tensor*, the unit vector and a constant $\beta = [-1; 1]$.

If β is equal to -1 or to 1 there is no change in the tangential components, if β is equal to 0 it is rolling without slipping at impact.

The theory of Jenkins and Richman [46] is applied to smooth spheres, with mass m , velocity u , angular momentum ω and inertial momentum I , and introducing a vector of velocity with three components (u_1, u_2, u_3) , the spin is defined as: $s = \omega(I/m)^{1/2}$

In analogy with the kinetic theory of molecular gases, the concept of ordinary temperature is replaced with the concept of granular temperature, which is a measurement of the fluctuations of the velocities of the granular phase. In particular, following Jenkins and Richman [46], the mean kinetic energy of the flow is governed by two types of temperature: one accounts for the fluctuations in the translational velocity ($\Theta = 1/2 \langle u_i^g u_i^g \rangle$) and the other measures the fluctuations in the spin ($\tilde{\Theta} = \langle u_3^2 \rangle$), where the brackets $\langle \rangle$ represent the average of all the particles, which, at each instant, are inside a control volume, that is, the *ensemble average*. $u_i'^g = u_i^g - \langle u_i^g \rangle$ represent the fluctuations of the vector of the velocity and $\langle u_i^g \rangle = u_i^g$ are the averaged components of the velocities. In this case, the flow is characterized by the continuum of partially elastic collisions among particles. It is evident that, since the granular temperature changes in space and in time, it represents the kinetic energy of the collisional regime. In analogy with the thermal temperature it is assumed that the granular temperature plays the same role in generating pressure and governing the mass, momentum and energy transports.

There are two cases in which the spin is negligible: in the case of slightly rough and nearly elastic particles ($\beta \simeq -1$ and $e \simeq 1$), and in the case of near reversal of contact velocities ($\beta \simeq 1$ and $e \simeq 1$) where the translational and spin temperatures are equal. The theories developed in this thesis concern cases in which the spin is negligible.

In the kinetic theory, all the proprieties of the flow fields, such as density, shape and size, are averaged over all possible collisions. The coefficient of

restitution e is less than 1 so a dissipation term is included in the energy balance.

Kinetic theory uses a spatial probability function based on the probable number of pairs of particles to collide. If the mean flow is homogeneous, the probability function is isotropic. The statistics of binary collisions are determined by the complete pair distribution function of the two particles' velocities, time and positions, integrated over all velocities.

In these processes, the dissipation gives an important contribution to the flux of linear momentum, and fluctuation in energy arises both from particles moving between collisions and from the transfer of energy in collisions. The dense flows of interest are dominated by the transfer mechanics.

The stresses due to collisions among particles are derived theoretically by Jenkins and Hanes [45], starting from the totally generic formulation by Chapman and Cowling [19]:

$$T_{ij}^{g-coll} = -p^{g-coll} \delta_{ij} + \tau_{ij}^{g-coll} \quad (1.19)$$

where T^{g-coll} is the collisional component of the stress tensor of the granular phase and δ_{ij} Kronecker's delta. p^{g-coll} is the isotropic collisional pressure of the granular phase and substantially depends on the granular temperature. Different relations between p^g and Θ , informally called the equation of state, are proposed. The thesis refers to the formulation of Lun et al. [55], which appears from experimental evidence [10] more appropriate to hyperconcentrated flows than the widely used formulation by Jenkins and Hanes [45].

The equation of state reads:

$$p^{g-coll} = f_1 \rho_s \Theta \quad (1.20)$$

The collisional shear stress is expressed as:

$$\tau_{ij}^{g-coll} = \mu^{g-coll} \left(\frac{\partial u_i}{\partial x_j} + \frac{\partial u_j}{\partial x_i} \right) \quad (1.21)$$

The collisional dynamic viscosity of the kinetic theory is scaled on the granular temperature, as the velocity scale, and on the diameter of the particles, as the length scale, and reads as:

$$\mu^{g-coll} = f_2 \rho_s \sqrt{\Theta} d \quad (1.22)$$

where:

$$f_1 = c(1 + 4c\eta_p g_o) \quad (1.23)$$

and:

$$f_2 = \frac{5\sqrt{\pi}}{96\eta_p(2 - \eta_p)} \left(1 + \frac{8}{5}\eta_p c g_o \right) \left(\frac{1}{g_o} + \frac{8}{5}\eta_p(3\eta_p - 2)c \right) + \frac{8/5}{\sqrt{\pi}}\eta_p c^2 g_o$$

are functions of the volume concentration. g_o is the *radial distribution function* that states that the probability of collisions between two particles also depends on the presence of other particles in the control volume [18]. Different expressions for g_o were proposed, differing in particular for higher values of concentration, where the kinetic theory lost its validity, for example the expression eq.(1.24) [35], and eq.(1.25) [54]:

$$g_o(c) = \frac{1}{\left(1 - \frac{c}{c^*}\right)^{1/3}} \quad (1.24)$$

$$g_o(c) = \frac{1}{\left(1 - \frac{c}{c^*}\right)^{2.5c^*}} \quad (1.25)$$

$\eta_p = \frac{(1+e)}{2}$ is a parameter that depends on the elastic coefficient of restitution e of particles. The kinetic theory of gases needs a further equation, which is the kinetic energy balance relevant to the granular temperature:

$$\rho_s \left(\frac{\partial \Theta}{\partial t} + u_j^g \frac{\partial \Theta}{\partial x_j} \right) = \frac{\partial}{\partial x_j} \left(k_\Theta \frac{\partial \Theta}{\partial x_j} \right) + \mu^{g-coll} \left(\frac{\delta u_i^g}{\delta x_j} + \frac{\delta u_j^g}{\delta x_i} \right)^2 - f_5 \rho_s \frac{\Theta^{1.5}}{d} \quad (1.26)$$

where the left side represents the inertial variation of the kinetic energy relevant to the granular temperature of the flow, and on the right side there are the terms due to the diffusion caused by the agitation of particles (k_Θ is the diffusion coefficient), due to the work done by the stresses of the granular phase and due to the dissipation of the inelastic component of collision. The expression of the diffusion coefficient, according to Lun et al. [55], is:

$$k_\Theta = f_4 \rho_s \sqrt{\Theta} d \quad (1.27)$$

where:

$$f_4 = \frac{25\sqrt{\pi}}{16\eta_p(41-33\eta_p)} \left(1 + \frac{12}{5}\eta_p c g_o \right) \left(\frac{1}{g_o} + \frac{12}{5}\eta_p^2(4\eta_p-3)c \right) + \frac{4}{\sqrt{\pi}}\eta_s c^2 g_o$$

and:

$$f_5 = \frac{12}{\sqrt{\pi}} c^2 g_o (1 - e^2)$$

1.4.2.1 Different formulations of the functions f_i

In the framework of the thesis, the expressions of the functions f_i of the kinetic theory involved were proposed by Lun et al. [55], subsequently by Mitarai and Nakanishi [58]. These are equivalent to that of the previous works by Jenkins and Savage [48] and Jenkins and Richman [46], if the particles are elastic, that is $e = 1$ and $\eta_p = 1$. In fact:

- the expression of f_1 is the same in the two formulations;
- the expression of f_2 by Lun et al. [55] can be written for $\eta_p = 1$:

$$f_2 = \frac{8}{\sqrt{\pi}} c^2 g_o \left[1 + \frac{\pi}{12} \left(1 + \frac{5}{8 c g_o} \right)^2 \right]$$

which is the same as the expression by Jenkins and Savage [48]:

$$f_{2-JS} = \frac{8}{5\sqrt{\pi}} c \frac{2-c}{2(1-c)^3} \left[1 + \frac{\pi}{12} \left(1 + \frac{5}{8} c \frac{2-c}{2(1-c)^3} \right)^2 \right]$$

- The expression of f_4 by Lun et al. [55] can be written for $\eta_p = 1$:

$$f_4 = \frac{4}{\sqrt{\pi}} c^2 g_o \left[1 + \frac{9\pi}{32} \left(1 + \frac{5}{12c} g_o \right)^2 \right] \quad (1.28)$$

which in Jenkins and Savage [48] is written:

$$f_{4-JS} = \frac{4}{\sqrt{\pi}} c^2 \frac{2-c}{2(1-c)^3} \left[1 + \frac{9\pi}{32} \left(1 + \frac{5}{12} c \frac{2-c}{2(1-c)^3} \right)^2 \right]$$

- The expression of f_5 by Lun et al. [55] for $\eta_p = 1$ is:

$$f_5(1 - e^2) = \frac{24}{\sqrt{\pi}} (1 - e) \eta_p c^2 g_o$$

which is the same expression as that by Jenkins and Savage [48]:

$$f_{5-JS} = \frac{24}{\sqrt{\pi}} (1 - e) c^2 \frac{2-c}{2(1-c)^3}$$

1.4.3 The generation of granular temperature

A detailed analysis of the mechanisms by which the granular temperature of a granular flows is generated is presented by Campbell [16]. In particular, for rapid granular flows, two modes are considered:

- *collisional temperature generation*: the granular temperature is generated from the transfer of momentum between particles when they collide and depends on the velocities of the particles and on the elastic coefficient of restitution of the collisions
- *streaming temperature generation* due to the presence of the particles with different shear rates such that the particles that move from their own layer accelerate or decelerate by colliding with the particles that they meet, with the same mechanism of the generation as Reynolds turbulent stresses. This mode dominates at very low density, and such that the region governed by the streaming mode is often neglect.

1.4.4 A model for chains of particles

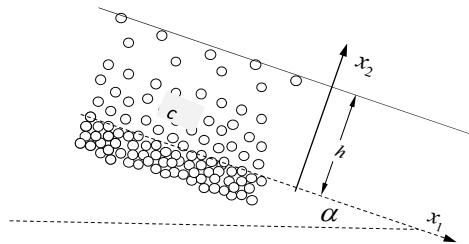


Figure 1.3: Sketch of the flow and notation.

A rheological Coulombian type model for describing the behaviour of dense assemblies of dry grains subjected to continuous shear deformation is represented in GDR-MiDi [34]. With reference to the notation of figure 1.3,

GDR-MiDi [34] proposed the following relation (1.29):

$$\mu = \mu_s + \frac{\mu_2 - \mu_s}{I_o + I} I = \frac{\mu_s I_o + \mu_2 I}{I_o + I} \quad (1.29)$$

where I is the *inertial number*, previously introduced by Ancy and Evesque [1]:

$$I = \frac{\dot{\gamma} d}{\sqrt{p^g/\rho_s}} \quad (1.30)$$

where $\dot{\gamma}$ is the shear rate, d the diameter of the particles, ρ_s the density of the solid phase and p^g the granular pressure. The *inertial number* is subsequently interpreted in term of ratio between the two temporal scales that govern the problem is given by da Cruz et al. [22]: a micro scale $d/\sqrt{p^g/\rho_s}$, which is the time in which a particle falls in a empty space, with dimension of the particle d by the action of a pressure p^g ; and a macro scale proportional to the local strain rate $\dot{\gamma} = \partial u_1/\partial x_2$, such that the *inertial number* is small for slow motions and becomes larger as the flows go faster. μ_s of equation (1.29) is "the critical value at zero shear rate" of the friction coefficient and μ_2 is "the limit value at high I ". The model is based on the observation that, for confined flows, different entities of chains of particles appear depending on the boundary conditions of pressure and shear rate.

In particular, this model seems to be affected by some fundamental weaknesses, which are:

- the $\mu(I)$ -model lacks of an *equation of state*. This is the reason why the authors assume that the concentration is constant. If the top layer is governed by the collisional regime, it seems obvious that the transition between the two layers is continuous and that it is unlikely that the flow maintains a concentration constant from the static loose bed, in which the concentration takes the maximum value (random packing), up to the top layer where the motion is governed by the collisional regime.

- for the rheological parameters μ_s , μ_2 and I_o in eq. (1.29), the authors choose the values given by the experimental data of flows on inclined plane: $\mu_s = \tan \theta_s$ with $\theta_s = 20.9$; $\mu_2 = \tan(\theta_2)$ with $\theta_2 = 32.76$; and $I_o = 0.279$. According to the Authors, "*...this choice means that no fit parameter exists when we shall compare results from the simulations to the experimental data.*" From this statement it can be deduced that these parameters are "universal" constants, or properties of the material, but they do not tell on which kind of property they depend (i.e. elasticity, stiffness, roughness, or other) and on what limit its value can be deduced. Furthermore, from the kinetic theory results that μ_2 is a property of the flow field, and its value cannot be known *a priori*.

Moreover, it seems that this model shows its biggest weaknesses when trying to simulate a granular flow saturated by water, e.g. in the case studied in this thesis. Experimental evidences [12] suggest that, in this situation, both the effect of buoyancy, that of the lubrication produced by water on the mechanisms of prolonged contact and the remarkable intensity of the drag forces inhibit the effects of the side walls, observed in the dry granular flows. In an immersed granular flows, the effect of the side walls is similar to that of fluid flows and the velocity measurements on the free surface show that the gradients of the velocity profile are practically negligible. Furthermore, in contrast with previous work on the $\mu(I)$ -model, da Cruz et al. [22] makes the hypothesis of a linear relationship between the concentration of the material and the inertial parameter I , in order to avoid the lack of the equation of state of the model and the limitation of considering the concentration constant across the flow depth. It is easy to realize that in this case the model reduces to a Coulombian model in which the angle of friction is a function of the concentration, a model previously proposed by several authors, but which has proved to be unreliable. Although this model has some inherent problems, which are also declared by the authors, especially in the early works, it is often present in the literature on enduring contacts. The $\mu(I)$ -model can be

interpreted as a weighted combination of two Coulombian models [3, 4]. In fact, Armanini [3] proves that the total shear stresses of the granular phase can be rewritten as a weighted linear combination of a collisional component and a frictional component, adopting for both components a Coulombian scheme. If I is the dimensionless parameter that governs the frictional regime, one of the two weight functions is I , because on the static bed $I = 0$, and the other is a constant, here set equal to I_o :

$$(I_o + I)\tau_{ij}^g = p^g (\tan \varphi^{fric} I_o + \tan \varphi^{coll} I) \quad (1.31)$$

that is:

$$\tau_{ij}^g = p^g \tan \varphi^{fric} \frac{I_o}{I_o + I} + p^g \tan \varphi^{coll} \frac{I}{I_o + I} \quad (1.32)$$

1.4.5 Granular flow regimes over fixed and mobile bed

The behaviour of a gravity-driven liquid-granular mixture was studied with a series of experiments in a special glass-walled open channel at the Hydraulic Laboratory of the University of Trento, Italy, [5]. The aim of the investigation was to observe the possible regimes occurring in uniform flow conditions and, in particular, distinguishing for the different profiles of velocities, concentration and granular temperature, four different regimes were measured, as it is reported in figure 1.4. In particular:

- *immature flow or over-saturated flow*: the solid material flows in the lower part of the flow, while approaching the free surface a region in which the presence of particles is occasional is observed, (figure 1.4(a));
- *mature flow or saturated flow*: the particles flow across the entire flow depth and the concentration decreases monotonically from the bottom to the free surface, (figure 1.4(b));
- *plug flow or under-saturated flow*: the concentration is such that the

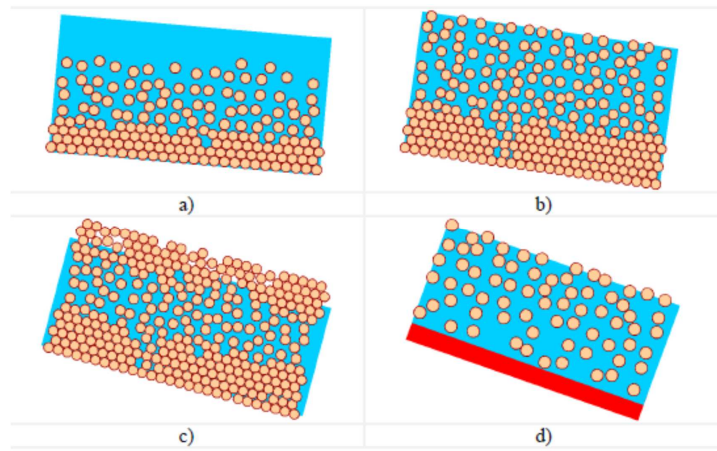


Figure 1.4: Different types of granular flows regimes: a) over-saturated erodible bed flow; b) saturated erodible bed flow; c) under-saturated erodible bed flow (plug-flow); d) rigid bed flow [5]. This figure belongs to [3].

upper part of the flow is unsaturated [32], (figure 1.4(c));

- *rigid bed flow*: in this case the layer of the loose static bed does not appear. The constant of elastic restitution of the collision among particles is inferior to that of the upper layers and as the distance from the wall increases, it becomes a property of the flow field (figure 1.4(d)). In cases (a)-(b)-(c) a static loose material composed of the same particles forms over the rigid bed on the channel.

The considerations proposed in this thesis regard a mature flow.

1.4.6 The coexistence of the collisional and the frictional regimes

The new and fundamental approach of the thesis is based on the observation of the coexistence of the frictional and the collisional regimes of submerged granular flows driven by gravity in a mature regime. From the visual record, in fact, is it observed a region of the flow where the two regimes are alternate in space and time, through a mechanism similar to that of the border

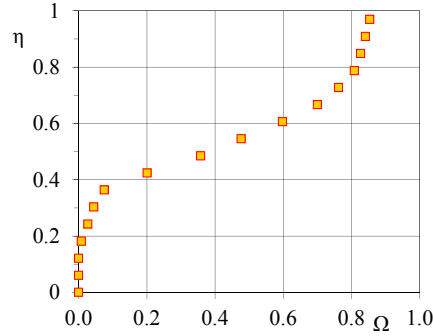


Figure 1.5: Distribution along the flow depth (η is the dimensionless vertical coordinate) of the intermittency function proposed by Armanini et al. [10]

of a turbulent boundary layer. This phenomenon is identified as intermittency. Armanini et al. [10] provide an explanation of the intermittency in granular flows in terms of time evolution of the vertical velocity of particles. Throughout the definition of a filter function f_c , which is equal to 1 when the kinetic component of the velocity exceeds a threshold and is null otherwise, the intermittency function, Ω , is expressed as [10]:

$$\Omega = \frac{\int_T f_c dt}{T} \quad (1.33)$$

where T is a long enough period to consider the process statistically stationary. In figure 1.5 the distribution across the of the intermittency function calculated in uniform flow condition of a mature granular flow is shown [3].

1.4.7 The coefficient of restitution of submerged granular flows

In submerged granular flows, the coefficient of restitution e has been observed to be highly dependent on the Stokes number. Armanini et al. [5, 10] proposed to choose the square of the granular temperature as the representative

velocity, such that the Stokes number reads as:

$$St = \frac{1}{18} \frac{\rho_s d \Theta^{0.5}}{\mu} \quad (1.34)$$

Experimental measurement [10] provided the following empirical relation for the coefficient of restitution e of granular flows.

$$e = 0.9 - 2.8St^{-0.5} \quad (1.35)$$

In the framework of this thesis the coefficient of restitution used is that of relation (1.35).

1.4.8 The two phase approach

Drew [26] was the pioneering work with respect to the two phase approach and provides the common features of dispersed two-phase flows from a continuum mechanical approach based on the idea that each material is a continuum. The role of the liquid phase on a submerged granular flows driven by gravity is detailed by Meruane et al. [57] by highlighting that the dynamic of the solid phase cannot be understood without the inclusion of the hydrodynamic fluid pressure and the drag interactions. With respect to the liquid phase, Meruane et al. [57] proposed the $k - \epsilon$ model, which is used to include the turbulence effects and to describe the stresses of the liquid phase.

1.4.8.1 The interphase force

Meruane et al. [57] provide the derivation of the relation for the interphase forces, the term F_i^β of eq.(1.1), that occurs without mass exchange between the two phases. The interaction force coincides with the surface forces between the constituents. In a control volume is V , a surface S of the interface

is identified, and its border is ∂V . In this respect the interaction force is:

$$F_i^g = \int_{\partial V} T_{ij}^g dS \quad (1.36)$$

and applying the divergence theorem eq.(1.36) becomes:

$$F_i^g = \int_V \frac{\partial T_{ij}^g}{\partial x_j} dV_s \quad (1.37)$$

where V_s is the volume of the solid fraction, that is $V_s = cV$. The tensor of the solid phase is given by the summation of a isotropic component and a deviatoric component and results:

$$F_i^g = -c \frac{\partial p^g}{\partial x_i} + c \frac{\partial \tau_{ij}^g}{\partial x_j} \quad (1.38)$$

Meruane et al. [57] show that the normal component of the interphase force is the fluid pressure, so p^g of relation (1.38) becomes p^f . Furthermore Meruane et al. [57] give a proper relation for the stresses components of eq.(1.38), which neglecting the virtual mass effects and the Basset effect, depends only on the drag effects relevant to the relative velocities between the two phases. Eq.(1.38) reduces to:

$$F_i^g = -c \frac{\partial p^f}{\partial x_i} + D_i \quad (1.39)$$

The definition of the drag D_i consists in the definition of the drag coefficient. In this respect, in the framework of the drag force of a granular flow, the literature is based on the work of di Felice [25]. This is a collection of experimental studies dealing with fluidized beds, attempting to describe a relation for the drag force of a granular flow. In particular, a *voidage function* is introduced to modify the known expression of the drag of a single particle and to account for the concentration. From the best fitting of these investigations

the *voidage function* is a power of the concentration of the liquid phase. All the data are collected for a concentration lower than 0.3. With respect to the discussion of Meruane et al. [57], it is proven [2] that the Archimedes' principle, applied to steep channel, is valid on the normal direction of the flow and not only in the vertical direction such that in the following the definition of the interaction forces provided by Meruane et al. [57], eq.(1.39), is modified as:

$$F_i^g = -c \left(\frac{\partial p^f}{\partial x_i} - \frac{\partial \tau_{ij}^f}{\partial x_j} \right) + D_i \quad (1.40)$$

Chapter 2

The rheology of the granular phase

In Chapter 2 a heuristic model for the rheology of the granular phase is presented. This is the main original contribution of the thesis and the results are published in Armanini et al. [11]. The set of equations of hyperconcentrated granular flow, in stationary and uniform conditions, under the hypothesis that the stresses of the liquid phase are negligible in the momentum balances, is numerically solved and the results are compared with experimental data. The numerical method was presented in Armanini et al. [6]. The chapter also contains considerations on the total energy balance of the granular phase and on the kinetic energy balance. The concept of core region and the effect of the sidewall are discussed.

2.1 Granular phase

A review of the literature dealing with the behaviour of the granular phase provides a theory, called *the kinetic theory of dense gases*, but its validity is restricted only to the collisional regime. In contrast, the problem of the rheology of the frictional regime is still open. The frictional regime becomes

important when the concentration increases. In this situation, in fact, the collisions among particles are not instantaneous, but become long lasting and involve various particles at the same time. Experimental evidences show that the frictional regime is always present in a granular gravity flow flowing over a loose bed composed of the same material [10]. In fact, the loose *static bed* forms because the solid concentration increases, proceeding downward up to a value (*random packing concentration*) for which the frictional shear stress is so high that the flow is inhibited.

In one of the earliest works on granular flows, Johnson and Jackson [49] observe that, while at least one conceptual scheme can be derived for the collisional regime on the basis of a micro-structural constitutive model, the rheological formulations of the frictional regime are essentially empirical. The situation has not changed much in the last 30 years: different schemes of empirical nature exist, but not a theory. Most of these schemes assume that the frictional regime is confined in a layer contiguous to the static bed, within which the shear stress is Coulombian, while the pressure is expressed as a function of concentration through a quite empirical relationship [49, 64, 50, 57].

2.1.1 A heuristic rheological model for the frictional regime

The experimental analysis of the flow [10] and the intuition suggest that the rheology of the frictional regime is shear dependent, like in liquids, but at the same time some pressure-dependent feature are presented, which can be expressed by a Coulombian model used for the rheology of solids, through a frictional angle, which is not a constant but depends on the kinematic properties of the flow. A dimension analysis of the forces involved predicts

that the frictional regime depends on the *Savage number* [63]:

$$I_s = \frac{\rho_s (\dot{\gamma} d)^2}{p^g} \quad (2.1)$$

where $\dot{\gamma} d^2$ dimensionally represents the kinematic viscosity of the granular flow, ρ_s is the density of the material and p^g the granular pressure. It is allowable that the rheology of the frictional regime depends also on other possible contact properties of the interstitial fluid and of the material composing the particles.

Furthermore, the relationship of the frictional shear stress must satisfy two asymptotic conditions. It must tend to a pure Coulombian regime on the boundary of the loose bed, and it must vanish when the parameter I_s tends to become large enough. A suitable relationship, satisfying the above conditions, is provided by Armanini et al. [11]:

$$\tau^{fric} = p^g \tan \varphi^{fric} \frac{I_{so}}{I_s + I_{so}} \quad (2.2)$$

where φ^{fric} is the friction angle of the material and I_{so} is a parameter that presumably depends on the contact properties of the interstitial fluid and of the solid material composing the particles; its value must be determined experimentally.

A hyperbolic relationship between the tangential stress and the inertia number is discussed also by Chialvo et al. [20].

A suitable equation of state for the granular frictional regime must be now identified. Eq. (2.2) suggests that $p^g I_{so}/(I_{so} + I_s)$ can be interpreted as the frictional component of the pressure (due to the prolonged contacts between particles). In other words, the equation for the pressure can be written in the following form:

$$p^{fric} = p^g \frac{I_{so}}{I_{so} + I_s} \quad (2.3)$$

where $p^{fric} = p^g - p^{coll}$ is the frictional component of the granular pressure. Equation (2.3) can be considered as the *equation of state* of the frictional regime, even if not *stricto sensu*, because of the presence of the shear rate embedded in I_s .

The rheological model proposed [11] is:

$$\tau_{ij}^g = p^g \tan \varphi^{fric} \frac{I_{so}}{I_{so} + I_s} \frac{D_{ij}}{\sqrt{D_{ij} D_{ji}}} + 2\rho_s f_2 d \Theta^{0.5} D_{ij} \quad (2.4)$$

$$p^g = p^g \frac{I_{so}}{I_{so} + I_s} + \rho_s f_1 \Theta \quad (2.5)$$

where $D_{ij} = 1/2 (\partial u_i / \partial x_j + \partial u_j / \partial x_i)$ is the shear rate tensor. Eq. (2.4) represents the deviatoric component of the stress tensor, which has been obtained by applying the Drucker-Prager failure criterion [24], calibrated on the results of the experimental tests in terms of the Mohr-Coulomb friction angle. Notice, however, that a more refined generalization to the 3D case would require a more complex failure criterion, taking into account the third invariant of the stress tensor. Although conceptually simple, this refinement is beyond the aims of this work.

Furthermore, it is possible to obtain the granular pressure p^g in explicit form from eq. (2.5), within the flow field:

$$p^g = \rho_s f_1 \Theta \frac{(\dot{\gamma}d)^2}{(\dot{\gamma}d)^2 - I_{so} f_1 \Theta} \quad (2.6)$$

A striking feature of eq. (2.6) is that it is valid except for the boundary where $\dot{\gamma} = \Theta = 0$, that is $I_s = 0$, i.e. on the static bed, which represents the boundary between the upper granular fluid and the lower static granular bed, which behaves as a granular solid. The lower side of this interface has to be considered as a solid, for which no relationship between the pressure and the kinematic properties of the flow field (shear rate or granular temperature) exists. On this side of the boundary interface, equation (2.3) then reduces to an identity.

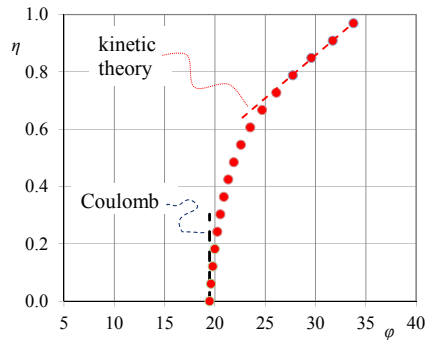


Figure 2.1: Distribution along the flow depth of measured values of the apparent friction angle, i.e. the inverse tangent of the ratio between shear stress and pressure in a uniform flow of spheres and water.

The granular temperature also influences the frictional regime, as will be explained in section 2.7, discussing the energy balance. On the other hand, when $c \rightarrow 0$ ($f_1 \rightarrow 0$), i.e. in the vicinity of the free surface, eq. (2.6) tends to the relation provided by the kinetic theory.

The same occurs for the rheological relationship (2.4). On the static bed boundary $\dot{\gamma} = \Theta = 0$, so $\tau_{ij}^g = p^g \tan \varphi^{fric}$. In contrast, approaching the free surface where $I_{so} p^g \ll (\dot{\gamma} d)^2 \rho_s$ the expression of the shear stress tends to that given by the kinetic theory.

These two conditions are confirmed also by the experimental data of figure 2.1, which refers to a gravity driven granular submerged uniform flow. In particular, in figure 2.1, the distribution across the flow depth of the measured values of the *apparent friction angle*, i.e. the inverse tangent of the ratio between shear stress and pressure, is reported. The experiments and the related results of our investigations will be explained in detail in sections 2.4 and 2.5, but for the sake of clarity it is worthwhile to highlight some results here. The figure 2.1 shows that, as the static bed is approached, the apparent friction angle tends to become constant and equal to the static angle, according to the purely Coulombian model. On the other hand, when approaching the free surface, the behaviour recovers that derived from kinetic

theory.

2.2 Steady state flow

The model was applied to a steady uniform two-phase flow in a prismatic wide channel. This relatively simple case is important not only *per se* because it can be verified experimentally with good accuracy, but also because the solution of the uniform flow, integrated on the depth (or on the cross-section), provides the closure relationships for the depth integrated numerical models (1DH and 2DH), employed in field applications to debris flows [9, 42]. In this situation, the distribution of the fluid pressure (the pore pressure) is hydrostatic [32]. Generally, the interaction force between the two-phase, F_i^β , reads [41]:

$$F_i^f = -F_i^g = c \frac{\partial p^f}{\partial x_i} - c \frac{\partial \tau_{ij}^f}{\partial x_j} - D_i^f \quad (2.7)$$

Please refer to section 3.1 for a better explanation of expression 2.7. Under the hypothesis of plane flow in the two directions x_1 , x_2 , the system (1.1) could be simplified and, by substituting the projections of eq. (2.7), the momentum balance equations reduce to the following for the liquid phase:

$$0 = -\rho_w(1-c)g \frac{\partial z}{\partial x_1} + \frac{\partial \tau_{21}^f}{\partial x_2} - c \frac{\partial \tau_{21}^f}{\partial x_2} - D_1^f \quad (2.8)$$

$$0 = -\rho_w(1-c)g \frac{\partial z}{\partial x_2} - \frac{\partial p^f}{\partial x_2} + c \frac{\partial p^f}{\partial x_2} - D_2^f \quad (2.9)$$

and for the granular phase:

$$0 = -\rho_s c g \frac{\partial z}{\partial x_1} + \frac{\partial \tau_{21}^g}{\partial x_2} + c \frac{\partial \tau_{21}^f}{\partial x_2} + D_1^f \quad (2.10)$$

$$0 = -\rho_s c g \frac{\partial z}{\partial x_2} - \frac{\partial p^g}{\partial x_2} - c \frac{\partial p^f}{\partial x_2} + D_2^f \quad (2.11)$$

By adding the momentum equations in the longitudinal direction x_1 for the two-phase (eq. 2.8 and eq. 2.10), it is obtained:

$$\frac{\partial \tau_{21}^g}{\partial x_2} + \frac{\partial \tau_{21}^f}{\partial x_2} = (\rho_s c + \rho_w (1 - c)) g \frac{\partial z}{\partial x_1} \quad (2.12)$$

In addition, accounting for $D_2^f = 0$, by eliminating the term $\partial p^f / \partial x_2$ between the two equations of momentum in the normal direction x_2 for the two-phase (eq. 2.9 and eq. 2.11), it is obtained:

$$-\frac{\partial p^g}{\partial x_2} = (\rho_s - \rho_w) c g \frac{\partial z}{\partial x_2} \quad (2.13)$$

If the particle concentration is large enough, the fluid shear stress τ_{21}^f is negligible compared to the granular stress, as will be better explained in section 2.4.1. Finally, it is obtained:

$$\frac{\partial \tau_{21}^g}{\partial x_2} = \left(1 + c \frac{\rho_s - \rho_w}{\rho_w} \right) \rho_w g \frac{\partial z}{\partial x_1} \quad (2.14)$$

$$-\frac{\partial p^g}{\partial x_2} = c \left(\frac{\rho_s - \rho_w}{\rho_w} \right) \rho_w g \frac{\partial z}{\partial x_2} \quad (2.15)$$

In a uniform flow condition the rheological relationships (eq. 2.4 and eq. 2.5) and the kinetic energy balance (eq. 1.26) become:

$$\tau_{21}^g = p^g \tan \varphi^{fric} \frac{I_{so} p^g}{I_{so} p^g + \left(\frac{\partial u_1^g}{\partial x_2} d \right)^2 \rho_s} + \rho_s f_2 d \Theta^{0.5} \frac{\partial u_1^g}{\partial x_2} \quad (2.16)$$

$$p^g = \rho_s f_1 \Theta \frac{\left(\frac{\partial u_1^g}{\partial x_2} d \right)^2}{\left(\frac{\partial u_1^g}{\partial x_2} d \right)^2 - I_{so} f_1 \Theta} \quad (2.17)$$

$$0 = \frac{\partial}{\partial x_2} \left(k_\Theta \frac{\partial \Theta}{\partial x_2} \right) + \mu^{coll} \left(\frac{\partial u_1^g}{\partial x_2} \right)^2 - f_5 \rho_s \frac{\Theta^{1.5}}{d} \quad (2.18)$$

The equations (2.14-2.18) form a nonlinear system of five differential algebraic equations (DAE) that must be solved with a suitable numerical method. The five unknowns of the problem are: u_1^g , c , Θ , τ_{21}^g and p^g . The boundary conditions are assigned at the bed, where $u_1^g = \partial u_1^g / \partial x_2 = \Theta = 0$, $c = c_*$ and, according to eq. (2.16), $\tau_{21}^g = p^g \tan \varphi^{fric}$.

2.3 Numerical method

This section is part of [6].

The governing equations of the proposed model can be written under the general form of a nonlinear system of differential algebraic equations (DAE) as follows:

$$\frac{d}{dt} \mathbf{E}(\mathbf{Q}(t)) = \mathbf{f}(\mathbf{Q}(t), t), \quad \mathbf{Q}(0) = \mathbf{Q}_0, \quad (2.19)$$

where $\mathbf{Q} = \mathbf{Q}(t) = (q_1(t), q_2(t), \dots, q_n(t)) \in \mathbb{R}^n$ is the unknown state vector, and $\mathbf{E}(\mathbf{Q}) \in \mathbb{R}^n$ and $\mathbf{f}(\mathbf{Q}, t) \in \mathbb{R}^n$ are two nonlinear functions of the state vector \mathbf{Q} and the independent variable t . \mathbf{Q}_0 is the known initial condition of the initial value problem eq.(2.19). For its numerical solution we use a Galerkin method, based on the following expression for the unknown solution vector:

$$\mathbf{Q}_h(t) = \sum_{l=0}^N \theta_l(t) \hat{\mathbf{Q}}_l := \theta_l \hat{\mathbf{Q}}_l, \quad (2.20)$$

where $\theta_l(t)$ represent piecewise polynomial basis functions of maximum degree N and $\hat{\mathbf{Q}}_l$ are the unknown coefficients of the numerical solution. In the above relation we have used classical tensor notation with the Einstein summation convention over two equal indices. Equation (2.20) is valid for

one timestep $\Delta t = t^{n+1} - t^n$, where t^n is the current solution time. To obtain the unknown coefficients $\hat{\mathbf{Q}}_l$, the DAE is multiplied with test functions $\theta_k(t)$ that are identical with the basis functions (classical Galerkin approach), and is subsequently integrated over a time step to obtain the following weak formulation of the DAE:

$$\int_{t^n}^{t^{n+1}} \theta_k(t) \left(\frac{d}{dt} \mathbf{E}(\mathbf{Q}_h(t)) - \mathbf{f}(\mathbf{Q}_h(t), t) \right) dt. \quad (2.21)$$

For the test and basis functions $\theta_k(t)$ it is chosen the Lagrange interpolation polynomials that pass through the $N + 1$ equidistant Newton-Cotes quadrature points, $t_l^n = t^n + (l - 1)/(N - 1)\Delta t$, hence it is used a *nodal basis*. Therefore, the numerical approximations of the nonlinear functions \mathbf{E} and \mathbf{f} are simply given by

$$\mathbf{E}_h(t) = \theta_l \hat{\mathbf{E}}_l, \quad \text{and} \quad \mathbf{f}_h(t) = \theta_l \hat{\mathbf{f}}_l, \quad (2.22)$$

with

$$\hat{\mathbf{E}}_l = \mathbf{E}(\hat{\mathbf{Q}}_l), \quad \text{and} \quad \hat{\mathbf{f}}_l = \mathbf{f}(\hat{\mathbf{Q}}_l, t_l^n) \quad (2.23)$$

due to the choice of the nodal basis. The weak formulation eq.(2.21) for the unknowns $\hat{\mathbf{Q}}_l$ therefore becomes

$$\left(\int_{t^n}^{t^{n+1}} \theta_k(t) \frac{d}{dt} \theta_l(t) dt \right) \hat{\mathbf{E}}_l = \left(\int_{t^n}^{t^{n+1}} \theta_k(t) \theta_l(t) dt \right) \hat{\mathbf{f}}_l, \quad (2.24)$$

or, in a more compact matrix-vector notation:

$$\mathbf{K}_{kl} \mathbf{E}(\hat{\mathbf{Q}}_l) - \mathbf{M}_{kl} \mathbf{f}(\hat{\mathbf{Q}}_l, t_l^n) = 0, \quad (2.25)$$

with $\hat{\mathbf{Q}}_0 = \mathbf{Q}(t^n)$, and the mass matrix \mathbf{M}_{kl} and the stiffness matrix \mathbf{K}_{kl} , which can both be precomputed once and for all. The resulting nonlinear algebraic equation system (2.25) of dimension $n(N + 1)$ is solved by a standard Newton method for systems with a line-search-type globalization strategy. The initial guess is provided using a second order Crank-Nicholson-type scheme for the DAE eq.(2.19) to initialize the nodal values $\hat{\mathbf{Q}}_l$ at all time levels t_l^n :

$$\frac{\mathbf{E}(\hat{\mathbf{Q}}_{l+1}) - \mathbf{E}(\hat{\mathbf{Q}}_l)}{t_{l+1}^n - t_l^n} = \frac{1}{2} \left(\mathbf{f}(\hat{\mathbf{Q}}_{l+1}, t_{l+1}^n) + \mathbf{f}(\hat{\mathbf{Q}}_l, t_l^n) \right). \quad (2.26)$$

Equation (2.26) is again a nonlinear algebraic equation system, however, of smaller dimension n , which is again solved by a globally convergent Newton method. The proposed Galerkin-type method, eq.(2.25), is theoretically of arbitrary order of accuracy in the independent variable t and can be used inside a classical *shooting method* for solving DAE boundary value problems of the type

$$\frac{d}{dt}\mathbf{E}(\mathbf{Q}(t)) = \mathbf{f}(\mathbf{Q}(t), t), \quad \mathcal{Q}(t_0) = \mathcal{Q}_0, \mathcal{Q}(t_1) = \mathcal{Q}_1, \quad (2.27)$$

where \mathcal{Q}_0 and \mathcal{Q}_1 are the known boundary values of the boundary value problem (BVP), eq.(2.27). The calculation is repeated by an iterative method, changing I_{so} to minimize the root mean square error of the granular velocity across the flow depth.

2.4 Experimental investigation

In the framework of the thesis the experimental data of Armanini et al. [5] are used. In particular, the data derived from an investigation on the behaviour of a gravity-driven liquid-granular mixture, done with a series of experiments in a special glass-walled open channel at the Hydraulic Laboratory of the

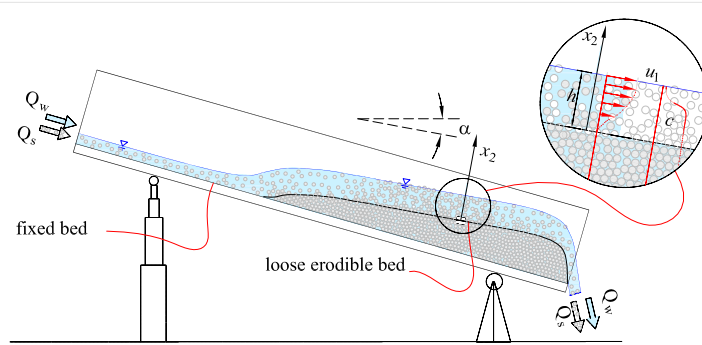


Figure 2.2: Representation of the glass-walled open channel used for the experimental analysis. This figure belongs to [8].

University of Trento, Italy.

For all the details regarding the flume (figure 2.2) and the experimental techniques please refer to Armanini et al. [5].

If liquid and solid discharges are kept constant in time (*stationary regime*) it is easy to prove that the only possible solution for the mobile bed is the uniform flow [7]. In this case the slopes of the free surface and of the mobile bed are the same. These conditions are also confirmed by the experiments. This situation is identified as an *equilibrium condition* between the granular flow and the static bed.

The granular phase is reproduced by perfectly identical spherical plastic particles, composed of barium sulfate and titanium dioxide dispersed on polystyrene. The particles have a diameter $d = 6$ mm and a specific gravity $\rho_s/\rho_w = 2.21$. The static friction angle was estimated to be 20° from geotechnical tests based on the tilting board [5]. The liquid and solid discharges ($Q_s = 0.38$ l/s and $Q_l = 1.45$ l/s) were measured at the same time using a volumetric technique, while the flow depth ($h = 0.062$ m) and the slope (of the free surface and of the static loose bed: $\alpha = 8^\circ$) of the flow were deduced from level measurement through the transparent sidewalls of the flume. Since the velocity profile is asymptotic to the mobile bed, it is

assumed that the interface of the static bed is located at the level where the velocity is less than 1% of the maximum velocity.

2.4.1 The internal stresses of the liquid phase

In uniform flow conditions, in the integration of momentum equations, the internal shear stresses of the liquid phase, either turbulent or laminar, are considered negligible compared to the internal stresses of the granular phase. Preliminary experiments of the variables of the liquid phase allows to check if this assumption is realistic. Notice that this analysis was carried out only in the upper part of the flow depth, where the velocity measurements of the liquid phase are more accurate.

The internal stress of the liquid phase are estimated as the difference between the longitudinal component of the gravity force of the liquid phase and the drag force (eq. 2.8). This force (per unit volume), D_1^f , is assumed according to Meruane et al. [57], as:

$$D_1^f = \frac{3}{4} C_D \frac{\rho_w}{d} f(c) c |u_1^f - u_1^g| (u_1^f - u_1^g) \quad (2.28)$$

where $C_D = (0.63 + 4.8/\sqrt{Re_d})^2$ is the drag coefficient [23]; $Re_d = \rho_w(1 - c)(u_1^f - u_1^g)d/\mu_w$ is the particle Reynolds number and $f(c) = (1 - c)^{1-m}$ ($m = 3.6 \div 3.7$ depending on the regime of the flow) is a function, proposed by di Felice [25], taking into account the effect of the particle concentration on the drag forces. According to this author the empirical expression for the voidage function is valid for all concentration values. On the other hand, further investigations provided a different relation for the voidage function in a submerged granular flows, but the considerations of section 3.2 does not invalidate the results obtained in Armanini et al. [11]. Figure 2.3(b) shows that the internal stresses are very small compared to the stresses of the granular phase and, hence, they can be neglected in eqs. (2.8) and (2.12). This assumption implies that the drag force is substantially balanced by the

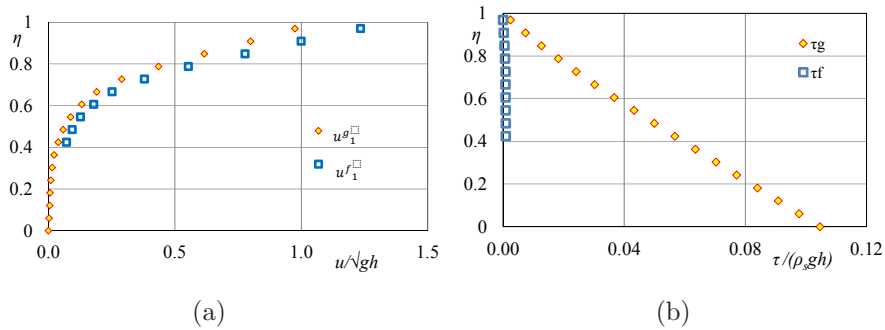


Figure 2.3: Distribution along the flow depth of the experimental: (a) velocity; (b) internal shear stresses of the granular and the liquid phases calculated from the momentum balance in the longitudinal direction assuming that the drag is totally balanced by the weight of the fluid phase.

weight of the liquid phase. This evidence is account for the discussion on the granular energy balance.

2.5 Results

The comparison between the experimental data and the prediction of the model is reported in the next figures. Data are expressed in non-dimensional form, assuming as reference scales the total flow depth h , the material density of the particles ρ_s and the gravity acceleration g . In particular, as already defined, $\eta = x_2/h$ represents the dimensionless distance from the static bed. In figures 2.4(a) and 2.4(b) the distributions of the concentration of the granular phase and of the granular temperature are reported. The calculated concentration profile shows minor discrepancy from the experimental data, while its value at the bed is well in agreement with the measurement of the random packing concentration obtained with a volumetric method. The distribution of the granular temperature, in figure 2.4(b), shows most mismatches in the proximity of the free surface, where the model prediction gives a value appreciably larger than the experimental data. It appears that the particle

concentration remains at values close to the maximum in a region near to the static bed which covers nearly 50% of the flow depth. In this region the granular temperature attains very low values. This zone is dominated by frictional stresses. In the upper half of the depth, ruled by collisional stresses, the concentration begins to decrease sharply while the granular temperature increases significantly. In figures 2.5(a) and 2.5(b) the normal distributions of the granular velocity and of its gradient are reported. The model reproduces both parameters quite well, even though the gradient shows minor disagreement, possibly related to the imprecision associated with the computation of the spatial derivatives from experimental data. In figures 2.6(b) and 2.6(a) the normal distributions of the granular shear stress and of the granular pressure are depicted. Despite some discrepancies between the computed results and the experimental data profiles shown in figure 2.4(a) and 2.4(b), the agreement between predicted and experimental data concerning granular shear stress and pressure is very good. It is likely that these deviations are reflected minimally in the pressure and shear stress distributions since they are close to zero near the free surface. In figure 2.7(a) and 2.7(b) the distributions of the collisional and the frictional components of the shear stresses and of the granular pressure are presented. These profiles exhibit

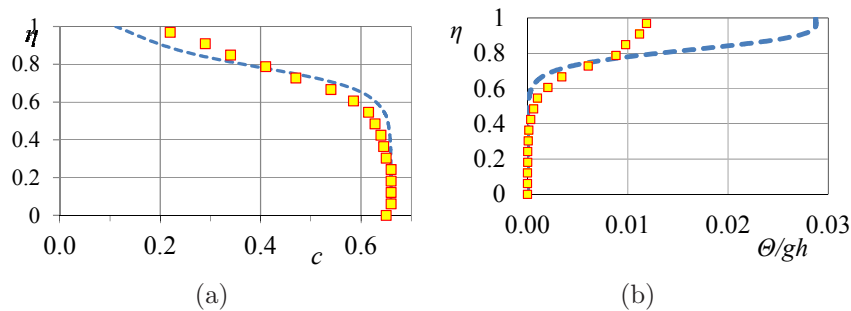


Figure 2.4: Comparison between results of the numerical simulation (line) and experimental data (symbols) of: (a) particle concentration profile; (b) granular temperature profile.

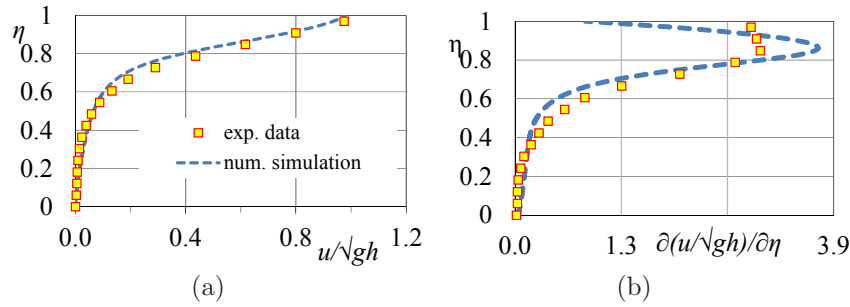


Figure 2.5: Comparison between results of the numerical simulation (line) and experimental data (symbols) of: (a) granular velocity profile; (b) granular velocity gradient profile.

a reasonably good agreement with the experimental data, and confirm the coexistence of the collisional and the frictional regimes across the flow depth, with the collisional component dominating the region close to the free surface, and the frictional component developed mostly in the region close to the static bed. As already observed for the concentration, around the middle of the flow depth, the dominance of one regime over the other is inverted, but in the region near the static loose bed the collisional component of both the tangential and the normal stresses is not negligible.

The only parameter of the model that needs to be calibrated is I_{so} . Its

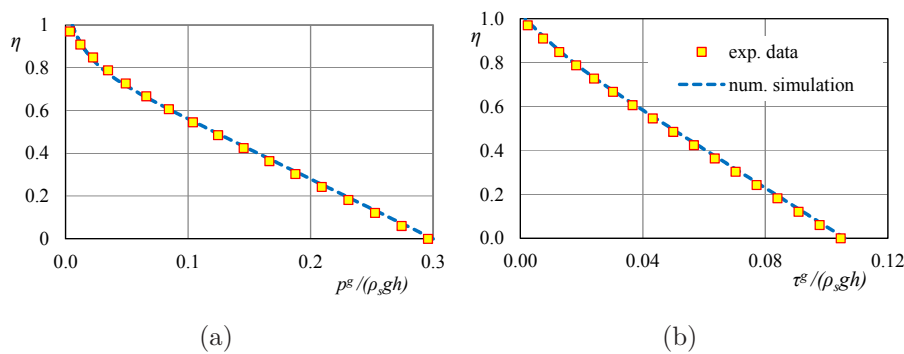


Figure 2.6: Comparison between computed (lines) and observed (symbols) of: (a) granular pressure profile; (b) granular shear stresses profile.

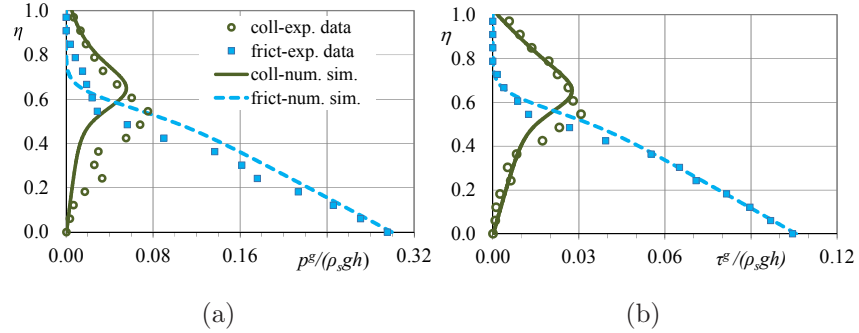


Figure 2.7: Collisional and frictional component of (a) pressure and of (b) shear stress. Comparison between computed (lines) and observed (symbols) values.

value affects the apportionment between the collisional and the frictional stresses, while the total stresses are influenced only minimally. From eq. 2.3 it is easy to deduce that I_{s0} is the value of I_s at the distance from the static bed where there is a perfect balance between frictional and collisional pressure ($p^{coll} = p^{fric}$). The value $I_{s0} = 0.04$ was obtained by best fitting the experimental velocity profile of the granular phase.

2.6 The kinetic energy balance

The mechanisms that regulate the energy balance have been analyzed. In figure 2.8 it is plotted the distribution of the different terms comprising the granular kinetic energy balance, eq.(2.18), measured in the experiments and calculated with the mathematical model. Notice that in the kinetic energy balance a term, which accounts for the fluctuating component of the interaction forces between the phases (drag force), and which contributes to the dissipative mechanism [40], is included as it is presented in section 3.5.

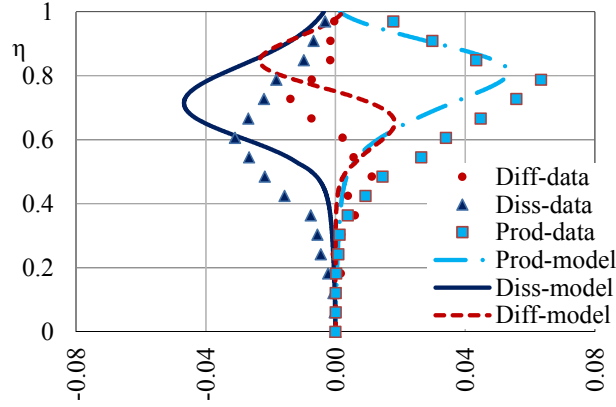


Figure 2.8: Distribution along the depth of the (dimensionless) terms of the kinetic energy balance of the collisional component eq.(2.18). Experimental data (symbols) and predictions of the model (lines)

2.7 The total energy balance of the granular phase

A further novelty of the *heuristic model*, with respect to previous models on the granular flows, is the analysis of the total energy balance of the granular phase. In fact, by multiplying each term of the granular momentum equations by the respective component of the granular velocity the energy balance of the granular phase reads:

$$\rho^g \left(\frac{\partial}{\partial t} + u_j^g \frac{\partial}{\partial x_j} \right) \frac{u_i^g u_i^g}{2} = \rho^g u_i^g g_i^g + \frac{\partial}{\partial x_j} u_i^g T_{ij}^g - T_{ij}^g \frac{\partial u_i^g}{\partial x_j} - F_i^g u_i^g \quad (2.29)$$

By restricting the scope of the analysis to the case of uniform flow, in which the average velocity has only the longitudinal component, the total energy balance becomes:

$$-u_1^g (c\rho_s + (1-c)\rho_w) g \frac{\partial z}{\partial x_1} + \frac{\partial}{\partial x_2} (u_1^g \tau_{21}^g) - \tau_{21}^{fric} \frac{\partial u_1^g}{\partial x_2} - \tau_{21}^{coll} \frac{\partial u_1^g}{\partial x_2} = 0 \quad (2.30)$$

In eq.(2.30) it is assumed that, as previously stated, the term $F_i^f = -F_i^g$ is balanced with a good approximation by the buoyancy forces and by the longitudinal component of the weight of the liquid phase. The terms of eq.(2.30) can be interpreted in analogy with the energy balance in a turbulent channel flow. The first term of the equation represents the work done by the gravity forces (in this case also including the interphase forces), the second term is the diffusion of the energy due to the total granular shear stress, the third term is the dissipation of kinetic energy due to the frictional stresses, while the last term is the work due to the collisional stresses. This term, with its sign changed, corresponds to the production of collisional kinetic energy in the collisional kinetic energy balance (second term of eq. 2.18). Figure 2.9 shows the distribution across the flow depth of the different dimensionless terms of the total energy balance.

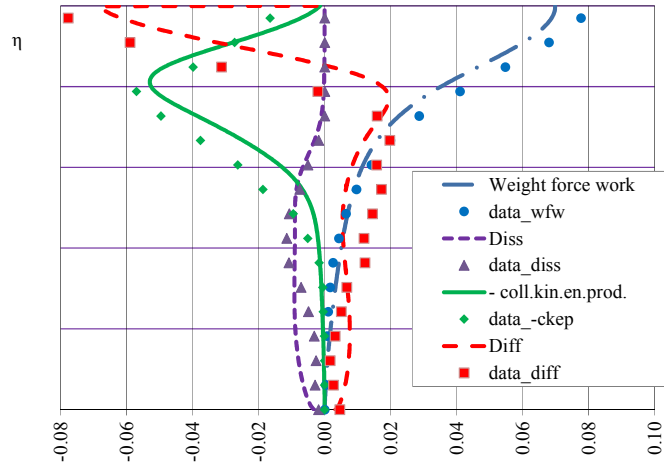


Figure 2.9: Distribution along the depth of the dimensionless terms of the total energy balance eq.(2.29). Each terms of eq.(2.29) is divided by $\rho_s g^{1.5} h^{0.5}$. Comparison between experimental data (symbols) and results of the model (lines).

2.8 The core region

Louge [53] introduces the concept of core region to indicate the region of the flow where the ratio between the stresses of the frictional regime over the total stresses of the granular phase, named η_{Lou} , depends on the concentration.

$$\eta_{Lou} = \frac{\tau^{fric}}{\tau^{tot}} = \frac{\tau^{fric}}{\tau^{fric} + \tau^{coll}} = \frac{1}{1 + \frac{\tau^{coll}}{\tau^{fric}}} \quad (2.31)$$

Louge [53] obtains a linear relationship between the volume concentration and the ratio between the frictional and the total shear stresses is found by interpolating the results of the particle simulation with a straight line, whose coefficients have to be calibrated *a posteriori*. On the other hand the results of the *heuristic model* [11] suggest that this ratio does not depend on the concentration in a constant manner. In fact, remembering the definition of

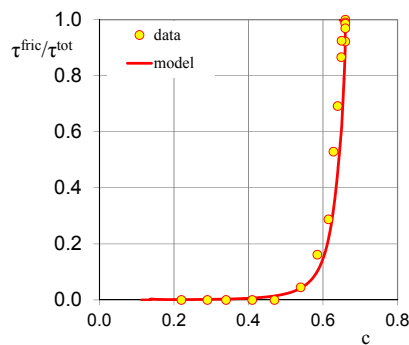


Figure 2.10: Comparison between computed (solid line) and observed (circles) values of the ratio of frictional to total stresses plotted versus volume concentration.

the stresses of the granular phase:

$$\tau^{coll} = f_2 \rho_s \sqrt{\Theta} d \dot{\gamma} \quad (2.32)$$

$$\tau^{fric} = p \tan \varphi \frac{I_{so}}{I_{so} + I_s} \quad (2.33)$$

and the equation of state for the pressure of the granular phase:

$$\begin{aligned} p (I_o^2 + I^2) &= p I_{so} + f_1 \rho_s \Theta (I_{so} + I_s) \\ p &= f_1 \rho_s \Theta \frac{(I_{so} + I_s)}{I_s} \end{aligned} \quad (2.34)$$

is it possible to rewrite the frictional stresses and to derive an expression of the parameter η_{Lou} :

$$\begin{aligned} \tau^{fric} &= f_1 \rho_s \Theta \frac{(I_{so} + I_s)}{I_s} \tan \varphi \frac{I_{so}}{I_{so} + I_s} \\ &= f_1 \rho_s \Theta \tan \varphi \frac{I_{so}}{I_s} \end{aligned} \quad (2.35)$$

$$\begin{aligned} \eta_{Lou} &= \frac{1}{1 + \frac{f_2 \sqrt{\Theta} d \dot{\gamma} I_s}{f_1 \Theta \tan \varphi I_{so}}} \\ &= \frac{1}{1 + \frac{f_2}{f_1} \frac{\dot{\gamma} d}{\sqrt{\Theta} \tan \varphi} \frac{I_s}{I_{so}}}, \end{aligned} \quad (2.36)$$

where I_s is eq.(2.1). By substituting the expression of the pressure of the granular phase 2.36 reduces to:

$$\eta_{Lou} = \frac{1}{1 + \frac{f_2}{f_1} \frac{\dot{\gamma} d}{\sqrt{\Theta} \tan \varphi} \left(\frac{\dot{\gamma}^2 d^2}{f_1 \Theta I_{so}} - 1 \right)} \quad (2.37)$$

Figure 2.10 represented the ratio τ^{fric}/τ^{tot} of the frictional to the total shear stress, as a function of the volume concentration. The agreement between the experiments and the model is fairly good. In particular, the model confirms

that the above ratio tends to vary linearly with the concentration when the concentration tends to its maximum [53].

2.9 The kinetic energy balance in the core region

Recently, Jenkins [44] proposed a model for the rheology of the granular phase that is based on an extension of the kinetic theory of gases to the dense regime. This model is based on the assumption that the concentration of the solid phase is constant in the core region of the flow and that the diffusion term is negligible in the kinetic energy balance. It means that in the core region the production of kinetic energy is totally balanced by the dissipation term. Figure 2.8 shows that the *heuristic model* is able to reproduce the terms of the kinetic energy balance with a reasonable degree of accuracy. In particular, both numerical and experimental data suggest that the diffusive term is *not* negligible and, hence, production does not balance dissipation, as is usually assumed [44]. An attempt to see if such a simplification is acceptable at least in the region dominated by the frictional regime is presented. A limit analysis is carried out for the behaviour of the collisional energy balance equation in the proximity of the static loose bed. Substituting the proper closure relationships in the kinetic energy equation (2.18), gives:

$$0 = \frac{\partial}{\partial x_2} f_4 d^2 \sqrt{\Theta} \frac{\partial \Theta}{\partial x_2} + f_2 d^2 \sqrt{\Theta} \left(\frac{\partial u_1^g}{\partial x_2} \right)^2 - f_5 \Theta^{1.5} \quad (2.38)$$

When the concentration tends to its maximum value ($c \rightarrow c_*$) then $g_o \rightarrow \infty$ and the asymptotic order of magnitude of the f_i functions ($i = 1, 5$) defined

by Lun et al. [55] is $\mathcal{O}(g_o)$. At this limit the equation of state (2.5) becomes:

$$\left(\frac{\partial u_1^g}{\partial x_2} d\right)^2 = I_{so} f_1 \Theta \quad (2.39)$$

Substituting (2.39) into the expression (2.38), yields:

$$0 = \frac{\partial}{\partial x_2} d^2 f_4 \sqrt{\Theta} \frac{\partial \Theta}{\partial x_2} + f_2 \sqrt{\Theta} f_1 \Theta I_{so} - f_5 \Theta^{1.5} \quad (2.40)$$

In conclusion when $(c \rightarrow c_*)$, $f_2 f_1 I_{so} \rightarrow \mathcal{O}(g_o^2)$ while $f_5 \rightarrow \mathcal{O}(g_o)$, so the dissipation term is negligible. Therefore, in the proximity of the mobile bed, where the frictional regime is dominant ($c \rightarrow c_*$), the production of kinetic collisional energy turns out to be balanced by the diffusion. Obviously this assumption cannot be extended in the region where the collisional regime is dominant.

A possible picture of the total kinetic energy balance (eq. 2.30) is the following: in the proximity of the static bed, the kinetic energy of the granular phase is produced by the work of the gravity forces. The flow in this region is characterized by a series of arrays of sliding particles moving along superimposed layers. Such a picture also corresponds to the idea of Jenkins [44], in which the length scale corresponds to a cluster of particles instead of a single particle size.

This relatively slow longitudinal movement forces the particles to move in horizontal strings [10], but their bouncing between inter-particle hollows induces their oscillation in the normal direction. This movement is unstable and some particles are affected by more intense fluctuations and start to collide: this collisional kinetic energy is diffused in the normal direction by the shear stress. The model predicts that the flux of the diffused fluctuating energy considerably exceeds the flux of fluctuating energy that is locally dissipated: the term of diffusion is, in fact, an order of magnitude larger than the dissipation and is balanced by the production. Furthermore, a possible explanation of the exchange among the different terms of the total

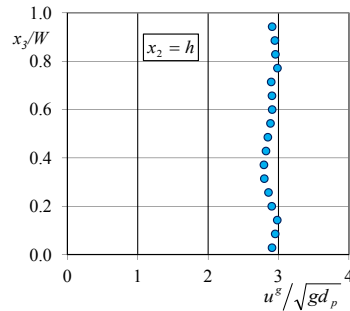


Figure 2.11: Distribution along the transversal direction x_3 of the non-dimensional longitudinal velocity of the granular phase u^g/\sqrt{gd} observed at the free surface in the experiment described in section 3. W denotes the width of the channel.

and of the collisional component of the kinetic energy of the granular flow and in order to clarify the mechanism of energy exchange in the region near the static loose bed, which seems to be dominated by the balance between production and diffusion, while the dissipation is an order of magnitude less than the other two terms, suggests the idea that the motion of the grains, even at concentrations close to that of packing, is always accompanied by a certain degree of granular temperature (which is present also in the rheology of the frictional component) according to Lois et al. [52]. This is reasonable, since partially elastic particles, in order to move at a concentration close to that of packing, are forced to bounce over the particles of the underlying layer and this mechanism generates granular temperature, which is diffused towards the upper layers.

2.10 The influence of the sidewall

Jop et al. [51], Taberlet et al. [65] performed a variety of experiments on the influences of the wall on the equations of granular flows. However, the transversal shear stresses have not been included in the momentum balance (eq. 2.14). In fact, in contrast to what occurs in dry granular flows, in a

submerged granular flow the presence of a liquid interstitial fluid inhibits the possible formation of chains of forces in the transverse direction. This effect is likely due to the buoyancy, the drag and the lubrication, which are determinant due to the high value of the density of water. This hypothesis is corroborated by an almost uniform transversal distribution of the longitudinal velocity measured on the free surface, as it is possible to appreciate in figure 2.11. This experimental observation allows us to consider, as a first approximation, the contribution of the stress τ_{31} to be negligible compared to τ_{21} in the longitudinal momentum balance. Further investigations are underway to ascertain the validity of this hypothesis, i.e. if the τ_{31} component of the shear stress is negligible everywhere in the channel cross-section.

Chapter 3

Further investigations on the interphase forces

In Chapter 3 the definition of the drag force for a hyperconcentrated granular flow is tackled, underlining its role in the momentum balances and in the energy balances. The definition of the average drag is discussed. Experimental investigations of the flow in the column and of the free fall flow are carried out in order to better understand these concepts. A part of this chapter is published in Nucci et al. [59] and the whole content is going to be submitted to a scientific journal.

3.1 Introduction

In submerged granular flows driven by gravity, described with the two-phase approach, the interaction force that occurs between the two phases, without mass exchange, is equal in value and opposite in sign due to the principle of reciprocity. Two effects are ascribed to the interaction: the buoyancy due to the gradient in the stresses of the liquid phase, induced by the presence of the particles, and the drag effect relevant to the difference in velocities of the two phases. The expression of the interaction forces is given by the integral

over the surface of the particles of the gradients of the normal and the shear stresses, as it is derived in section 1.4.8.1, and it is:

$$F_i^f = -F_i^g = -c \left(\frac{\partial p^f}{\partial x_i} - \frac{\partial \tau_{ij}^f}{\partial x_j} \right) - D_i \quad (3.1)$$

where $D_i^\beta \propto u_i^f - u_i^g$ is the drag force. The definition of the drag of a cluster of particles is derived from the known relation of the drag of a single particle [2], through a function that takes into account for the presence of the assemble of particles, called *voidage function*, which is a function of the concentration. The drag force exercised by the liquid phase on a single spherical particle per unit area is:

$$D_{sp-i} = \frac{\alpha_2 d^2}{\alpha_3 d^3} \rho_w C_D \frac{U_{r-i}^2}{2} \quad (3.2)$$

where: α_2 and α_3 are a shape factors (i.e. for spherical particles $\alpha_2 = \pi/4$ and $\alpha_3 = \pi/6$), $U_{r-i} = u_i^f - u_i^g$ is the relative velocity between the two phases and C_D is the drag coefficient of a single sphere, which is a function of the Reynolds number. Although lots of expressions of the drag coefficient exist in literature, in the framework of the thesis, the relation by Dallavalle [23], which is valid for a large range of Reynolds number, is assumed:

$$C_D = \left(\frac{4.8}{\sqrt{Re}} + 0.63 \right)^2 \quad (3.3)$$

whit $Re = \rho_w d(u_i^f - u_i^g)/\mu_w$ is the Reynolds number. The aim of this chapter is to clarify the role of the drag in the momentum balances and in the energy balances. A review of the literature of the topic supplies several works, relevant, in particular, to industrial and low concentration applications. In the framework of this thesis the definition of the *voidage function* valid also for hyperconcentrated flow driven by gravity is reached. Furthermore the thesis tackles the analysis of the fluctuations in the drag force, and attempts to

explain of the role of these terms in the momentum and energy balances.

3.2 Voidage function

As it is reported in section 2.4.1, the drag force in a submerged granular flows (per unit volume), D_i^f , is derived according to Meruane et al. [57], as:

$$D_i^f = \frac{3}{4} C_D \frac{\rho_w}{d} f(c) c |\mathbf{u}^f - \mathbf{u}^g| (u_i^f - u_i^g) \quad (3.4)$$

The function $f(c)$ of eq.(3.4) represents the *voidage function*. An available relation of the *voidage function* was given by di Felice [25], deduced by the best fitting of different experimental investigations of fluidized bed, that is:

$$f(c) = (1 - c)^{1-m} \quad (3.5)$$

where $m = 3.6 \div 3.7$ depending on the regime of the flow. The collection of works in [25] regards diluted cases, that is, $c < 0.3$.

When the concentration of the solid phase increases, that is, when its value tends to the maximum value (random package), for a submerged granular flow driven by gravity, it is possible to consider that the flow of the liquid phase tends to a flow in porous media, probably in laminar regime and the relation (3.4) can be written as (3.6):

$$D_i^f = \frac{3}{4} \frac{\rho_w}{d} C_D f(c) U_{r-i}^2 \quad (3.6)$$

The relative velocity of the expression (3.6) is the velocity in porous media, $U_{r-i} = u_i^{fil} / (1 - c)$. The factor $(1 - c)$ is such that the Darcy's velocity is the velocity in pores. In fact, the mass conservation equation of the liquid phase in uniform flow conditions is: $Q_l = u_i^f (1 - c) A$, while the discharge in the Darcy regime is: $Q_l = u_i^{fil} A$, where Q_l is the liquid discharge and A the surface of the section. The velocity in porous media is related to

the hydraulic gradient by the hydraulic conductivity K : $u_i^{fil} = K \partial h^* / \partial x_i$. In particular, in uniform flow conditions, the hydraulic gradient coincides with the slope of the free surface, which is also the slope of the mobile bed, $\partial h^* / \partial x_i = \sin \alpha$. With respect to the hydraulic conductivity K , it is a property of the flow field usually expressed as a function of the permeability k that is a property of the porous media only, and dimensionally is a surface ($K = kg/\nu_w$). In laminar regime, the permeability can be expressed by the Kozeny Carman equation: $k = (1 - c)^3 c^{-2} d^2 180^{-1}$ [17]. Furthermore, the drag coefficient, in this condition, is expressed by the Stocks relation: $C_D = 24/Re_d$. Armanini et al. [11] prove that, when the concentration is large enough, in the momentum balance of the liquid phase in the longitudinal direction, the internal stresses of the liquid phase are negligible compared to the other terms of the balance and thus the drag is balanced by the weight of the liquid phase per unit volume. With simple steps, the theoretical expression of the *voidage function* at this limit is derived:

$$\begin{aligned} \rho_w(1 - c)g \sin \alpha &= \frac{3}{4} \frac{\rho_w}{d} U_r^2 \frac{24\nu_w}{d(1 - c)U_r} cf(c) \\ &= \frac{3}{4} \frac{\rho_w}{d} U_r \frac{24\nu_w}{d(1 - c)} cf(c) \\ &= \frac{3}{4} \frac{\rho_w}{d} \frac{(1 - c)^3}{c^2} \frac{gd^2}{180\nu_w} \sin \alpha \frac{24\nu_w}{d(1 - c)} cf(c) \end{aligned}$$

and results that:

$$f(c) = 10 \frac{c}{(1 - c)} \quad (3.7)$$

In figure 3.1 it is reported the distribution of the voidage function derived under the hypothesis of laminar flow eq.(3.7) (dot line). Of course, this relation is valid only at the limit when the concentration c tends to its maximum value c^* , which is reported in figure 3.1 in dashed line. In figure 3.1 the relation (3.7) is compared with the expression proposed by di Felice [25]. The

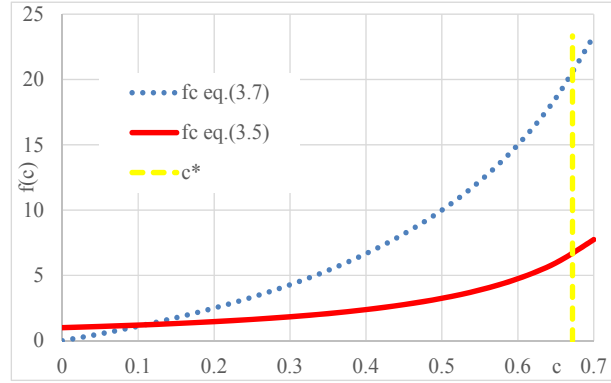


Figure 3.1: The dot line represents the voidage function according to the theoretical relation derived eq.(3.7) while the red line represents the voidage function according to eq.(3.5). In dashed line the maximum value of the concentration is reported.

gap between the two relation is significant when the concentration increases. This observation confirms that the relation of di Felice [25] is no more valid at this limit. A relation of the *voidage function* valid for all the values of concentration, can be obtained as a combination of generalization of the expression by di Felice [25] and the theoretical relations derived at the limit when the concentration tends to the maximum value, such as:

$$f = \frac{1}{(1-c)^n} \frac{c^* - c}{c^*} + 10 \frac{c}{1-c} \left(1 - \frac{c^* - c}{c^*} \right) \quad (3.8)$$

where n is a suitable parameter, which in principle is a function of the concentration. The simplest expression is to consider $n = 0$ such that eq.(3.8) reads:

$$f \simeq 1 - \frac{c}{c^*} \frac{1 - 11c}{1 - c} \quad (3.9)$$

3.3 The drag force fluctuations

In order to account for the temporal and spatial variation of the phenomenon, a statistical approach is proposed. It means that the drag can be expressed as an average component, \overline{D} , and a fluctuating component, D' . Choosing a period T sufficiently long to make the averaged flow statistically stationary, the average drag is defined as:

$$\overline{D} = \frac{1}{T} \int_T D dt \quad (3.10)$$

The definition of average can be applied also to the velocity and to the concentration:

$$\overline{u_i^\beta} = \frac{1}{T} \int_T u_i^\beta dt \quad (3.11)$$

$$\overline{c} = \frac{1}{T} \int_T c dt \quad (3.12)$$

The Reynolds decomposition is applied to the expression of the drag in the case that the liquid phase is faster than the granular phase ($u_i^f > u_i^g$), which is presumable because the viscosity of the liquid phase is smaller than the viscosity of the granular phase. It is observed that the average drag, \overline{D} , differs from the drag calculated by the average of velocities and concentration, $D(\overline{c}, \overline{U})$, and this difference is named residual drag D_R , that is:

$$\overline{D} = D(\overline{c}, \overline{U}) + D_R \quad (3.13)$$

Following the steps reported in Appendix B, it is derived an approximated expression for the drag of the average velocities and concentration:

$$\begin{aligned} D(\overline{c}, \overline{U}) &\simeq 17.28 \frac{\mu_w}{d^2} \frac{\overline{c}}{(1 - \overline{c})^{n+1}} (\overline{u^f} - \overline{u^g}) \\ &+ 4.44 \frac{\sqrt{\mu_w} \sqrt{\rho_w}}{d^{1.5}} \frac{\overline{c}}{(1 - \overline{c})^{n+0.5}} (\overline{u^f} - \overline{u^g})^{1.5} + \end{aligned}$$

$$+0.297 \frac{\rho_w}{d} \frac{\bar{c}}{(1-\bar{c})^n} (\bar{u}^f - \bar{u}^g)^2 \quad (3.14)$$

while the residual drag results:

$$\begin{aligned}
D_R \simeq & \left\{ \left[17.28 \frac{\mu_w}{d^2} \left((n+1) \frac{\bar{c}}{(1-\bar{c})^{n+2}} + \frac{1}{(1-\bar{c})^{n+1}} \right) \right] \right. \\
& + \left[4.44 \frac{\sqrt{\mu_w} \sqrt{\rho_w}}{d^{1.5}} \left(\frac{1}{(1-\bar{c})^{n+0.5}} + (n+0.5) \frac{\bar{c}}{(1-\bar{c})^{n+1.5}} \right) (1.5(\bar{u}^f - \bar{u}^g)^{0.5}) \right] \\
& \left. - \left[0.297 \frac{\rho_w}{d} 2 \left(\frac{1}{(1-\bar{c})^n} + n \frac{\bar{c}}{(1-\bar{c})^{n+1}} \right) (\bar{u}^f - \bar{u}^g) \right] \right\} \overline{c'(u'_f - u'_g)} \\
& + \left\{ \left[17.28 \frac{\mu_w}{d^2} \frac{n+1}{(1-\bar{c})^{n+2}} (\bar{u}^f - \bar{u}^g) \right] \right. \\
& + \left[4.44 \frac{\sqrt{\mu_w} \sqrt{\rho_w}}{d^{1.5}} \frac{(n+0.5)}{(1-\bar{c})^{n+1.5}} (\bar{u}^f - \bar{u}^g)^{1.5} \right] \\
& \left. + \left[0.297 \frac{\rho_w}{d} \frac{1}{(1-\bar{c})^{n+1}} (\bar{u}^f - \bar{u}^g)^2 \right] \right\} \overline{c'c'} \\
& + \left\{ 17.28 \frac{\mu_w}{d^2} \frac{(n+1)}{(1-\bar{c})^{n+2}} + 4.44 \frac{\sqrt{\mu_w} \sqrt{\rho_w}}{d^{1.5}} \frac{(n+0.5)}{(1-\bar{c})^{n+1.5}} 1.5(\bar{u}^f - \bar{u}^g)^{0.5} \right. \\
& \left. - 0.297 \frac{\rho_w}{d} 2n \frac{1}{(1-\bar{c})^{n+1}} (\bar{u}^f - \bar{u}^g) \right\} \overline{c'c'(u'_f - u'_g)} \\
& + 0.297 \frac{\rho_w}{d} \frac{\bar{c}}{(1-\bar{c})^n} \overline{(u'_f - u'_g)^2} \\
& + 0.297 \frac{\rho_w}{d} \left(\frac{1}{(1-\bar{c})^n} + n \frac{\bar{c}}{(1-\bar{c})^{n+1}} \right) \overline{c'(u'_f - u'_g)^2} \\
& + 0.297 \frac{\rho_w}{d} n \frac{1}{(1-\bar{c})^{n+1}} \overline{c'c'(u'_f - u'_g)^2} \quad (3.15)
\end{aligned}$$

The relation (3.15) can be simplified and expressed in dimensionless variables as:

$$\begin{aligned}
\widehat{D}_R = & \chi_1 \overline{c'(u'_f - u'_g)} + \chi_2 \overline{c'c'} + \chi_3 \overline{c'c'(u'_f - u'_g)} + \chi_4 \overline{(u'_f - u'_g)^2} \\
& + \chi_5 \overline{c'(u'_f - u'_g)^2} + \chi_6 \overline{c'c'(u'_f - u'_g)^2} \quad (3.16)
\end{aligned}$$

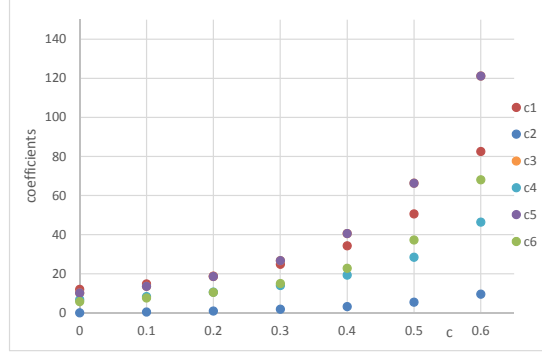


Figure 3.2: Magnitude of each coefficient of the fluctuating components of the drag force as a function of the concentration.

where the hat stays for dimensionless residual drag, and where:

$$\begin{aligned} \chi_1 &= \left(17.28 \frac{1}{Re} + 4.44 \frac{1}{\sqrt{Re}} (1.5(\overline{u^f} - \overline{u^g})^{0.5}) - 0.594(\overline{u^f} - \overline{u^g}) \right) \\ &\quad \left(n \frac{\bar{c}}{(1 - \bar{c})^{n+1}} + \frac{1}{(1 - \bar{c})^n} \right) \\ \chi_2 &= \left(17.28 \frac{1}{Re} (\overline{u^f} - \overline{u^g}) + 4.44 \frac{1}{\sqrt{Re}} (\overline{u^f} - \overline{u^g})^{1.5} + 0.297(\overline{u^f} - \overline{u^g})^2 \right) \\ &\quad \frac{n}{(1 - \bar{c})^{n+1}} \\ \chi_3 &= \left(17.28 \frac{1}{Re} + 4.44 \frac{1}{Re} 1.5(\overline{u^f} - \overline{u^g})^{0.5} - 0.594(\overline{u^f} - \overline{u^g}) \right) \\ &\quad n \frac{1}{(1 - \bar{c})^{n+1}} \\ \chi_4 &= 0.297 \frac{\bar{c}}{(1 - \bar{c})^n} \\ \chi_5 &= 0.297 \left(\frac{1}{(1 - \bar{c})^n} + n \frac{\bar{c}}{(1 - \bar{c})^{n+1}} \right) \\ \chi_6 &= 0.297 n \frac{1}{(1 - \bar{c})^{n+1}} \end{aligned}$$

Figure 3.2 shows the entity of the coefficients χ_i with respect to the concen-

tration.

3.4 Experimental investigations

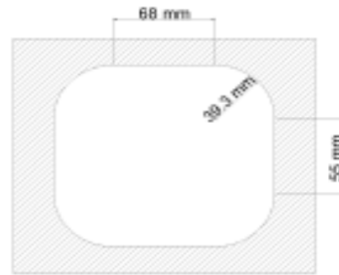


Figure 3.3: Section of the column in the x_1, x_2 plane. This figure belongs to [56].

Experimental investigations on the interphase force of a submerged granular flow were carried out in the Hydraulics Laboratory of DICAM (Department of Civil, Environmental and Mechanical engineering) of the University



Figure 3.4: Column sets up in the hydraulic laboratory with the two cameras for videos. This figure belongs to [56].

of Trento. In particular, the flow in the column and the free fall flow were reproduced in a column setup. The solid phase was composed of heavy identical spherical particles with $d = 6 \text{ mm}$ and $\rho_s = 2210 \text{ kg/m}^3$. The liquid phase was water and there was no cohesion. The column is 2 meters high and the section square as it is reported in figure 3.3. For a better explanation of the experimental method of acquisition and elaboration of the data please refer to section 2.4 and to Armanini et al. [5].

In the case of the column, the data was recorded by two cameras (figure 3.4). The cameras were 1 meter from the lateral side of the column, with a 512×1024 pixel resolution, and two different frequencies of acquisition were used (60 fps and 500 fps).

3.4.1 The measurement of the concentration

With the measurement technique adopted, the value of the concentration that is measured refers to the surface concentration. On the other hand, the equations of the mass and momentum conservation are written with respect to the volume concentration.

It is possible to deduce a relation between these two concentrations based on geometrical considerations. In figure 3.5 a sketch of a general disposition of the particles is given. In the case of spherical particles, Bagnold [13] proposes a relation between the linear concentration, which is defined as the ratio between the diameter of the particle and the distance between two

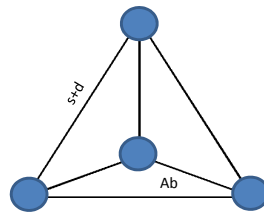


Figure 3.5: Hypothetical disposition of particles

particles ($\lambda = d/s$), and the volume concentration, that is:

$$\lambda = \frac{c^{1/3}}{c_*^{1/3} - c^{1/3}} \quad (3.17)$$

The surface concentration, λ_a , is given by the ratio between the surface of a particle and the average surface. Referring to figure 3.5, the area of the base of the pyramid is:

$$A_b = \frac{(s+d)^2 \sqrt{3}}{2} \quad (3.18)$$

which must be projected as:

$$A_{bv} = \frac{(s+d)^2 \sqrt{3}}{2} \delta \quad (3.19)$$

with δ assuming values between 1 and $\sqrt{3}/2$.

$$\lambda_a = \frac{A_{particles}}{A_{section}} = \frac{(\pi d^2/4)}{(s+d)^2 \sqrt{3}/4\delta} = \frac{\pi}{2\sqrt{3}\delta} \left(\frac{\lambda}{\lambda+1} \right)^2 \quad (3.20)$$

This means that:

$$\frac{\lambda}{\lambda+1} = (\lambda_a 2\sqrt{3}\delta/\pi)^{1/2} \quad (3.21)$$

and from eq. (3.17):

$$\frac{c}{c_*} = \left(\frac{\lambda}{1+\lambda} \right)^3 \quad (3.22)$$

so:

$$\frac{c}{c_*} = (\lambda_a 2\sqrt{3}\delta/\pi)^{3/2} \quad (3.23)$$

The expression 3.23 is calibrated with measurements obtained by introducing

a coefficient ξ , which is probably a function of the concentration:

$$\frac{c}{c_*} = (\lambda_a 2\sqrt{3}\delta/\pi)^{3/2} \xi \quad (3.24)$$

From experimental interpolation ξ is more or less equal to 1.

3.4.2 Flow in the column

The column is filled by a solid volume of known weight and is fed from the bottom with a discharge of water that makes the bed move. A precise system of filters is designed to avoid most of the oscillations generated during the inclusion of water: a cylinder of gravel, of section slightly smaller than that of the column, was added, to avoid phenomena of abrupt narrowing on entering the column and abrupt enlargement on output from the tube; a plastic honeycomb was placed in the entrance to make the input stream as homogeneous as possible. Finally, in the gap between the honeycomb and the base of the column, two meshes were inserted: a rigid metal mesh and a plastic mesh suitable to assume the best form useful to dissipate the current above. The system of equations (1.1) is rewritten for a 3D flow in the three directions $x = (x_1, x_2, x_3)$, with x_3 the vertical such that $g = (0, 0, -g)$ and with $u^\beta = (u_1^\beta, u_2^\beta, u_3^\beta)$ the vector of velocities, where the superscript $\beta = f$

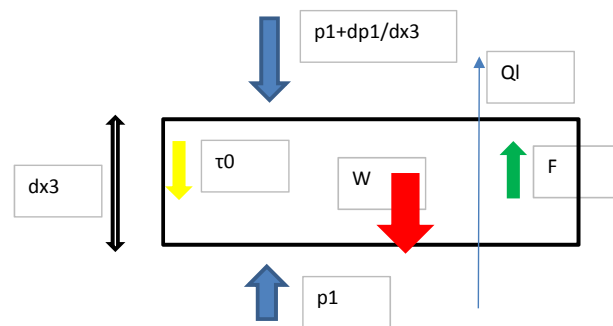


Figure 3.6: Scheme of the forces involved in the momentum balances.

stands for the liquid phase and $\beta = g$ for the solid phase. The scheme of the forces involved, in uniform flow conditions, is represented in figure 3.6. The system (1.1) becomes (3.25):

$$\begin{aligned}
& \frac{\partial}{\partial t} \rho_s c + \frac{\partial}{\partial x_1} \rho_s c u_1^g + \frac{\partial}{\partial x_2} \rho_s c u_2^g + \frac{\partial}{\partial x_3} \rho_s c u_3^g = 0 \\
& \frac{\partial}{\partial t} \rho_s c u_1^g + \frac{\partial}{\partial x_1} \rho_s c u_1^g u_1^g + \frac{\partial}{\partial x_2} \rho_s c u_1^g u_2^g + \frac{\partial}{\partial x_3} \rho_s c u_1^g u_3^g = \\
& \quad - \frac{\partial p^g}{\partial x_1} + \frac{\partial \tau_{11}^g}{\partial x_1} + \frac{\partial \tau_{21}^g}{\partial x_2} + \frac{\partial \tau_{31}^g}{\partial x_3} + F_1^g \\
& \frac{\partial}{\partial t} \rho_s c u_2^g + \frac{\partial}{\partial x_1} \rho_s c u_2^g u_1^g + \frac{\partial}{\partial x_2} \rho_s c u_2^g u_2^g + \frac{\partial}{\partial x_3} \rho_s c u_2^g u_3^g = \\
& \quad - \frac{\partial p^g}{\partial x_2} + \frac{\partial \tau_{12}^g}{\partial x_1} + \frac{\partial \tau_{22}^g}{\partial x_2} + \frac{\partial \tau_{32}^g}{\partial x_3} + F_2^g \\
& \frac{\partial}{\partial t} \rho_s c u_3^g + \frac{\partial}{\partial x_1} \rho_s c u_3^g u_1^g + \frac{\partial}{\partial x_2} \rho_s c u_3^g u_2^g + \frac{\partial}{\partial x_3} \rho_s c u_3^g u_3^g = \\
& \quad - \rho_s c g - \frac{\partial p^g}{\partial x_3} + \frac{\partial \tau_{13}^g}{\partial x_1} + \frac{\partial \tau_{23}^g}{\partial x_2} + \frac{\partial \tau_{33}^g}{\partial x_3} + F_3^g \\
& \frac{\partial}{\partial t} \rho_w (1 - c) + \frac{\partial}{\partial x_1} \rho_w (1 - c) u_1^f + \frac{\partial}{\partial x_2} \rho_w (1 - c) u_2^f + \frac{\partial}{\partial x_3} \rho_w (1 - c) u_3^f = 0 \\
& \frac{\partial}{\partial t} \rho_w (1 - c) u_1^f + \frac{\partial}{\partial x_1} \rho_w (1 - c) u_1^f u_1^f + \frac{\partial}{\partial x_2} \rho_w (1 - c) u_1^f u_2^f = \\
& \quad + \frac{\partial}{\partial x_3} \rho_w (1 - c) u_1^f u_3^f - \frac{\partial p^f}{\partial x_1} + \frac{\partial \tau_{11}^f}{\partial x_1} + \frac{\partial \tau_{21}^f}{\partial x_2} + \frac{\partial \tau_{31}^f}{\partial x_3} + F_1^f \\
& \frac{\partial}{\partial t} \rho_w (1 - c) u_2^f + \frac{\partial}{\partial x_1} \rho_w (1 - c) u_2^f u_1^f + \frac{\partial}{\partial x_2} \rho_w (1 - c) u_2^f u_2^f + \\
& \quad + \frac{\partial}{\partial x_3} \rho_w (1 - c) u_2^f u_3^f = - \frac{\partial p^f}{\partial x_2} + \frac{\partial \tau_{12}^f}{\partial x_1} + \frac{\partial \tau_{22}^f}{\partial x_2} + \frac{\partial \tau_{32}^f}{\partial x_3} + F_2^f \\
& \frac{\partial}{\partial t} \rho_w (1 - c) u_3^f + \frac{\partial}{\partial x_1} \rho_w (1 - c) u_3^f u_1^f + \frac{\partial}{\partial x_2} \rho_w (1 - c) u_3^f u_2^f + \\
& \quad \frac{\partial}{\partial x_3} \rho_w (1 - c) u_3^f u_3^f = - \rho_w (1 - c) g - \frac{\partial p^f}{\partial x_3} + \frac{\partial \tau_{13}^f}{\partial x_1} + \frac{\partial \tau_{23}^f}{\partial x_2} + \frac{\partial \tau_{33}^f}{\partial x_3} \\
& \quad + F_3^f \tag{3.25}
\end{aligned}$$

In the first instance the flow is stationary and uniform in the vertical direction. Under these hypothesis the average value of the velocity of the solid phase is null because there is no solid discharge, while the averaged value of the liquid phase is constant and is derived from the continuity equation. The system of eqs.(3.25) reduce to:

$$\begin{aligned} \frac{\partial}{\partial x_3} \rho_s \overline{c u_3^{g'} u_3^{g'}} + \frac{\partial}{\partial x_3} \rho_s \overline{c' u_3^{g'} u_3^{g'}} &= -\rho_s \overline{c} g - \frac{\partial p^g}{\partial x_3} + \frac{\partial \tau_{31}^g}{\partial x_1} + \frac{\partial \tau_{32}^g}{\partial x_2} \\ &+ \frac{\partial \tau_{33}^g}{\partial x_3} - \overline{c} \frac{\partial p^f}{\partial x_3} + \overline{c} \left(\frac{\partial \tau_{31}^f}{\partial x_1} + \frac{\partial \tau_{32}^f}{\partial x_2} + \frac{\partial \tau_{33}^f}{\partial x_3} \right) \\ &+ \overline{D_3} + \overline{D'_3} \end{aligned} \quad (3.26)$$

$$\begin{aligned} \frac{\partial}{\partial x_3} \rho_w \left(\overline{u_3^f u_3^f} + \overline{u_3^{f'} u_3^{f'}} - \overline{c u_3^f u_3^f} - \overline{c' u_3^{f'} u_3^{f'}} - 2 \overline{u_3^f u_3^{f'} c} - \overline{c' u_3^{f'} u_3^f} \right) \\ = -\rho_w (1 - \overline{c}) g - (1 - \overline{c}) \frac{\partial p^f}{\partial x_3} + (1 - \overline{c}) \left(\frac{\partial \tau_{31}^f}{\partial x_1} + \frac{\partial \tau_{32}^f}{\partial x_2} + \frac{\partial \tau_{33}^f}{\partial x_3} \right) \\ - \overline{D_3} - \overline{D'_3} \end{aligned} \quad (3.27)$$

3.4.2.1 Experimental results

A collection of investigations, differing in the liquid discharge, that is, different concentration, were carried out in a uniform steady state flow in the x_3 vertical direction. The results are reported in the following figures, distinguishing the measurements along the direction x_3 from the measurements in the plane of the section of the column x_1, x_2 . In particular, with respect to the vertical direction, figures represent: the profile of the concentration (figure 3.7); the averaged value of the velocities in the vertical direction x_3 (figure 3.8(a)); the fluctuations of the velocities (figure 3.9(a)) and the terms due to the correlations of the fluctuations of the velocities and the concentration (figures 3.10(a) and 3.11(a)). Figure 3.8(a) shows that the velocity of the granular phase is approximately null, while the velocity of the liquid

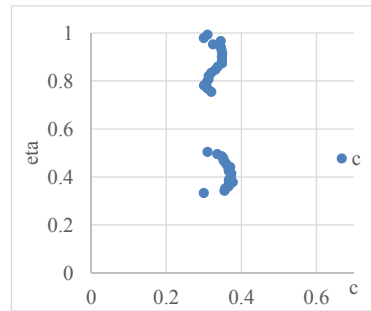


Figure 3.7: Distribution across the flow depth of concentration.

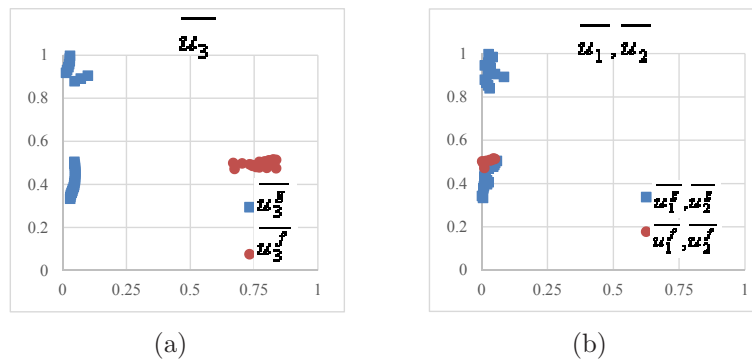


Figure 3.8: Distribution along the flow depth of the average value of the velocity (a) in the vertical direction x_3 ; (b) the average value of the velocity in the horizontal plane x_1, x_2 .

phase is constant. While, with respect to the horizontal plane x_1, x_2 , figures represent: the averaged value of the velocities (figure 3.8(b)); the fluctuations of the velocities (figure 3.9(b)) and the terms due to the correlations of the fluctuations of the velocities and the concentration (figures 3.10(b) and 3.11(b)). From the experimental evidences it emerges that:

1. there is no gradient of concentration (figure 3.7)
2. From figures 3.9(a), 3.9(b), 3.10(a), 3.10(b), 3.11(a), 3.11(b) it is clear that the fluctuations of the velocities, the correlations of the fluctua-

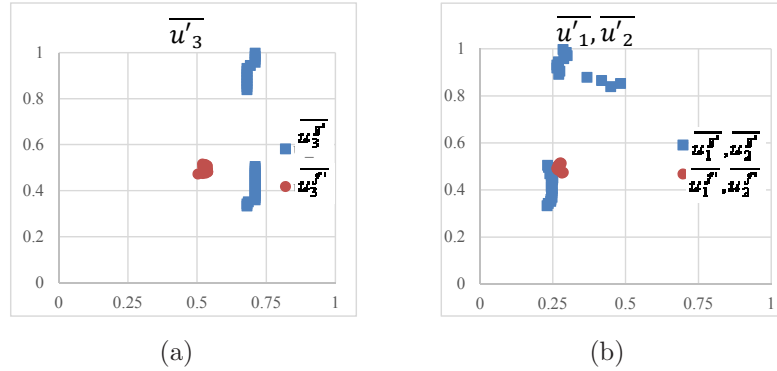


Figure 3.9: Distribution along the flow depth of the fluctuations of the velocities: (a) in the vertical direction x_3 ; (b) in the horizontal plane x_1, x_2 . In blue the measurement of the granular phase and in red of the liquid phase.

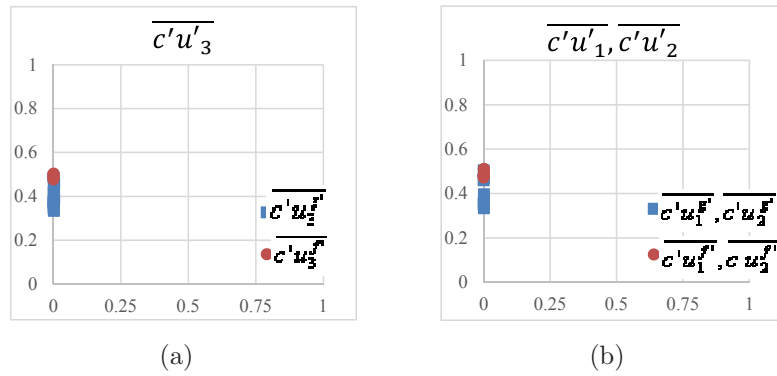


Figure 3.10: Distribution along the flow depth of the dimensionless correlations of the fluctuations of the velocities and the concentration: (a) in the vertical direction x_3 ; (b) in the horizontal plane x_1, x_2 . In blue the measurement of the granular phase and in red of the liquid phase.

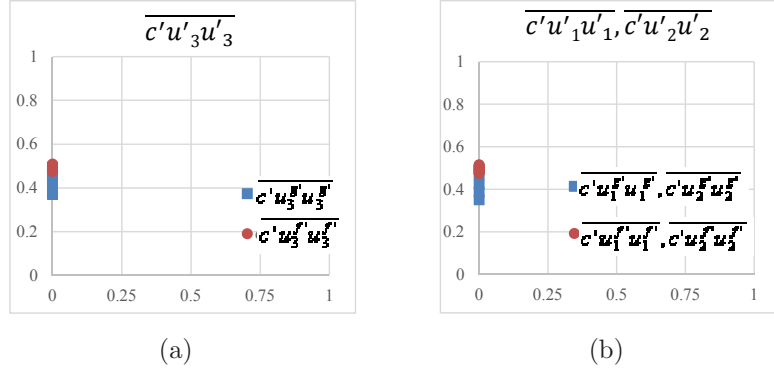


Figure 3.11: Distribution along the flow depth of the correlations of the dimensionless fluctuations of the velocities and concentration: (a) in the vertical direction x_3 ; (b) in the horizontal plane x_1, x_2 . In blue the measurement of the granular phase and in red of the liquid phase.

tions of the velocities and the concentration are small. In this respect, the gradients of these terms are considered negligible.

3. the hypothesis that the gradients of the velocities are negligible allows the shear stresses, of the liquid and of the solid, to be considered null except in a restricted layer near the wall.
4. in first assumption it is assumed that $\overline{D'_3}$ is null.

Following the steps in appendix A the system (3.25) reduces to:

$$0 = -\rho_w(1 - \bar{c})g - (1 - \bar{c})\frac{\partial p^f}{\partial x_3} + (1 - \bar{c})\frac{\tau_{r3}^f}{R_h} - \overline{D_3} \quad (3.28)$$

$$0 = -\rho_s \bar{c}g - \frac{\partial p^g}{\partial x_3} - \bar{c}\frac{\partial p^f}{\partial x_3} + \bar{c}\frac{\tau_{r3}^f}{R_h} + \overline{D_3} \quad (3.29)$$

where τ_{r3}^f is the shear stresses normal to the section of the column in the vertical direction, and R_h is the hydraulic radius of the section of the column. Adding together eq.(3.28) and eq.(3.29) it results:

$$0 = -\rho_s c g - \rho_w(1 - c)g - \frac{\partial p^g}{\partial x_3} - \frac{\partial p^f}{\partial x_3} + \frac{\tau_{r3}^f}{R_h} \quad (3.30)$$

Because $u_3^g = 0$ and the concentration is high enough it is assumed that:

$$\frac{\partial p^g}{\partial x_3} = -\rho_s c g \quad (3.31)$$

so:

$$0 = -\rho_w(1-c)g - \frac{\partial p^f}{\partial x_3} + \frac{\tau_{r3}^f}{R_h} \quad (3.32)$$

Figure 3.12 reports the distribution of the measured drag as a function of the concentration, derived from the balance (3.32):

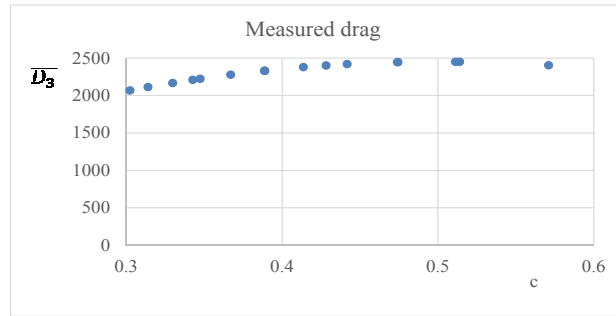


Figure 3.12: Distribution of the drag vs concentration. Measurements of the flow in the column.

3.4.2.2 The velocity of the liquid phase

The drag force represents the component of the interaction force that depends on the difference between the velocities of the two phases. Up to now the continuity equation of the liquid phase is sufficient to deduce the average values of the velocities, since the fluid discharge is imposed. In order to quantify the fluctuations of the velocities of the fluid phase and to obtain measurements of the different correlation terms, the velocities of the liquid phase were measured by using smaller and lighter particles and by assuming that the velocities of these particles are the velocities of the liquid phase. 3 runs with different liquid discharges were done. In figure 3.13 the results

obtained for the test with liquid discharge of 160 [l/min], is reported: From

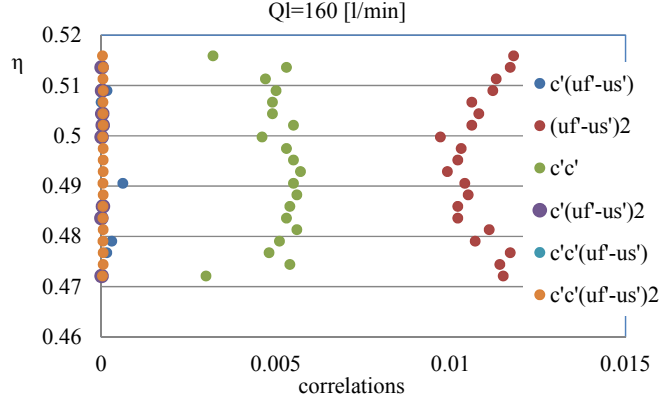


Figure 3.13: Different terms of the correlations of the fluctuations of the momentum balance for different runs: with a liquid discharge of 160 [l/min]

figure 3.13 appears that the only correlations that should be taken into account are $\overline{c'c'}$ and $\overline{(u^f - u^s)^2}$, such that the residual component of the drag force, eq.(3.16), reduces to.

$$D_R \simeq \left\{ \left[0.297 \frac{\rho_w}{d} \frac{\bar{1}}{(1 - \bar{c})^{n+1}} (\overline{u^f} - \overline{u^g})^2 \right] \overline{c'c'} + 0.297 \frac{\rho_w}{d} \frac{\bar{c}}{(1 - \bar{c})^n} \overline{(u^f - u^g)^2} \right\} \quad (3.33)$$

3.4.2.3 The pressure of the liquid phase

The water pressure in the column was measured using a differential piezometer. The flow is confined such that the pressure is constant in the layer of the column where there is only water. However, the water pressure varies linearly, increasing going towards the bottom of the column, due to the presence of the solid phase. The graph in figure 3.14 summarizes the pressure measured in the investigations of the flow in the column: The order of magnitude of the pressure measurement is verified through a pressure gauge installed in the column.

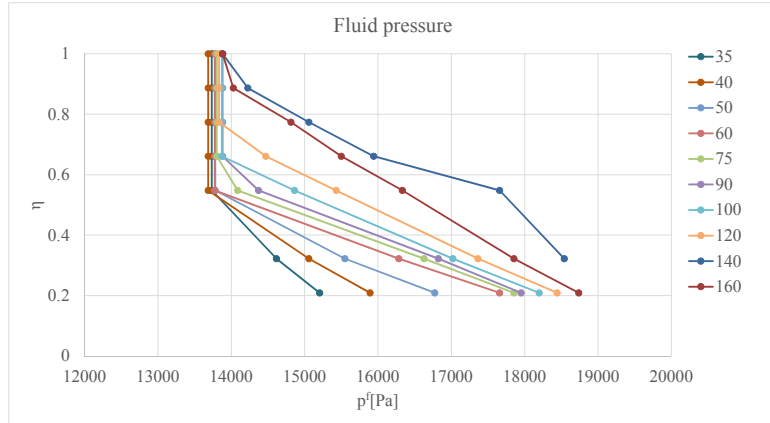


Figure 3.14: Measurements of the fluid pressure for different discharges.

3.4.3 Free fall flow

The setup of the column is that the solid material is released instantaneously (with a guillotine mechanism) from the top into still water. In free fall flow in still water, the pressure of the liquid phase is hydrostatic. Under the hypothesis that the granular pressure is balanced by the weight of the solid phase, eqs. (3.28) and (3.29) reduce to:

$$0 = (1 - \bar{c}) \frac{\tau_{r3}^f}{R_h} - \overline{D}_3 \quad (3.34)$$

$$0 = -\bar{c} \rho_w g + \bar{c} \frac{\tau_{r3}}{R_h} + \overline{D}_3 \quad (3.35)$$

Figure 3.15 shows the distribution of the average drag, derived from the balances (3.34) and (3.35), as a function of the concentration.

3.4.4 Preliminary results

In order to summarize the results obtained in the framework of the experimental investigation on the column, the data presented in figures 3.12 and 3.15 are combined in 3.16: The experiments confirm that the drag force increases when the concentration becomes higher. The voidage function is

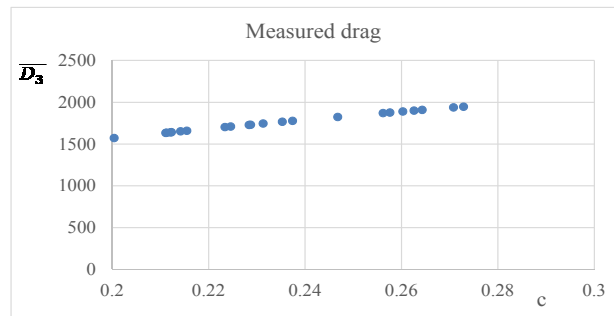


Figure 3.15: Distribution of the average drag vs concentration. Measurements of the free fall flow.

deduced by the ratio of the measured drag over the drag of the single sphere.

Moreover the voidage function should satisfy two boundary conditions: that are the voidage function is one when there is no concentration of particles ($c = 0$) and that the voidage function tends to the value derived for the flow in porous media when the concentration tends to its maximum. The experimental data obtained are analyzed and then compared with the relations derived in section 3.2 as well as with the empirical relation by di Felice [25]. From figure 3.17 it is deduced that the experimental data are in accordance with the expression of di Felice [25] for concentrations lower than 0.3 but it is not able to reproduce the boundary condition of the flow in porous media. On the other hand the simpler relation derived in section 3.2, that is

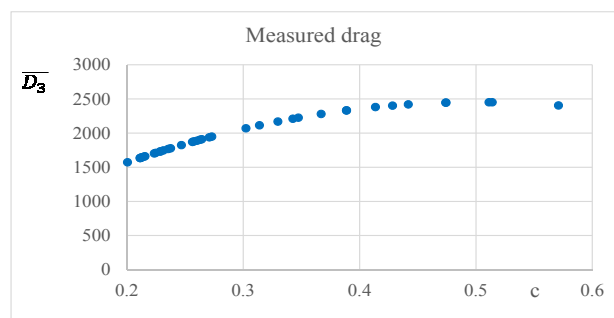


Figure 3.16: Distribution of the average drag vs concentration. Summary of the measured data.

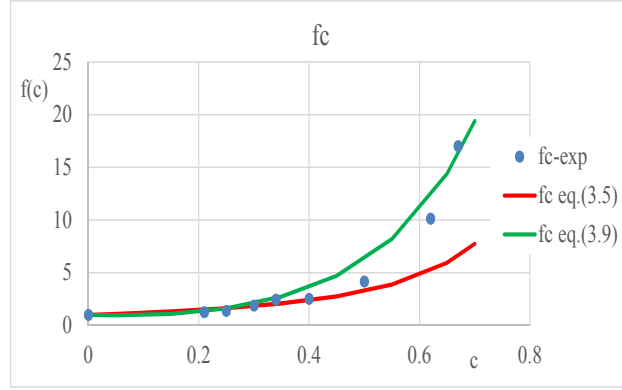


Figure 3.17: The voidage function calculated from the experimental data is shown in blue dot. The red line represents the voidage function according to eq.(3.5), while the green line is the voidage function according to eq.(3.9)

eq.(3.9), satisfies the boundary conditions and reproduces the behaviour of the experimental data.

3.5 The fluctuations of the drag in the kinetic energy balance

An other consequence of the fluctuations of the drag force is that an additional dissipation mechanism, $\overline{u^g D'}$ also appears in the kinetic energy balance, which in uniform flow conditions reads as:

$$0 = \frac{\partial}{\partial x_2} \left(k_{\Theta} \frac{\partial \Theta}{\partial x_2} \right) + \mu^{coll} \left(\frac{\partial u_1^g}{\partial x_2} \right)^2 - \hat{f}_5 \rho_s (1 - e^2) \frac{\Theta^{1.5}}{d} + \overline{u^g D'} \quad (3.36)$$

where $\hat{f}_5 = f_5 / (1 - e^2)$ and e , the elastic coefficient of restitution, is constant. This further dissipation rate results from the velocity and concentration fluctuations on a scale much larger than the grain size. Such large-scale fluctuations would not exist if the sediment was not in the turbulent flow of the fluid [40]. There are different approaches to account for the effect on the

dissipation rate in the kinetic energy balance due to the fluctuations in the drag. In Armanini et al. [11] it is embedded in the coefficient of restitution e , which in this case is assumed to be dependent on the Stokes number relevant to the granular temperature $St = \rho_s d \Theta^{0.5} / (18 \mu_w)$ [10]:

$$e = e_o - 2.85 St^{-0.5} \quad (3.37)$$

where e_o represents the value of the restitution coefficient in the absence of interstitial fluid. According to the kinetic theory:

$$\hat{f}_5 (1 - e_o^2) \rho_s \frac{\Theta^{1.5}}{d} \quad (3.38)$$

is the dissipation rate due to inelastic collisions. Then, following Armanini et al. [10], the dissipation due to the fluctuations is expressed as:

$$\overline{u^{g'} D'} = \hat{f}_5 (2.85^2 St^{-1} - 2e_o 2.85 St^{-0.5}) \frac{\Theta^{1.5}}{d} \quad (3.39)$$

In Nucci et al. [59], the approach of the *heuristic model* is compared with the diffusive model proposed by Hsu et al. [40], that is:

$$\overline{u^{g'} D'} = -2c \frac{\rho_w}{d} U_r C_D f(c) K_s \quad (3.40)$$

where K_s is the oscillatory component of the solid phase, and U_r the relative velocity between the phases.

In figure 3.18 is reported a comparison of the distributions across the flow depth of the dissipation rate of the term of the correlations according to the approach by Armanini et al. [11] and the approach by Hsu et al. [40]. Figure 3.18 also includes the distribution across the flow depth of the term of the dissipation rate due to the inelastic collisions $\hat{f}_5 (1 - e_o^2) \rho_s \Theta^{1.5} / d$ of eq. (1.26), in order to highlight the different order of magnitude.

From figure 3.18 it appears evident that the two ways of defining the fluc-

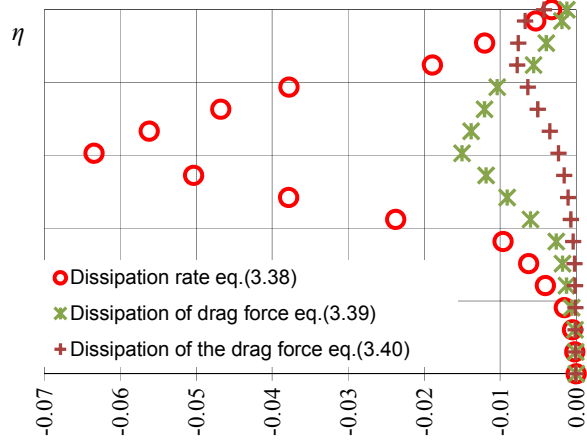


Figure 3.18: Comparison between the dissipation rate in the kinetic energy balance, obtained according to different formulations. The stars represent the dissipation rate due to the drag fluctuations, obtained following Armanini *et al.* (2014), eq.(3.39). The crosses represent the dissipation rate of the drag fluctuations obtained according to the diffusive hypothesis by Hsu *et al.* (2004), eq.(3.40). The circles represent the kinetic energy dissipation rate due to the inelastic collisions, eq.(3.38). The experimental data are presented in Armanini *et al.* (2009).

tuating components give different results, but it is not possible to determine which is the most reliable. However, it should be noted that:

- the results depend on the value of the dry coefficient of restitution e_o and this contribution is predominant across the entire flow depth;
- in the approach by Hsu *et al.* [40] the velocity fluctuations are divided into two contributions: a term at the scale of Θ that represents the correlations of the small-scale fluctuations of particle velocities, and a term at the scale of k_s that represents the large-scale sediment velocity fluctuations. However some preliminary, and not yet published, measurements of the instantaneous velocities show that this separation is somehow arbitrary, because the spectrum of the particle velocity fluctuations is continuous and monotonically decreasing;

- it is, however, proved [11] that the kinetic theories of dense gases, modified as in Jenkins and Hanes [45], interpret quite well the flow of the granular phase also in the upper part of the flow depth, where the fluctuations in the drag could become important. For this reason the calculation of eq. (3.40) adopts $K_s = \Theta$.

Chapter 4

Further investigations on the diluted flow conditions

In Chapter 4 a review of the literature regarding the definition of the closure relation of the stresses of the liquid phase of submerged granular flows is developed. Some relations are proposed. The set of equations solved in Chapter 2 is written adding the equations of the liquid phase. Preliminary numerical results are compared with experimental data.

4.1 Introduction

A complete description of the dynamics of the solid phase is given only including the role of the interstitial fluid. However, often studies of granular flows neglect the presence of the liquid phase, with different justifications. For example, Campbell [16] considers the particles to be much denser than the interstitial fluid and thus assumes that the dynamics of the phenomena is described only by the interactions among particles, e.g. the internal stresses of the granular phase. From a review of the literature, two different approaches treating the mixture of the two phases, differing for the basic assumptions, are presented, called the *mixture theory* and the *two-phase model*. The *mixture theory*

ture theory was formulated to study the dynamics of mixtures through a generalization of the principles of continuous mechanics. The key abstraction in this theory is that, at any time, every point in space is occupied simultaneously by one particle of each constituent [67]. The mixture theory had been the only approach to study granular flows up to the formulation of the kinetic theory was formulated, and it was widely used [66, 64, 41]. Among these, Iverson [41] derived from the model proposed by Savage and Hutter [64] a model for submerged granular flow where the presence of the interstitial fluid alters the behaviour of the flow, and developed a system of mass and momentum equations for the mixture, in order to study snow avalanches.

The *two-phase model* works on the fluid particle flow with a phase-averaged formulation that means an average of the mass and momentum balance laws for fluid and solid constituents over time or volume [26]. In this formulation the control volume is sufficiently larger than the particles and sufficiently small to be considered infinitesimal. Please refer to the considerations on the different types of averaging in section 1.3.1.

4.2 Literature review

Among the pioneering work in this field, Drew [26] examines the common features of dispersed two-phase flows, based on the ideas that each material is continuum. The equations proposed by Drew [26] are basic and generic and consist in the average balance equations for average mass and momentum for a general two-phase flow. Furthermore, Drew [26] defines closure relations for the stresses of each phase and a relation for the interaction force. With respect to the original Favre average two-phase equations [26], Hsu et al. [40] proposes a closure for the correlations between the velocity fluctuations with respect to the collisional component of the stresses of the granular phase. It is observed that, because of the flow turbulence, the sediment concentration

fluctuates on a scale much larger than the grain size, and this is the reason why a second averaging process needs to be carried out in order to calculate the large scale turbulence. In fact, the Reynolds stresses describe the correlation of velocity fluctuations within a region smaller than several grain diameters. However, for river flow, it is important to take into account the effects of large-scale turbulence that may involve boundary layers or breaking waves. In particular Hsu et al. [40] proposes a correlation between the velocity of the solid and the liquid phase using a coefficient α . The theory is applied to a steady open channel, two-dimensional, unidirectional, free surface, driven by gravity flows, with small inclination, and, in particular to the dilute regions, neglecting collisional stress and large-scale Reynolds stress in the sediment-phase momentum equations. Furthermore the small-scale Reynolds stress in fluid-phase momentum equation is negligible.

Another work on the governing equations for a two-phase model is by Zhang and Reese [68]. The interphase momentum correlation, that is, the drag force, is modeled by considering the effect of solid-particle fluctuations. The influence of particles on the $\kappa - \epsilon$ turbulence model parameters is tackled, and the constitutive equations for the particulate stresses, which account for the effect of the gas turbulence, are given. Zhang and Reese [68] introduce a coefficient k_{12} relating to the autocorrelation of the force experienced by a representative particle. The correlation time is taken to be comparable to the collision interval and the force acting on a particle is the drag force. Meruane et al. [57] suggest a set of governing equations describing the role of the interstitial fluid on the dynamics of gravitational granular flows. The system of equations is based on fundamental principles of the mixture theory, where the granular flow is considered compressible. A satisfactory explanation on why the liquid phase can or cannot be negligible is given. It is demonstrated that the normal component of the interphase force is product of the gradient of the fluid pressure and the solid concentration. Furthermore, with respect to the stress component of the interphase force, Meruane et al. [57] neglect

both virtual mass effect and Basset force and consider only the drag force effects. To consider the turbulence modulation Meruane et al. [57] add the work of the interphase force as a product term in both the κ and ϵ equations. Following the mixture theory approach proposed in Truesdell [67], Meruane et al. [57] propose the governing equations for a dense granular flow consisting of a heterogeneous mixture of solid particles and a Newtonian ambient fluid are obtained.

4.3 Stresses tensor of the liquid phase

Assuming that the state variables of the governing equations are mean quantities obtained by Reynolds averaging of the equations, the stress tensor for the liquid phase can be written as:

$$\tau_{ij}^f = \mu_f \left(\frac{\partial u_i^f}{\partial x_j} + \frac{\partial u_j^f}{\partial x_i} \right) - \overline{\rho_w u_i^{f'} u_j^{f'}} \quad (4.1)$$

where μ_f is the dynamic viscosity of the fluid and $\overline{\rho_w u_i^{f'} u_j^{f'}}$ is a generic term of the Reynolds stresses. According to the diffusive model of Boussinesq [15], the term due to turbulent fluctuations can be expressed as a linear function of the shear rate:

$$-\overline{u_i^{f'} u_j^{f'}} = \nu_t \left(\frac{\partial u_i^f}{\partial x_j} + \frac{\partial u_j^f}{\partial x_i} \right) \quad (4.2)$$

where ν_t is derived in analogy with the kinematic viscosity of the flow but it represents a kinematic property of the flow. In first instance it is assumed that ν_t is a scalar and it is noted that this hypothesis is not general and it falls in default when applied to the normal stresses of the Reynolds tensor. Anyway, the closure suggested by Boussinesq [15] can be applied when there are few terms of the turbulent tensor efforts that count in the balance of

momentum. In the case of fluid-particle flows is more complicated than that for the case of pure fluid flows, as the solid particles modify the structure and intensity of the fluid turbulence, thus altering the transport rate of momentum [31]. A detailed description of the mechanism relevant to the turbulence in granular flows is proven by Elghobashi and Truesdell [31] ”...*In gravitational environment, particles also transfer their momentum to the small-scale motion but in an anisotropic manner. The pressure-strain correlation acts to remove this anisotropy by transferring energy from the direction of gravity to the other two directions, but at the same wave number, i.e., to the small-scale motion in directions normal to gravity. This input of energy in the two directions with lowest energy content causes a reverse cascade. This reverse cascade tends to build up the energy level at lower wave numbers, thus reducing the decay rate of energy as compared to that of particle-free turbulence. This reduction of the energy decay rate slows down the rate of growth of the integral length scale. The associated augmentation of the dissipation rate reduces the Kolmogorov length scale...*”.

4.3.1 Dynamic viscosity of interstitial fluid

The presence of particles in the pore fluid influences the effective fluid viscosity. The influence is complex and has been the object of systematic research [41]. In the framework of sediment transport in river bed, Einstein [30] proposes an expression to modify the viscosity of water, taking into account the solid grains, that is: $\mu_e = \mu_f(1 + 2.5c)$ where μ_e is the effective viscosity. Although the relation proposed by Einstein was derived in the mono-phase approach and it is valid in diluted region, it represents the basic approach to treat the problem, i.e. to derive a relation for the viscosity of the liquid phase that is a function of the concentration.

4.3.2 Closure models for the Reynolds stresses in granular flows

From a dimensional point of view, the diffusive coefficient ν_t introduced by Boussinesq [15] is the product between a length and a velocity, such that in general:

$$\nu_t = [\Lambda][U] \quad (4.3)$$

Different models for expressing the diffusive coefficient, improperly also called eddy viscosity exists. In this chapter some closure relation of the stresses of the liquid phase in two-phase flows are provided.

4.3.2.1 Mixing length models in granular flows

The mixing-length model by Prandtl [61] is the first proper model to describe the distribution of the eddy viscosity of the turbulence. Following an analogy with the kinetic theory of gases, the eddy viscosity is scaled on the mean fluctuation velocity and on a mixing length. For two-phase granular flows the idea is to use the mixing length as the length scale and the shear rate of the liquid phase dot the mixing length as the velocity scale, and to express the mixing length as a function of the concentration. In this respect different expressions for the mixing length are evaluated, eqs.(4.4)-(4.9):

$$\ell_1 = \kappa\eta \left(\frac{c^* - c}{c^*} \right)^a h \quad (4.4)$$

$$\ell_2 = \kappa\eta \left(\frac{c^* - c}{c^*} \right) \frac{d}{\lambda} \quad (4.5)$$

$$\ell_3 = \kappa\eta \left(\frac{c^* - c}{c^*} \right) h + \frac{d}{\lambda} \quad (4.6)$$

$$\ell_4 = \kappa\eta \left(\frac{c^* - c}{c^*} \right)^b \frac{d}{\lambda} \quad (4.7)$$

$$(4.8)$$

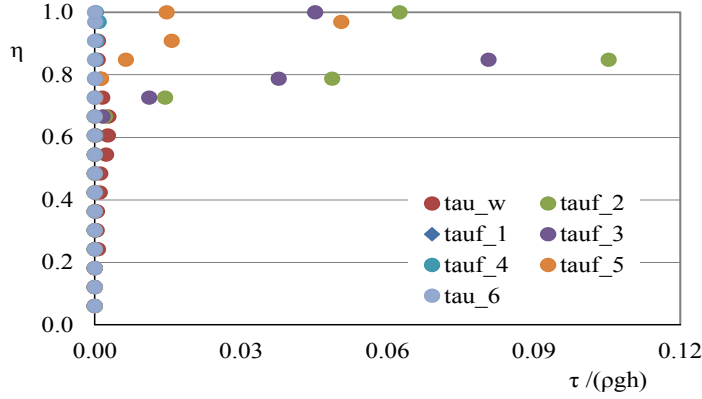


Figure 4.1: Comparison among the expression of the stresses of the liquid phase following different relations of the mixing length of a two phase flow. Furthermore, the red dot represents the stresses according to relation (4.11).

$$\ell_5 = \kappa \left(\frac{d}{g_o} \right) \quad (4.9)$$

where: κ is the von Karman constant, η the non-dimensional normal coordinate, h the water depth of the flow, c^* the maximum value of the concentration, d the diameter of the particles, λ the linear concentration [13], g_o the radial distribution function [54] and a and b constant. In uniform flow conditions the stresses of the liquid phase reads:

$$\tau_{12}^f = \rho_w (1 - c) \ell^2 \left(\frac{\partial u_1^f}{\partial x_2} + \frac{\partial u_2^f}{\partial x_1} \right)^2 \quad (4.10)$$

In figure 4.1 a comparison of the different entities of the shear stresses of the liquid phase, evaluated for the different relations of the mixing length ℓ_i , choosing $a = 2, b = 0.1$ and making dimensionless by the water depth, the density of the solid phase and the gravity vector, is presented. The experimental data used for these considerations were obtained in Armanini et al. [5]. From figure 4.1, the relations named 2, 3, 5 made the entity of the internal stresses of the liquid phase too big for the type of flow under consideration. Furthermore, from this previous analysis we see that none of

the equations proposed, eqs.(4.4)-(4.9), are able to reproduce the free surface flows. In fact, a valid expression of the mixing length must take into account that the shear stresses of the liquid phase are zero at the free surface. In this respect, a proper relation is:

$$\tau_{ij}^f = \rho_w(1-c)(\kappa\eta)(1-\eta)h^2 \left(\frac{\partial u_i^f}{\partial x_j} + \frac{\partial u_j^f}{\partial x_i} \right)^2 f_2(c) \quad (4.11)$$

where $f_2(c)$ is a function of the concentration that take into account the influence of the particles. This model is valid when is applied to the wall turbulence.

4.3.2.2 $k - \epsilon$ models in granular flows

A standard turbulence energy-dissipation model for the turbulence of the liquid phase is the $k - \epsilon$ model [62], where k is the energy of the turbulence ($k = 1/3(u_1^{f'} + u_2^{f'} + u_3^{f'})$) and ϵ is the dissipation rate, such that, according to Meruane et al. [57] the eddy viscosity is:

$$\nu_t = c_\mu \frac{k^2}{\epsilon} \quad (4.12)$$

where c_μ is a constant. The equations of the two-phase approach are completed with the energy balances of the $k - \epsilon$ model, although there are no general turbulent closures for the liquid phase in the case of two-phase flows. In the literature there is still an ambiguity and this issue is currently dealt with using different approaches. Meruane et al. [57] and Crowe et al. [21] include a source term in the kinetic energy equation of the liquid phase, which represents the irreversible work on the fluid associated with the drag force on the particles:

$$0 = \frac{\partial}{\partial x_2} \left(\frac{\mu_t}{\sigma_t} \frac{\partial k}{\partial x_2} \right) + \mu_t \left(\frac{\partial u^f}{\partial x_2} \right)^2 + D|u^f - u^g|^2 - \frac{\rho_w}{\rho_s}(1-c)\epsilon \quad (4.13)$$

$$0 = c_{1\epsilon} \frac{\epsilon}{k} \left[\mu_t \left(\frac{\partial u^f}{\partial x_2} \right)^2 + D |u^f - u^g|^2 \right] + \frac{\partial}{\partial x_2} \left(\frac{\mu_t}{\sigma_\epsilon} \frac{\partial \epsilon}{\partial x_2} \right) - c_{2\epsilon} \frac{\rho_w}{\rho_s} (1-c) \frac{\epsilon^2}{k} \quad (4.14)$$

where $\mu_t = \rho_w \nu_t$. In contrast, Hsu et al. [39] considered the work on the fluid associated with the drag force on the particles as dissipative terms in the energy balances of the $k - \epsilon$ model.

4.4 Preliminary results

The set of equations that governs the two-phase uniform steady flow, in the x_1 longitudinal direction, proposed in Chapter 2, are written for the dilute flows, where the stresses of the fluid phase are not neglected, as:

$$\frac{\partial \tau_{21}^f}{\partial x_2} = \rho_w g \frac{\partial z}{\partial x_1} + \frac{1}{1-c} D_1 \quad (4.15)$$

$$\frac{\partial \tau_{21}^g}{\partial x_2} = c(\rho_s - \rho_w) g \frac{\partial z}{\partial x_1} - \frac{1}{1-c} D_1 \quad (4.16)$$

$$\frac{\partial p^g}{\partial x_2} = -c(\rho_s - \rho_w) g \frac{\partial z}{\partial x_2} \quad (4.17)$$

Please refer to appendix C for further explanation. In the following the system of equations (4.15)-(4.17) is solved with the numerical procedure described in section 2.3. The closure relations are the relations of the *heuristic model* for the granular stresses, the drag expression derived in Chapter 4, while for the stresses of the liquid phase a mixing length model, as in eq.(4.11), is proposed:

$$\tau_{21}^g = \mu^{g-coll} \dot{\gamma} + \tan \varphi p^g \frac{I_{so}}{I_{so} + I_s} \quad (4.18)$$

$$p^g = p^g \frac{I_{so}}{I_{so} + I_s} + f_1 \Theta \quad (4.19)$$

$$\tau_{21}^f = (\mu_e + \mu_t) \frac{\partial u_1^f}{\partial x_2} f_2(c) \quad (4.20)$$

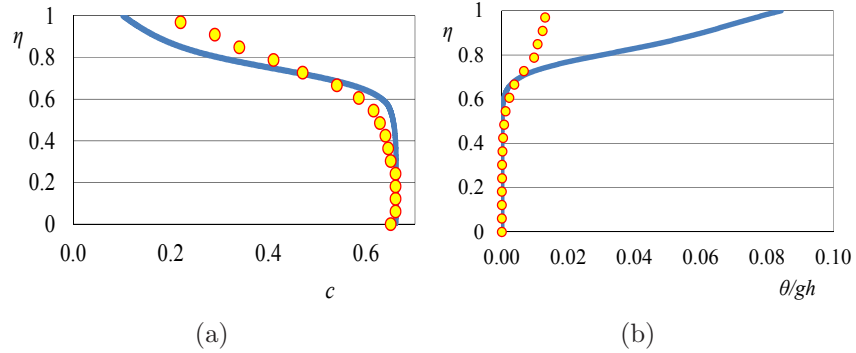


Figure 4.2: Comparison between results of the numerical simulation (solid line) and experimental data (circles) of: (a) particle concentration profile; (b) granular temperature profile.

$$D_1 = \frac{3}{4} C_D c \frac{\rho_w}{\rho_s d} (u_1^f - u_1^s) |u_1^f - u_1^s| f(c) \quad (4.21)$$

In first instance it is assumed that $f_2(c) = 0$, and the shear stresses of the liquid phase are considered null. This hypothesis allows the set of equations (4.15)-(4.17) to be solved, and the results of this investigation to be compared with the measurement of the velocity of the liquid phase published in Armanini et al. [11] (figure 4.3(a)).

With respect to the results proposed in Armanini et al. [11], the set of equations (4.15)-(4.17) is solved with a further variable, which is the velocity of the liquid phase. Moreover the interaction force is expressed through the voidage function derived in chapter 3, eq.(3.17). The preliminary considerations proposed in section 2.4.1 are confirmed by the distribution across the flow depth of the velocity of the liquid phase (figure 4.3(a)) obtained under the hypothesis that the stresses of the liquid phase are negligible compared with the other terms of the balance of the liquid phase in the longitudinal direction (figure 4.5).

A preliminary analysis of the nature of the solution of the complete set of equations (4.17), including the closure for the internal stresses of the liquid phase, shows that the velocity of the liquid phase, even in the simplest case of

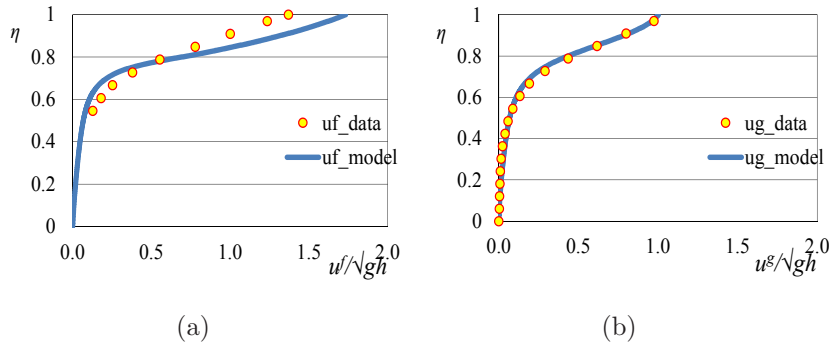


Figure 4.3: Comparison between results of the numerical simulation (solid line) and experimental data (circles) of: (a) velocity of the liquid phase; (b) velocity of the granular phase.

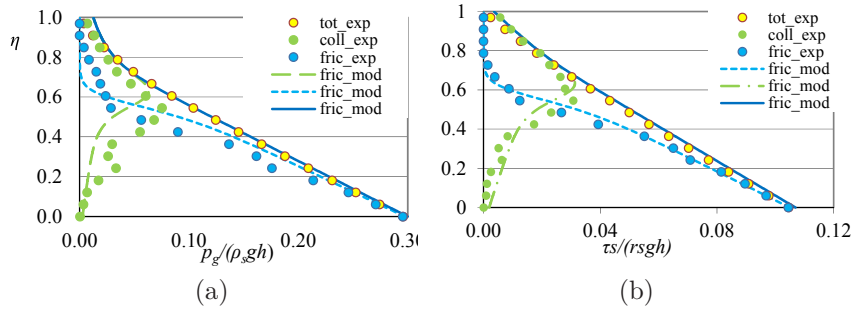


Figure 4.4: Collisional and frictional component of (a) pressure and of (b) shear stress. Comparison between computed (solid line) and observed (circles) values.

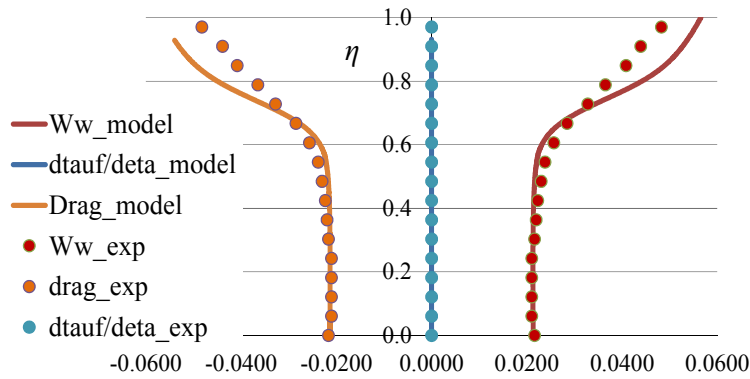


Figure 4.5: Terms of the momentum equation in x_1 of the liquid phase

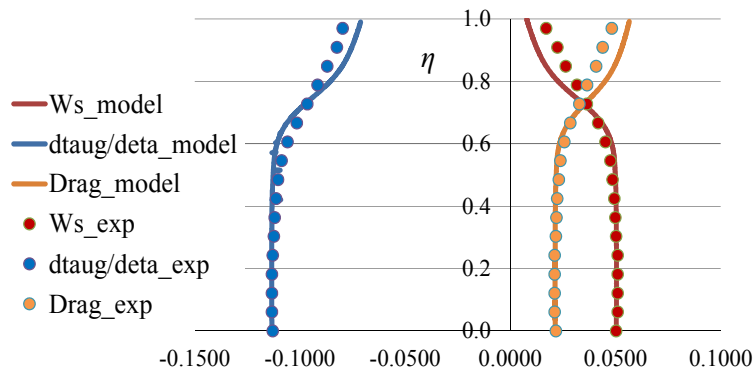


Figure 4.6: Terms of the momentum equation in x_1 of the solid phase.

laminar regime with constant viscosity, has four possible solutions real and non-real, depending on the absolute value of the difference in velocities of the two phases. The numerical resolutions of the complete set of equations is still an open issue.

Chapter 5

The extension to the 2D model

Chapter 5 tackles the extension of the complete system of equations of Chapter 4 to the non-uniform and non-stationary 2D case. The set of equations are implemented in a numerical model proposed by Dumbser [27]. A description of the numerical model, the geometry and the boundary conditions are presented. A set of adaptations of the numerical model for the application to granular flows are presented. The chapter concludes with some preliminary results.

5.1 Introduction

The system of equations (1.1) for a non-stationary flow in the plane x_1, x_2 , is:

$$\begin{aligned} \frac{\partial \rho_w(1-c)}{\partial t} + \frac{\partial \rho_w(1-c)u_1^f}{\partial x_1} + \frac{\partial \rho_w(1-c)u_2^f}{\partial x_2} &= 0 \\ \frac{\partial \rho_w(1-c)u_1^f}{\partial t} + \frac{\partial \rho_w(1-c)u_1^f u_1^f}{\partial x_1} + \frac{\partial \rho_w(1-c)u_1^f u_2^f}{\partial x_2} &= \\ -\rho_w(1-c)g \frac{\partial z}{\partial x_1} - (1-c) \frac{\partial p^f}{\partial x_1} + (1-c) \frac{\partial \tau_{11}^f}{\partial x_1} &+ \end{aligned} \quad (5.1)$$

$$+(1-c)\frac{\partial\tau_{21}^f}{\partial x_2} - D_1 \quad (5.2)$$

$$\begin{aligned} & \frac{\partial\rho_w(1-c)u_2^f}{\partial t} + \frac{\partial\rho_w(1-c)u_2^f u_1^f}{\partial x_1} + \frac{\partial\rho_w(1-c)u_2^f u_2^f}{\partial x_2} \\ & = -\rho_w(1-c)g\frac{\partial z}{\partial x_2} - (1-c)\frac{\partial p^f}{\partial x_2} + (1-c)\frac{\partial\tau_{22}^f}{\partial x_2} \\ & + (1-c)\frac{\partial\tau_{12}^f}{\partial x_1} - D_2 \end{aligned} \quad (5.3)$$

$$\frac{\partial\rho_s c}{\partial t} + \frac{\partial\rho_s c u_1^g}{\partial x_1} + \frac{\partial\rho_s c u_2^g}{\partial x_2} = 0 \quad (5.4)$$

$$\begin{aligned} & \frac{\partial\rho_s c u_1^g}{\partial t} + \frac{\partial\rho_s c u_1^g u_1^g}{\partial x_1} + \frac{\partial\rho_s c u_1^g u_2^g}{\partial x_2} \\ & = -\rho_s c g\frac{\partial z}{\partial x_1} - \frac{\partial p^g}{\partial x_1} + \frac{\partial\tau_{11}^g}{\partial x_1} + \frac{\partial\tau_{21}^g}{\partial x_2} - c\frac{\partial p^f}{\partial x_1} + c\frac{\partial\tau_{11}^f}{\partial x_1} \\ & + c\frac{\partial\tau_{21}^f}{\partial x_2} + D_1 \end{aligned} \quad (5.5)$$

$$\begin{aligned} & \frac{\partial\rho_s c u_2^g}{\partial t} + \frac{\partial\rho_s c u_2^g u_1^g}{\partial x_1} + \frac{\partial\rho_s c u_2^g u_2^g}{\partial x_2} \\ & = -\rho_s c g\frac{\partial z}{\partial x_2} - \frac{\partial p^g}{\partial x_2} + \frac{\partial\tau_{22}^g}{\partial x_2} + \frac{\partial\tau_{12}^g}{\partial x_1} - c\frac{\partial p^f}{\partial x_2} + c\frac{\partial\tau_{22}^f}{\partial x_2} \\ & + c\frac{\partial\tau_{12}^f}{\partial x_1} + D_2 \end{aligned} \quad (5.6)$$

$$\begin{aligned} & \frac{\partial\rho_s c \Theta}{\partial t} + \frac{\partial\rho_s c \Theta u_1^g}{\partial x_1} + \frac{\partial\rho_s c \Theta u_2^g}{\partial x_2} \\ & \frac{\partial}{\partial x_1} \left[\kappa_\theta \frac{\partial \Theta}{\partial x_1} \right] + \frac{\partial}{\partial x_2} \left[\kappa_\theta \frac{\partial \Theta}{\partial x_2} \right] + \mu^g \gamma \dot{g}^2 - f_5 \frac{\Theta^{1.5}}{d} \end{aligned} \quad (5.7)$$

where z is the vertical coordinate. The resulting system consists of a set of partial differential equations, (5.1)-(5.7), whose conservative part is hyperbolic, and can be written in the compact formulation, eq.(5.8):

$$\frac{d\mathbf{Q}}{dt} + \underline{\underline{\mathbf{A}}}(\mathbf{Q}) \cdot \nabla \mathbf{Q} = \mathbf{S}(\mathbf{Q}), \quad (5.8)$$

5.2 The numerical model for PDE equations

Recently Dumbser [27] developed a high-order, path conservative, WENO finite volume scheme, which solves the element interface with the new generalized Osher–type scheme [29], and is able to solve the BaerNunziato model for compressible multiphase flows. The domain Ω is discretized with an unstructured mesh, triangular for 2D flows. The sides of the triangles are called T_i . The numerical solutions is given as $u_h^n \in V_h$ where V_h is the space of piecewise polynomials of degree N . The numerical approximation is $w_h^n \in W_h$ where W_h is the space of piecewise polynomials of degree M , with $M \geq N$. The reconstruction is done by defining a stencil S_i containing the element T_i and an appropriate set of neighbors of T_i . The reconstructed solution is found by imposing a weak identity between the numerical and the approximated solutions, (5.9):

$$[\phi_k, w_h^n]_{T_j} = [\phi_k, u_h^n]_{T_j} \quad \forall T_j \in S_i \quad (5.9)$$

i.e. eq.(5.9) must hold at least exactly in the element T_i under consideration. ϕ_k is the test function of the space V_h used to evolve w_h^n inside each element with the local space-time Galerkin approach. The monotonicity is ensured using the unstructured WENO scheme. The governing PDE's, eqs.(5.8), are multiplied by θ_k , which is a test function $\in Z_h$ of the space of piecewise polynomials of degree M , and the resulting system is then integrated in time:

$$\begin{aligned} \left([\theta_k, q_h]_{T_i}^{t^{n+1}} - \left\langle \frac{\partial}{\partial t} \theta_k, q_h \right\rangle_{T_i} \right) + \langle \theta_k, \underline{\underline{A}}(q_h) \cdot \nabla q_h \rangle_{T_i} \\ = [\theta_k, w_h^n]_{T_i}^{t^n} + \langle \theta_k, S(q_h) \rangle_{T_i} \end{aligned} \quad (5.10)$$

The initial condition is the reconstructed solutions at time t^n , w_h^n . The result of the local system is called the predictor solution q_h , an element that is local in space and in time. The system can be solved very efficiently using

the one-step finite-volume and discontinuous Galerkin schemes developed in Dumbser et al. [28]. Finally, in order to update the numerical solution u_h^n from the time level t^n to the new time level t^{n+1} , a path-conservative $P_N P_M$ scheme is implemented, eq.(5.11):

$$\begin{aligned} [\phi_k, u_h^{t^{n+1}}]_{T_i}^{t^{n+1}} - [\phi_k, u_h^n]_{T_i}^{t^n} + \langle \phi_k, \underline{A}(q_h) \cdot \nabla q_h \rangle_{T_i, \partial T_i} \\ + \phi_k, D_{i+\frac{1}{2}}(q_h^-, q_h^+) \cdot \vec{n}_{\partial T_i} = \langle \phi_k, S(q_h) \rangle_{T_i} \end{aligned} \quad (5.11)$$

To solve the interface between the two elements of the volume, $D_{i+\frac{1}{2}}(q_h^-, q_h^+)$, a Osher-type scheme is used.

5.3 The equation of state of the liquid phase

In order to ensure that the pressure of the liquid phase is hydrostatic, the Tait equation of state [14], named EOS, is included by Dumbser [27]. This closure relation is also very common in weakly compressible smooth particle hydrodynamics (SPH) schemes, for the simulation of free surface flows. This simplification is in good agreement with the real behaviour of water in typical environmental flow conditions, i.e. close to atmospheric pressure and typical ambient temperatures.

The fluid pressure is expressed as:

$$p^f = k_f \left(\frac{\rho_f}{\rho_{fo}} - 1 \right)^\gamma \quad (5.12)$$

where k_f is a constant that governs the compressibility of the fluid and hence the speed of sound, ρ_f is the liquid density, ρ_{fo} is the liquid reference density at atmospheric standard conditions and γ is a parameter that is used to fit the EOS with experimental data. In the application to free surface flows, the Tait equation of state yields a relative pressure with respect to the atmospheric reference pressure ($p^f(\rho_{fo}) = 0$).

5.4 The equation of state of the granular phase

The pressure of the granular phase is given by the equation of state of the *heuristic model*. As is better explained in chapter 2, the equation of state is derived in analogy with the rheological formulation, and in uniform flow conditions satisfies the two boundary conditions: approaching the free surface it tends to the expression of the kinetic theory, while, at the boundary with the loose static bed, it reduces to an identity. From a theoretical point of view, in fact, this boundary represents the transition between the liquid and the solid behaviour of the granular flows, where the pressure cannot depend on the kinematic properties of the flow field such as the granular temperature. The equation of state of the *heuristic model* is given by an implicit expression depending on the *Savage number*:

$$p^g = p^g \frac{I_{so}}{I_{so} + I_s} + \rho_s f_1 \Theta \quad (5.13)$$

The formulation eq.(5.13) can be made explicit with simple steps, by substituting the expression of the *Savage number*:

$$(I_{so} + I_s)p^g = p^g I_{so} + f_1 \Theta (I_{so} + I_s) \quad (5.14)$$

$$\frac{(\dot{\gamma}d)^2}{p^g} p^g = f_1 \Theta \left(I_{so} + \frac{(\dot{\gamma}d)^2}{p^g} \right) \quad (5.15)$$

$$p^g (\dot{\gamma}d)^2 = f_1 \Theta p^g I_{so} + (\dot{\gamma}d)^2 f_1 \Theta \quad (5.16)$$

$$p^g ((\dot{\gamma}d)^2 - f_1 \Theta I_{so}) = (\dot{\gamma}d)^2 f_1 \Theta \quad (5.17)$$

which results in:

$$p^g = \frac{(\dot{\gamma}d)^2 f_1 \Theta}{(\dot{\gamma}d)^2 - f_1 \Theta I_{so}} \quad (5.18)$$

However, from a numerical point of view, the explicit formulation of the equation of state of the *heuristic model*, at the limit with the loose static

bed, exhibits two solutions:

- 1: $(\dot{\gamma}d)^2 = f_1\Theta I_{so}$
- 2: $(\dot{\gamma}d)^2 \gg f_1\Theta I_{so}$

To avoid this ambiguity, and in order to supply an equation of state that is also valid in the solid state of the granular flows, in analogy to the Tait equation used for the fluid pressure, a compressible behaviour of the solid state is included:

$$p^{g-com} = k_s \left(\frac{\rho_s}{\rho_{so}} - 1 \right)^\gamma \quad (5.19)$$

such that the equation of state for the granular phase becomes:

$$p^g = p^{g-com} + p^g \frac{I_{so}}{I_{so} + I_s} + f_1 \rho_s \Theta \quad (5.20)$$

The hypothesis that the solid phase is compressible is also proposed in the literature of the numerical modelization of two phase granular flows [60]. Since a new variable is introduced, ρ_s , a further partial differential equation is needed and the final system to solve consists of 8 equations:

$$\begin{aligned} \frac{\partial \rho_w(1-c)}{\partial t} + \frac{\partial \rho_w(1-c)u_1^f}{\partial x_1} + \frac{\partial \rho_w(1-c)u_2^f}{\partial x_2} &= 0 \quad (5.21) \\ \frac{\partial \rho_w(1-c)u_1^f}{\partial t} + \frac{\partial \rho_w(1-c)u_1^f u_1^f}{\partial x_1} + \frac{\partial \rho_w(1-c)u_1^f u_2^f}{\partial x_2} + \frac{\partial(1-c)p^f}{\partial x_1} \\ &= -\rho_w(1-c)g \frac{\partial z}{\partial x_1} - p^f \frac{\partial c}{\partial x_1} + \frac{\partial(1-c)\tau_{11}^f}{\partial x_1} + \tau_{11}^f \frac{\partial c}{\partial x_1} \\ &\quad + \frac{\partial(1-c)\tau_{21}^f}{\partial x_2} + \tau_{21}^f \frac{\partial c}{\partial x_2} - D_1 \quad (5.22) \\ \frac{\partial \rho_w(1-c)u_2^f}{\partial t} + \frac{\partial \rho_w(1-c)u_2^f u_1^f}{\partial x_1} + \frac{\partial \rho_w(1-c)u_2^f u_2^f}{\partial x_2} + \frac{\partial(1-c)p^f}{\partial x_2} &= \end{aligned}$$

$$\begin{aligned}
&= -\rho_w(1-c)g\frac{\partial z}{\partial x_2} - p^f\frac{\partial c}{\partial x_2} + \frac{\partial(1-c)\tau_{22}^f}{\partial x_2} + \tau_{22}^f\frac{\partial c}{\partial x_2} \\
&\quad + \frac{\partial(1-c)\tau_{12}^f}{\partial x_1} + \tau_{12}^f\frac{\partial c}{\partial x_1} - D_2
\end{aligned} \tag{5.23}$$

$$\frac{\partial\rho_s c}{\partial t} + \frac{\partial\rho_s c u_1^g}{\partial x_1} + \frac{\partial\rho_s c u_2^g}{\partial x_2} = 0 \tag{5.24}$$

$$\begin{aligned}
&\frac{\partial\rho_s c u_1^g}{\partial t} + \frac{\partial\rho_s c u_1^g u_1^g}{\partial x_1} + \frac{\partial\rho_s c u_1^g u_2^g}{\partial x_2} + \frac{\partial c p^f}{\partial x_1} + \frac{\partial f_1 \rho_s \Theta}{\partial x_1} + \frac{\partial p^{g-com}}{\partial x_1} \\
&= -\rho_s c g \frac{\partial z}{\partial x_1} - \frac{\partial}{\partial x_1} p^g \frac{I_{so}}{I_{so} + I_s} + \frac{\partial}{\partial x_1} \tan \varphi p^g \frac{I_{so}}{I_{so} + I_s} + \frac{\partial}{\partial x_1} \mu^{g-coll} \frac{\partial u_1^g}{\partial x_1} \\
&\quad + \frac{\partial}{\partial x_2} \tan \varphi p^g \frac{I_{so}}{I_{so} + I_s} + \frac{\partial}{\partial x_2} \mu^{g-coll} \left(\frac{\partial u_2^g}{\partial x_1} + \frac{\partial u_1^g}{\partial x_2} \right) + p^f \frac{\partial c}{\partial x_1} \\
&\quad + \frac{\partial c \tau_{11}^f}{\partial x_1} - \tau_{11}^f \frac{\partial c}{\partial x_1} + \frac{\partial \tau_{21}^f c}{\partial x_2} - \tau_{21}^f \frac{\partial c}{\partial x_2} + D_1
\end{aligned} \tag{5.25}$$

$$\begin{aligned}
&\frac{\partial\rho_s c u_2^g}{\partial t} + \frac{\partial\rho_s c u_2^g u_1^g}{\partial x_1} + \frac{\partial\rho_s c u_2^g u_2^g}{\partial x_2} + \frac{\partial c p^f}{\partial x_2} + \frac{\partial f_1 \rho_s \Theta}{\partial x_2} + \frac{\partial p^{g-com}}{\partial x_2} \\
&= -\rho_s c g \frac{\partial z}{\partial x_2} - \frac{\partial}{\partial x_2} p^g \frac{I_{so}}{I_{so} + I_s} + \frac{\partial}{\partial x_2} \tan \varphi p^g \frac{I_{so}}{I_{so} + I_s} + \frac{\partial}{\partial x_2} \mu^{g-coll} \frac{\partial u_2^g}{\partial x_2} \\
&\quad + \frac{\partial}{\partial x_1} \tan \varphi p^g \frac{I_{so}}{I_{so} + I_s} + \frac{\partial}{\partial x_1} \mu^{g-coll} \left(\frac{\partial u_1^g}{\partial x_2} + \frac{\partial u_2^g}{\partial x_1} \right) + p^f \frac{\partial c}{\partial x_2} \\
&\quad + \frac{\partial c \tau_{22}^f}{\partial x_2} - \tau_{22}^f \frac{\partial c}{\partial x_2} + \frac{\partial c \tau_{12}^f}{\partial x_1} - \tau_{12}^f \frac{\partial c}{\partial x_1} + D_2
\end{aligned} \tag{5.26}$$

$$\begin{aligned}
&\frac{\partial\rho_s c \Theta}{\partial t} + \frac{\partial\rho_s c \Theta u_1^g}{\partial x_1} + \frac{\partial\rho_s c \Theta u_2^g}{\partial x_2} \\
&\quad \frac{\partial}{\partial x_1} \left[\kappa_\theta \frac{\partial \Theta}{\partial x_1} \right] + \frac{\partial}{\partial x_2} \left[\kappa_\theta \frac{\partial \Theta}{\partial x_2} \right] + \mu^g \gamma^{g^2} - f_5 \frac{\Theta^{1.5}}{d}
\end{aligned} \tag{5.27}$$

$$\frac{\partial\rho_s}{\partial t} + \frac{\partial\rho_s u_1^g}{\partial x_1} + \frac{\partial\rho_s u_2^g}{\partial x_2} = 0 \tag{5.28}$$

5.4.1 The numerical formulation

For the numerical formulation, the system of equations (5.21)-(5.28), which shows 8 real eigenvalues, is written as:

$$\partial W_t + \partial F_x(W) + \partial F_y(W) + \partial G_x(W; \nabla W) + \partial G_y(W; \nabla W) + NC_x + NC_y = S \quad (5.29)$$

where the vector W is of the conservative variables is:

$$\begin{aligned} W(1) &= \rho_w(1 - c) \\ W(2) &= \rho_w(1 - c)u_1^f \\ W(3) &= \rho_w(1 - c)u_2^f \\ W(4) &= \rho_s c \\ W(5) &= \rho_s c u_1^g \\ W(6) &= \rho_s c u_2^g \\ W(7) &= \rho_s c \Theta \\ W(8) &= \rho_s \end{aligned}$$

The vector of the fluxes in the x_1 longitudinal direction is:

$$\begin{aligned} F_x(1) &= W(2) \\ F_x(2) &= W(2)W(2)/W(1) + (1 - c)p_w \\ F_x(3) &= W(3)W(2)/W(1) \\ F_x(4) &= W(5) \\ F_x(5) &= W(5)W(5)/W(4) + cp_w + f_1\rho_s\Theta + p^{g-com} \\ F_x(6) &= W(5)W(6)/W(4) \\ F_x(7) &= W(7)W(5)/W(4) \\ F_x(8) &= W(8)W(5)/W(4) \end{aligned}$$

The vector of fluxes in the y normal directions is:

$$\begin{aligned}
F_y(1) &= W(3) \\
F_y(2) &= W(2)W(3)/W(1) \\
F_y(3) &= W(3)W(3)/W(1) + (1 - c)p_w \\
F_y(4) &= W(6) \\
F_y(5) &= W(5)W(6)/W(4) \\
F_y(6) &= W(6)W(6)/W(4) + cp_w + f_1\rho_s\Theta + p^{g-com} \\
F_y(7) &= W(7)W(6)/W(4) \\
F_y(8) &= W(8)W(6)/W(4)
\end{aligned}$$

The vector of viscous fluxes, in the x longitudinal direction, is:

$$\begin{aligned}
G_x(1) &= 0 \\
G_x(2) &= (1 - c)2\mu_w \frac{\partial u_1^f}{\partial x_1} \\
G_x(3) &= (1 - c)\mu_w \left(\frac{\partial u_1^f}{\partial x_2} + \frac{\partial u_2^f}{\partial x_1} \right) \\
G_x(4) &= 0 \\
G_x(5) &= -p^g \frac{I_{so}}{I_{so} + I_s} + \tan \varphi p^g \frac{I_{so}}{I_{so} + I_s} + 2\mu^{g-coll} \frac{\partial u_1^g}{\partial x_1} + 2c\mu_w \frac{\partial u_1^f}{\partial x_1} \\
G_x(6) &= \tan \varphi p^g \frac{I_{so}}{I_{so} + I_s} + \mu^{g-coll} \left(\frac{\partial u_1^g}{\partial x_2} + \frac{\partial u_2^g}{\partial x_1} \right) + c\mu_w \left(\frac{\partial u_1^f}{\partial x_2} + \frac{\partial u_2^f}{\partial x_1} \right) \\
G_x(7) &= k_\Theta \frac{\partial \Theta}{\partial x_1} \\
G_x(8) &= 0
\end{aligned}$$

The vector of viscous fluxes, in the y normal direction, is:

$$\begin{aligned}
G_y(1) &= 0 \\
G_y(2) &= (1 - c)\mu_w \left(\frac{\partial u_1^f}{\partial x_2} + \frac{\partial u_2^f}{\partial x_1} \right) \\
G_y(3) &= (1 - c)2\mu_w \frac{\partial u_2^f}{\partial x_2} \\
G_y(4) &= 0 \\
G_y(5) &= \tan \varphi \frac{I_{so}}{I_{so} + I_s} + \mu^{g-coll} \left(\frac{\partial u_1^g}{\partial x_2} + \frac{\partial u_1^g}{\partial x_1} \right) + c\mu_w \left(\frac{\partial u_1^f}{\partial x_2} + \frac{\partial u_2^f}{\partial x_1} \right) \\
G_y(6) &= p^g \frac{I_{so}}{I_{so} + I_s} + \tan \varphi p^g \frac{I_{so}}{I_{so} + I_s} + 2\mu^{g-coll} \frac{\partial u_2^g}{\partial x_2} + 2c\mu_w \frac{\partial u_2^f}{\partial x_2} \\
G_y(7) &= k_\Theta \frac{\partial \Theta}{\partial x_2} \\
G_y(8) &= 0
\end{aligned}$$

the vector of non-conservative terms, in the x longitudinal direction, is:

$$\begin{aligned}
NC_x(1) &= 0 \\
NC_x(2) &= -p_w c + 2\mu_w \frac{\partial u_1^f}{\partial x_1} c \\
NC_x(3) &= \mu_w \left(\frac{\partial u_1^f}{\partial x_2} + \frac{\partial u_2^f}{\partial x_1} \right) c \\
NC_x(4) &= 0 \\
NC_x(5) &= p_w c - 2\mu_w \frac{\partial u_1^f}{\partial x_1} c \\
NC_x(6) &= -\mu_w \left(\frac{\partial u_1^f}{\partial x_2} + \frac{\partial u_2^f}{\partial x_1} \right) c \\
NC_x(7) &= 0 \\
NC_x(8) &= 0
\end{aligned}$$

The vector of non-conservative terms, in the y normal direction, is:

$$\begin{aligned}
NC_y(1) &= 0 \\
NC_y(2) &= \mu_w \left(\frac{\partial u_1^f}{\partial x_2} + \frac{\partial u_2^f}{\partial x_1} \right) c \\
NC_y(3) &= -p_w c + 2\mu_w \frac{\partial u_2^f}{\partial x_2} c \\
NC_y(4) &= 0 \\
NC_y(5) &= -\mu_w \left(\frac{\partial u_1^f}{\partial x_2} + \frac{\partial u_2^f}{\partial x_1} \right) c \\
NC_y(6) &= p_w c - 2\mu_w \frac{\partial u_2^f}{\partial x_2} c \\
NC_y(7) &= 0 \\
NC_y(8) &= 0
\end{aligned}$$

and finally the vector of the source terms is:

$$\begin{aligned}
S(1) &= 0 \\
S(2) &= -\rho_w g(1 - c) \sin \alpha - D_1 \\
S(3) &= -\rho_w g(1 - c) \cos \alpha - D_2 \\
S(4) &= 0 \\
S(5) &= -\rho_s g c \sin \alpha + D_1 \\
S(6) &= -\rho_s g c \cos \alpha + D_2 \\
S(7) &= -f_5 \frac{\Theta^{1.5}}{d} \\
S(8) &= 0
\end{aligned}$$

5.4.1.1 Modifications of the numerical model

The Bear–Nunziato model is solved under the hypothesis that the interaction among the different phases is negligible [27]. For submerged granular flows



Figure 5.1: Geometry in Gambit.

the interaction between the liquid and the solid phase plays an important role (please refer to the content of the Chapter 3). The numerical model is then modified to include the fact that the fluxes also depend on the gradient of the vector of conservative variables.

5.4.2 Geometry and Boundary Conditions

As a preliminary analysis of the *PDE solve* numerical model, the experimental configuration and the data from the laboratory investigations proposed in section 2.4 are reproduced.

The domain is designed using *Gambit2D* and represents the channel of figure 2.2. In figure 5.1 the channel is reproduced by a rectangle 2 *m* long and 0.0617 *m* in height. Furthermore, *Gambit 2D*, setup on the generic solver, allows to assign the boundary conditions and to create a triangular mesh of data spacing.

Different types of boundary conditions are considered: wall, Lagrangian wall, space-time dependent, constant Dirichlet boundaries and periodic boundaries. In particular, in order to reproduce the case studied in section 2.4, at the bottom a wall type boundary is assigned, while at the free surface constant Dirichlet type boundary conditions are imposed. In order to reproduce the re-circulation of the channel setup, the two vertical sides are periodic boundaries type.

The output of *Gambit 2D* is the geometry designed, with the boundaries assigned, and discretized by a mesh. It is exported in a file.neu and represents the domain of calculus.

The numerical model *PDE solve* reads a file including all input information:

-
- number of space dimensions ($2D$ or $3D$)
 - equation subtype, i.e. a number that identifies the set of equations to solve
 - the number of variables of the PDE system
 - the number of auxiliary variables
 - the name and values of the constant of the problem:
 - the constants of compressibility of the liquid phase and of the solid phase ($k_f = k_s$) and the constant γ ;
 - the reference densities (ρ_{fo} and ρ_{so}),
 - the value of the parameter of the *heuristic model*, I_{so} ,
 - the water depth h ,
 - the diameter of the spherical particles d
 - the value of the maximum packing concentration c^*
 - the initial conditions
 - the boundary conditions
 - the file name of the mesh and the type of discretization
 - the numerical inputs: the local space-time Galerkin predictor type; the initial guess type in time, the orders of the original basis and of the reconstructed solution, the type of the reconstructed solver, the method to solve the numerical fluxes and some numerical parameters such as the CFL number, the minimum interval of time discretization and the tolerance.
 - finally the instruction for where and how to write the outputs

5.5 Preliminary results

A preliminary test of the numerical model is to reproduce the uniform flow conditions that are the output of the simulation proposed in Chapter 2.

The boundary conditions and the initial conditions for the PDE model are the data out of the DAE model. Figures 5.2(a), 5.2(b), 5.3(a) ad 5.3(b) show the distributions across the flow depth of the inputs of the numerical simulation of Chapter 2, named *DAE*, with line, while the inputs of the *PDE* are in dots. It seems that the *PDE* are able to reproduce in a correct way the primitive variables. Furthermore, the comparison reported in figures 5.4(a) and 5.4(b) shows that the numerical model *PDEs* is able to correctly compute the distributions across the flow depth of the stresses of the granular phase of *DAEs*.

With respect to the results of *DAEs*, the equation of state of the *heuristic model* is modified to include the compressibility of the solid phase, and it seems from figure 5.4(a) that this hypothesis gives reasonable results. The mismatches of figure 5.4(b) near the free surfaces are probably due to the different computational procedure of the gradients of the variables of the two numerical solvers compared.

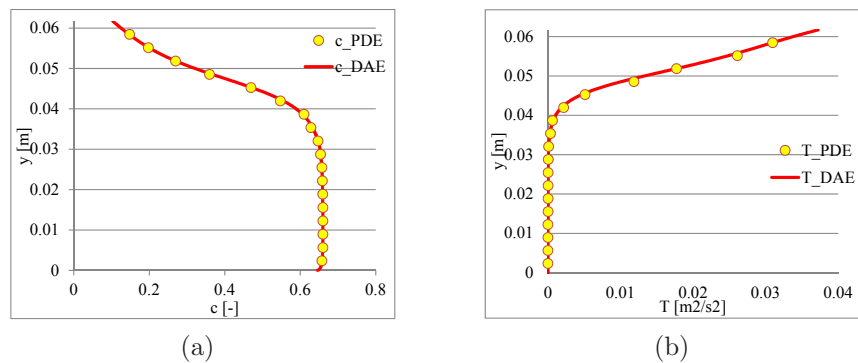


Figure 5.2: Comparison between results of the numerical simulation DAE (solid line) and results of the numerical simulation PDE (circles) of: (a) particle concentration profile; (b) granular temperature profile.

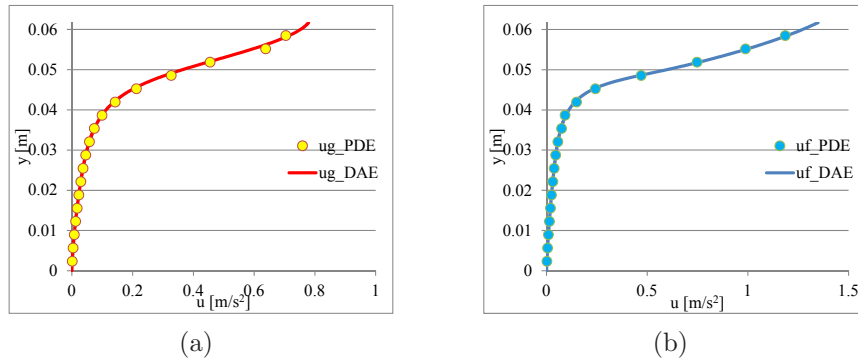


Figure 5.3: Comparison between results of the numerical simulation DAE (solid line) and results of the numerical simulation PDE (circles) of: (a) granular velocity profile; (b) liquid velocity gradient profile.

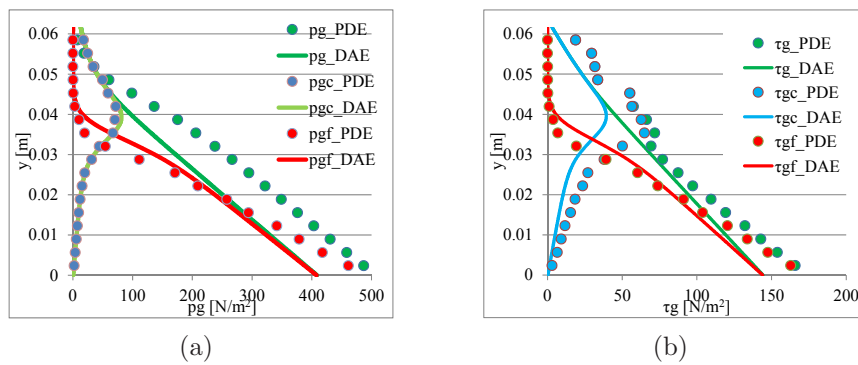


Figure 5.4: Comparison between results of the numerical simulation DAE (solid line) and results of the numerical simulation PDE (circles) of: (a) granular pressure profile; (b) granular shear stresses profile.

The content of this chapter is a preliminary dissertation on the numerical method proposed in order to simulate the unsteady flow of granular fluids, such as a dam break, and then, passing to the 3D formulation, the flow in enlargements and narrowing of granular flows. In the hydraulic laboratory of the University of Trento some data on dam breaks have already been analyzed [33] while we are working on analyzing the experimental data for the non-uniform motion.

Chapter 6

Conclusions

The thesis tackles the mechanics of granular flows. In particular, focusing on submerged granular flows driven by gravity, two phases are observed. In the framework of the thesis, the interstitial fluid is water, while the solid phase is composed of identical spherical heavy particles with constant diameter. From a physical point of view, the more reliable way to describe the behaviour of the solid phase is to treat it as a granular flow. The phenomenon is characterized by an absence of mass exchange between the two phases. The mechanics is described by the set of mass and momentum conservation equations, written separately for each phase. The closure relations for the stresses of the granular phase, of the interstitial fluid and of the interphase forces are needed. The thesis discusses these three aspects.

The main contributions of the thesis regard the rheology of the granular phase. It is observed that in uniform flow conditions, the granular phase behaves like a gas approaching the free surface, like a solid in a mobile static bed composed of the same material, and like a liquid in an intermediate region [5]. The mechanics of the granular phase is based on the types of contacts among particles: if the contacts are instantaneous, the regime is called *collisional*, while if the contacts become long lasting and involve several particles at the same time, the regime is called *frictional*. The experimental

evidence [5] shows, in fact, that in uniform flow conditions, the collisional regime dominates approaching the free surface, while the frictional regime becomes relevant approaching the loose static bed. The novelty of the approach adopted in the thesis is to consider the collisional regime and the frictional regime as coexisting across the flow depth, with a mechanism of intermittency similar to that of the turbulent boundary layer on smooth wall [10]. The collisional regime is described by the kinetic theory of dense gases [55], which, in analogy with the kinetic theory, replaces the concept of ordinary temperature with the concept of granular temperature, which is a measurement of the fluctuations of the granular phase, and adds a dissipation term, due to the inelastic collisions among particles, to the kinetic energy balance.

Regarding the frictional regime, the observations and the intuition suggest that the rheology shows, at the same time, both shear-dependent and shear-independent features. In this respect, an analysis of the forces involved identifies the *Savage number* as the dimensionless parameter that governs the frictional regime. A heuristic relation for the shear stress of the frictional regime is derived as a function of the *Savage number*. In analogy an equation of state for the frictional regime is derived. Since the literature of the frictional regime of granular flows lacks a theory, the considerations reported in Chapter 2 represent the major contribution of the thesis. The model, named the *heuristic model*, is solved numerically, [6], and the results are compared with experimental data [11]. With respect to previous works [64, 34, 22, 44, 20], the formulation of the *heuristic model* allows the concentration of the solid phase to become an independent variable of the problem, in order to avoid the assumption that the concentration is constant, which is in contrast with experimental evidence, and to avoid any empirical formulations.

A further novelty of the *heuristic model*, [11], regards the equation of the total energy balance of the granular phase. An attempt to explain the mechanisms of exchange of energy, among different terms of the total energy

balance and of the kinetic energy balance and between the terms of the two balances is provided. An analysis of the order of magnitudes of the terms of the kinetic energy balance suggests that the granular temperature also plays a role in the frictional regime.

Concerning the interphase forces, a proper relation, valid also for hyper-concentrated flows, is theoretically derived. A specific experimental investigation is carried out in order to understand the difference between the drag averaged over time and the drag calculated with respect to the average velocities. This difference between the two drags, named residual drag, represents the contribution to the drag due to the correlations between the fluctuating components of the concentration and of the velocities. Moreover, the role of this correlation in the kinetic energy balance is analyzed, comparing different approaches [39, 11].

Regarding the rheology of the interstitial fluid, it is water treated with a Newtonian rheology. In the framework of the thesis different relations for the stresses of the liquid phase are provided. For the laminar regime, the viscosity of water is modified to account for the presence of particles [30]. For the turbulent regime different models are considered: the simplest approach is to modify the mixing-length model with a mixing length dependent on the concentration of the granular phase, while a more complicated approach is to modify the equations of the $k - \epsilon$ model of turbulence through a term due to the work done by the granular phase [57].

Finally, the application to non-stationary and non-uniform flow conditions of the theory developed in the thesis in two dimensions is implemented with preliminary results.

Bibliography

- [1] Ancey, C. and P. Evesque (2000). Frictional-collisional regime for granular suspension flows down an inclined channel. *Physical Review E* 62(6), 8349.
- [2] Armanini, A. (2005). *Principi di Idraulica Fluviale*. Bios. in Italian.
- [3] Armanini, A. (2010). Models of two-phase liquid and granular flows keynote lecture. *Proceedings of the XXXII Italian congress of hydraulic and hydraulic engineering Farina Editore*. in Italian.
- [4] Armanini, A. (2013). Granular flows driven by gravity. *Journal of Hydraulic Research* 51(2), 111–120.
- [5] Armanini, A., H. Capart, L. Fraccarollo, and M. Larcher (2005). Rheological stratification in experimental free-surface flows of granular-liquid mixtures. *Journal of Fluid Mechanics* 532, 269–319.
- [6] Armanini, A., M. Dumbser, E. Nucci, and M. Larcher (2012). Dynamics of submerged gravitational granular flows. *Numerical Methods for Hyperbolic Equations*, 157.
- [7] Armanini, A., L. Fraccarollo, and M. Larcher (2003). *Debris flow*. Encyclopedia of Hydrological Sciences - Wiley Online Library.
- [8] Armanini, A., L. Fraccarollo, and M. Larcher (2008). Liquid-granular channel flow dynamics. *Powder Technology* 182(2), 218–227.

-
- [9] Armanini, A., L. Fraccarollo, and G. Rosatti (2009). Two-dimensional simulation of debris flows in erodible channels. *Computers & Geosciences* 35(5), 993–1006.
- [10] Armanini, A., M. Larcher, and L. Fraccarollo (2009). Intermittency of rheological regimes in uniform liquid-granular flows. *Physical Review E* 79(5), 051306.
- [11] Armanini, A., M. Larcher, E. Nucci, and M. Dumbser (2014). Submerged granular channel flows driven by gravity. *Advances in Water Resources* 63, 1–10.
- [12] Armanini, A. and A. Paris (2009). Global relations for liquid-granular flows over mobile bed in a wide range of slope values. *Proceedings of the 32nd IAHR Congress*, 9–14.
- [13] Bagnold, R. A. (1954). Experiments on a gravity-free dispersion of large solid spheres in a newtonian fluid under shear. *Proceedings of the Royal Society of London. Series A. Mathematical and Physical Sciences* 225(1160), 49–63.
- [14] Batchelor, G. K. (2000). *An introduction to fluid dynamics*. Cambridge university press.
- [15] Boussinesq, J. (1877). Essai sur la thorie des eaux courantes. *Memoires de l'Academie des sciences de l'Institut de France* 231, 252260.
- [16] Campbell, C. S. (1990). Rapid granular flows. *Annual Review of Fluid Mechanics* 22(1), 57–90.
- [17] Carman, P. C. (1956). *Flow of gases through porous media*. Butterworths Scientific Publications London.
- [18] Carnahan, N. F. and K. E. Starling (1969). Equation of state for nonattracting rigid spheres. *The Journal of Chemical Physics* 51(2), 635–636.

-
- [19] Chapman, S. and T. Cowling (1971). The mathematical theory of nonuniform gases, (cambridge, 1952). *For the same form of the second side of (18) see GH Wannier: American Journal of Physics 39, 281.*
- [20] Chialvo, S., J. Sun, and S. Sundaresan (2012). Bridging the rheology of granular flows in three regimes. *Physical Review E 85(2)*, 021305.
- [21] Crowe, C., T. Troutt, and J. Chung (1996). Numerical models for two-phase turbulent flows. *Annual Review of Fluid Mechanics 28(1)*, 11–43.
- [22] da Cruz, F., S. Emam, M. Prochnow, J.-N. Roux, and F. Chevoir (2005). Rheophysics of dense granular materials: Discrete simulation of plane shear flows. *Physical Review E 72(2)*, 021309.
- [23] Dallavalle, J. (1948). *Micrometrics*. Pitman.
- [24] Desai, C. and H. J. Siriwardane (1984). *Constitutive laws for engineering materials, with emphasis on geologic materials*. New Jersey: Prentice-Hall Inc. Englewood Cliffs.
- [25] di Felice, R. (1995). Hydrodynamics of liquid fluidisation. *Chemical Engineering Science 50(8)*, 1213–1245.
- [26] Drew, D. (1983). Mathematical modeling of two-phase flow. *Annual review of fluid mechanics 15(1)*, 261–291.
- [27] Dumbser, M. (2011). A simple two-phase method for the simulation of complex free surface flows. *Computer Methods in Applied Mechanics and Engineering 200(9)*, 1204–1219.
- [28] Dumbser, M., D. S. Balsara, E. F. Toro, and C.-D. Munz (2008). A unified framework for the construction of one-step finite volume and discontinuous galerkin schemes on unstructured meshes. *Journal of Computational Physics 227(18)*, 8209–8253.

-
- [29] Dumbser, M. and E. F. Toro (2011). A simple extension of the osher riemann solver to non-conservative hyperbolic systems. *Journal of Scientific Computing* 48(1-3), 70–88.
- [30] Einstein, A. (1906). A new determination of molecular dimensions. *Annual Physics* 19, 289–306. in German.
- [31] Elghobashi, S. and G. Truesdell (1993). On the two-way interaction between homogeneous turbulence and dispersed solid particles. i: Turbulence modification. *Physics of Fluids A: Fluid Dynamics (1989-1993)* 5(7), 1790–1801.
- [32] Fraccarollo, L., M. Larcher, and A. Armanini (2007). Depth-averaged relations for granular-liquid uniform flows over mobile bed in a wide range of slope values. *Granular Matter* 9(3-4), 145–157.
- [33] Fraccarollo, L. and E. F. Toro (1995). Experimental and numerical assessment of the shallow water model for two-dimensional dam-break type problems. *Journal of hydraulic research* 33(6), 843–864.
- [34] GDR-MiDi (2004). On dense granular flows. *European Physical Journal E* 14, 341–365.
- [35] Gidaspow, D. and L. Huilin (1998). Equation of state and radial distribution functions of fcc particles in a cfb. *AIChE Journal* 44(2), 279–293.
- [36] Goldhirsch, I. (2008). Introduction to granular temperature. *Powder Technology* 182(2), 130–136.
- [37] Gray, J. M. N. T., M. Wieland, and K. Hutter (1999). Gravity-driven free surface flow of granular avalanches over complex basal topography. *Proceedings of the Royal Society A: Mathematical, Physical and Engineering Sciences* 455(1985), 1841–1874.

-
- [38] Hill, H. M. (1966). Bed forms due to a fluid stream. *Journal of the Hydraulics Division, Proc. ASCE* 92, 127–143.
- [39] Hsu, T.-J., J. T. Jenkins, and P. L.-F. Liu (2003). On two-phase sediment transport: Dilute flow. *Journal of Geophysical Research: Oceans (1978–2012)* 108(C3).
- [40] Hsu, T.-J., J. T. Jenkins, and P. L.-F. Liu (2004). On two-phase sediment transport: sheet flow of massive particles. *Proceedings of the Royal Society of London. Series A: Mathematical, Physical and Engineering Sciences* 460(2048), 2223–2250.
- [41] Iverson, R. M. (1997). The physics of debris flows. *Reviews of geophysics* 35(3), 245–296.
- [42] Iverson, R. M. (2012). Elementary theory of bed-sediment entrainment by debris flows and avalanches. *Journal of Geophysical Research* 117(F3), F03006.
- [43] Jaeger, H. M., S. R. Nagel, and R. P. Behringer (1996). Granular solids, liquids, and gases. *Reviews of Modern Physics* 68(4), 1259.
- [44] Jenkins, J. T. (2007). Dense inclined flows of inelastic spheres. *Granular Matter* 10(1), 47–52.
- [45] Jenkins, J. T. and D. M. Hanes (1998). Collisional sheet flows of sediment driven by a turbulent fluid. *Journal of Fluid Mechanics* 370, 29–52.
- [46] Jenkins, J. T. and M. W. Richman (1985). Kinetic theory for plane flows of a dense gas of identical, rough, inelastic, circular disks. *Physics of Fluids (1958-1988)* 28(12), 3485–3494.
- [47] Jenkins, J. T. and M. W. Richman (1988). Plane simple shear of smooth inelastic circular disks: the anisotropy of the second moment in the dilute and dense limits. *Journal of Fluid Mechanics* 192, 313–328.

-
- [48] Jenkins, J. T. and S. B. Savage (1983). A theory for the rapid flow of identical, smooth, nearly elastic, spherical particles. *Journal of Fluid Mechanics* 130, 187–202.
- [49] Johnson, P. C. and R. Jackson (1987). Frictional-collisional constitutive relations for granular materials, with application to plane shearing. *Journal of Fluid Mechanics* 176, 67–93.
- [50] Johnson, P. C., P. Nott, and R. Jackson (1990). Frictional-collisional equations of motion for particulate flows and their application to chutes. *Journal of Fluid Mechanics* 210, 501–535.
- [51] Jop, P., Y. Forterre, and O. Pouliquen (2005). Crucial role of sidewalls in granular surface flows: consequences for the rheology. *Journal of Fluid Mechanics* 541(1), 167.
- [52] Lois, G., A. Lemaître, and J. Carlson (2005). Numerical tests of constitutive laws for dense granular flows. *Physical Review E* 72(5), 051303.
- [53] Louge, M. Y. (2003). Model for dense granular flows down bumpy inclines. *Physical review. E, Statistical, nonlinear, and soft matter physics* 67, 061303.
- [54] Lun, C. and S. Savage (1986). The effects of an impact velocity dependent coefficient of restitution on stresses developed by sheared granular materials. *Acta Mechanica* 63(1-4), 15–44.
- [55] Lun, C., S. Savage, D. Jeffrey, and N. Chepuruiy (1984). Kinetic theories for granular flow: inelastic particles in couette flow and slightly inelastic particles in general flow field. *Journal of Fluids Mechanics* 140, 223–256.
- [56] Mancabelli, R. (2014). Interazione solido liquida nei miscugli granulari. *DICAM, University of Trento*. Master Thesis, a.a. 2012-2013, in Italian.

-
- [57] Meruane, C., A. Tamburrino, O. Roche, et al. (2010). On the role of the ambient fluid on gravitational granular flow dynamics. *Journal of Fluid Mechanics* 648, 381.
- [58] Mitarai, N. and H. Nakanishi (2004). Density profile of dense granular flow down a rough slope. *Physical Review Letters* 94, 128001.
- [59] Nucci, E., A. Armanini, and M. Larcher (2014). The role of interphase forces in submerged granular flows driven by gravity. *Proceedings of River-Flows 2014*, 859–866.
- [60] Pitman, E. B. and L. Le (2005). A two-fluid model for avalanche and debris flows. *Philosophical transactions. Series A, Mathematical, physical, and engineering sciences* 363(1832), 1573–601.
- [61] Prandtl, L. (1925). Bericht über untersuchungen zur ausgebildeten turbulenz. *ZAMM - Journal of Applied Mathematics and Mechanics* 5(2), 136–139.
- [62] Rodi, W. (1993). *Turbulence models and their application in hydraulics*. CRC Press.
- [63] Savage, S. B. (1984). The mechanics of rapid granular flows. *Advances in applied mechanics* 24, 289–366.
- [64] Savage, S. B. and K. Hutter (1991). The dynamics of avalanches of granular materials from initiation to runout. Part I: Analysis. *Acta Mechanica* 86(1-4), 201–223.
- [65] Taberlet, N., P. Richard, A. Valance, W. Losert, J. M. Pasini, J. T. Jenkins, and R. Delannay (2003). Superstable granular heap in a thin channel. *Physical review letters* 91(26), 264301.
- [66] Takahashi, T. (1991). *Debris flow*. Balkema.

- [67] Truesdell, C. (1984). *The elements of continuum mechanics*. Springer.
- [68] Zhang, Y. and J. M. Reese (2003). Gas turbulence modulation in a two-fluid model for gassolid flows. *AIChE Journal* 49(12), 3048–3065.

Appendix A

Equations of the flow in the column

The flow in the column is a 3D flow in $x = (x_1, x_2, x_3)$, where x_3 the vertical direction such that the gravity acceleration vector is $g = (0, 0, -g)$. The vector $u^\beta = (u_1^\beta, u_2^\beta, u_3^\beta)$ represent the velocities in the three direction and the superscript is $\beta = g, f$ for the granular or the liquid phase respective. In the following, the steps needed to derives the simplified system of equation, proposed in Chapter 3, are treated separated for the solid phase and for the liquid phase. In both the systems the flow is assumed to be statistically stationary in order to define the average of each as: $\bar{u}(\mathbf{x}) = \frac{1}{T} \lim_{T \rightarrow \infty} \int u(\tau, \mathbf{x}) d\tau$, and $\bar{c}(\mathbf{x}) = \frac{1}{T} \lim_{T \rightarrow \infty} \int c(\tau, \mathbf{x}) d\tau$. The Reynolds decomposition is applied to the equations, that is to write each variable as the summation of the averaged value and the instantaneous value $u = \bar{u} + u'$ and to average it time, for example: $\bar{u} = \bar{\bar{u}} + \bar{u'}$ with $\bar{\bar{u}} = \bar{u}$ and $\bar{u'} = 0$.

A.1 Equations of the solid phase

$$\frac{\partial}{\partial t}\rho_s c + \frac{\partial}{\partial x_1}\rho_s c u_1^g + \frac{\partial}{\partial x_2}\rho_s c u_2^g + \frac{\partial}{\partial x_3}\rho_s c u_3^g = 0 \quad (\text{A.1})$$

$$\begin{aligned} \frac{\partial}{\partial t}\rho_s c u_1^g + \frac{\partial}{\partial x_1}\rho_s c u_1^g u_1^g + \frac{\partial}{\partial x_2}\rho_s c u_1^g u_2^g + \frac{\partial}{\partial x_3}\rho_s c u_1^g u_3^g = & -\frac{\partial p^g}{\partial x_1} \\ & + \frac{\partial \tau_{11}^g}{\partial x_1} + \frac{\partial \tau_{21}^g}{\partial x_2} + \frac{\partial \tau_{31}^g}{\partial x_3} + F_1^g \end{aligned} \quad (\text{A.2})$$

$$\begin{aligned} \frac{\partial}{\partial t}\rho_s c u_2^g + \frac{\partial}{\partial x_1}\rho_s c u_2^g u_1^g + \frac{\partial}{\partial x_2}\rho_s c u_2^g u_2^g + \frac{\partial}{\partial x_3}\rho_s c u_2^g u_3^g = & -\frac{\partial p^g}{\partial x_2} \\ & + \frac{\partial \tau_{12}^g}{\partial x_1} + \frac{\partial \tau_{22}^g}{\partial x_2} + \frac{\partial \tau_{32}^g}{\partial x_3} + F_2^g \end{aligned} \quad (\text{A.3})$$

$$\begin{aligned} \frac{\partial}{\partial t}\rho_s c u_3^g + \frac{\partial}{\partial x_1}\rho_s c u_3^g u_1^g + \frac{\partial}{\partial x_2}\rho_s c u_3^g u_2^g + \frac{\partial}{\partial x_3}\rho_s c u_3^g u_3^g = & -\rho_s c g \\ & -\frac{\partial p^g}{\partial x_3} + \frac{\partial \tau_{13}^g}{\partial x_1} + \frac{\partial \tau_{23}^g}{\partial x_2} + \frac{\partial \tau_{33}^g}{\partial x_3} + F_3^g \end{aligned} \quad (\text{A.4})$$

Since there is no a solid discharge filled in the column, for the solid phase in uniform flow conditions it is assumed that $u^g = 0, 0, u_3^g$ and that $\partial/\partial x_1 = \partial/\partial x_2 = 0$, so A.4 becomes:

$$\frac{\partial}{\partial t}\rho_s c + \frac{\partial}{\partial x_3}\rho_s c u_3^{g'} = 0 \quad (\text{A.5})$$

$$\frac{\partial \tau_{31}^g}{\partial x_3} = -F_1^g \quad (\text{A.6})$$

$$\frac{\partial \tau_{32}^g}{\partial x_3} = -F_2^g \quad (\text{A.7})$$

$$\frac{\partial}{\partial t}\rho_s c u_3^{g'} + \frac{\partial}{\partial x_3}\rho_s c u_3^{g'} u_3^{g'} = -\rho_s c g - \frac{\partial p^g}{\partial x_3} + \frac{\partial \tau_{33}^g}{\partial x_3} + F_3^g \quad (\text{A.8})$$

then averaging eq.A.8, it results:

$$\frac{\partial}{\partial t}\rho_s \bar{c} + \frac{\partial}{\partial x_3}\overline{\rho_s c' u_3^{g'}} = 0 \quad (\text{A.9})$$

$$\frac{\partial \tau_{31}^g}{\partial x_3} = -F_1^g \quad (\text{A.10})$$

$$\frac{\partial \tau_{32}^g}{\partial x_3} = -F_2^g \quad (\text{A.11})$$

$$\begin{aligned} \frac{\partial}{\partial t} \overline{\rho_s c' u_3^{g'}} + \frac{\partial}{\partial x_3} \overline{\rho_s \bar{c} u_3^{g'} u_3^{g'}} + \frac{\partial}{\partial x_3} \overline{\rho_s c' u_3^{g'} u_3^{g'}} = -\rho_s \bar{c} g - \frac{\partial p^g}{\partial x_3} \\ + \frac{\partial \tau_{13}^g}{\partial x_1} + \frac{\partial \tau_{23}^g}{\partial x_2} + \frac{\partial \tau_{33}^g}{\partial x_3} + F_3^g \end{aligned} \quad (\text{A.12})$$

The interaction forces in the three directions are:

$$F_1^g = \bar{c} \frac{\partial \tau_{31}^f}{\partial x_3} \quad (\text{A.13})$$

$$F_2^g = \bar{c} \frac{\partial \tau_{32}^f}{\partial x_3} \quad (\text{A.14})$$

$$F_3^g = -\bar{c} \frac{\partial p^f}{\partial x_3} + \bar{c} \frac{\partial \tau_{13}^f}{\partial x_1} + \bar{c} \frac{\partial \tau_{23}^f}{\partial x_2} + \bar{c} \frac{\partial \tau_{33}^f}{\partial x_3} + \overline{D_3} + \overline{D'} \quad (\text{A.15})$$

Substituting A.15 in A.12 the final system of averaged in time equations results:

$$\frac{\partial}{\partial t} \rho_s \bar{c} + \frac{\partial}{\partial x_3} \overline{\rho_s c' u_3^{g'}} = 0 \quad (\text{A.16})$$

$$\frac{\partial \tau_{31}^g}{\partial x_3} = -\bar{c} \frac{\partial \tau_{31}^f}{\partial x_3} \quad (\text{A.17})$$

$$\frac{\partial \tau_{32}^g}{\partial x_3} = -\bar{c} \frac{\partial \tau_{32}^f}{\partial x_3} \quad (\text{A.18})$$

$$\begin{aligned} \frac{\partial}{\partial t} \overline{\rho_s c' u_3^{g'}} + \frac{\partial}{\partial x_3} \overline{\rho_s \bar{c} u_3^{g'} u_3^{g'}} + \frac{\partial}{\partial x_3} \overline{\rho_s c' u_3^{g'} u_3^{g'}} = -\rho_s \bar{c} g - \frac{\partial p^g}{\partial x_3} + \frac{\partial \tau_{13}^g}{\partial x_1} + \frac{\partial \tau_{23}^g}{\partial x_2} \\ + \frac{\partial \tau_{33}^g}{\partial x_3} - \bar{c} \frac{\partial p^f}{\partial x_3} + \bar{c} \frac{\partial \tau_{13}^f}{\partial x_1} + \bar{c} \frac{\partial \tau_{23}^f}{\partial x_2} + \bar{c} \frac{\partial \tau_{33}^f}{\partial x_3} + \overline{D_3} + \overline{D'} \end{aligned} \quad (\text{A.19})$$

From the experimental evidence the mean flow is in the vertical direction, so is the momentum equation in x_3 to be analyzed. Then, eliminating all the

terms negligible, it reads as:

$$0 = -\rho_s \bar{c} g - \frac{\partial p^g}{\partial x_3} - \bar{c} \frac{\partial p^f}{\partial x_3} + \bar{c} \frac{\partial \tau_{13}^f}{\partial x_1} + \bar{c} \frac{\partial \tau_{23}^f}{\partial x_2} + \overline{D_3} + \overline{D'} \quad (\text{A.20})$$

Furthermore eq.(A.20) is averaged over the section of column (A) and reads:

$$0 = -\rho_s \bar{c} g - \frac{\partial p^g}{\partial x_3} - \bar{c} \frac{\partial p^f}{\partial x_3} + \bar{c} \frac{\tau_{r3}}{R_h} + \overline{D_3} \quad (\text{A.21})$$

A.2 Equations of the liquid phase

$$\begin{aligned} & \frac{\partial}{\partial t} \rho_w (1-c) + \frac{\partial}{\partial x_1} \rho_w (1-c) u_1^f + \frac{\partial}{\partial x_2} \rho_w (1-c) u_2^f \\ & \quad + \frac{\partial}{\partial x_3} \rho_w (1-c) u_3^f = 0 \\ & \frac{\partial}{\partial t} \rho_w (1-c) u_1^f + \frac{\partial}{\partial x_1} \rho_w (1-c) u_1^f u_1^f + \frac{\partial}{\partial x_2} \rho_w (1-c) u_1^f u_2^f \\ & \quad + \frac{\partial}{\partial x_3} \rho_w (1-c) u_1^f u_3^f = -\frac{\partial p^f}{\partial x_1} + \frac{\partial \tau_{11}^f}{\partial x_1} + \frac{\partial \tau_{21}^f}{\partial x_2} + \frac{\partial \tau_{31}^f}{\partial x_3} + F_1^f \\ & \frac{\partial}{\partial t} \rho_w (1-c) u_2^f + \frac{\partial}{\partial x_1} \rho_w (1-c) u_2^f u_1^f + \frac{\partial}{\partial x_2} \rho_w (1-c) u_2^f u_2^f \\ & \quad + \frac{\partial}{\partial x_3} \rho_w (1-c) u_2^f u_3^f = -\frac{\partial p^f}{\partial x_2} + \frac{\partial \tau_{12}^f}{\partial x_1} + \frac{\partial \tau_{22}^f}{\partial x_2} + \frac{\partial \tau_{32}^f}{\partial x_3} + F_2^f \\ & \frac{\partial}{\partial t} \rho_w (1-c) u_3^f + \frac{\partial}{\partial x_1} \rho_w (1-c) u_3^f u_1^f + \frac{\partial}{\partial x_2} \rho_w (1-c) u_3^f u_2^f \\ & \quad + \frac{\partial}{\partial x_3} \rho_w (1-c) u_3^f u_3^f = -\rho_w (1-c) g - \frac{\partial p^f}{\partial x_3} + \frac{\partial \tau_{13}^f}{\partial x_1} + \frac{\partial \tau_{23}^f}{\partial x_2} \\ & \quad + \frac{\partial \tau_{33}^f}{\partial x_3} + F_3^f \end{aligned} \quad (\text{A.22})$$

A constant discharge of water is filled in the column, and from the continuity equation is found that the velocity of the liquid phase is constant because

a uniform flow condition is assumed, and the vector of the velocity reads as: $u = 0, 0, u_3^f$. Furthermore, in this condition $\partial/\partial x_1 = \partial/\partial x_2 = 0$. A.22 becomes:

$$\begin{aligned} \frac{\partial}{\partial t} \rho_w(1-c) + \frac{\partial}{\partial x_3} \rho_w(1-c)u_3^f &= 0 \\ \frac{\partial \tau_{33}^f}{\partial x_3} &= -F_1^f \\ \frac{\partial \tau_{32}^f}{\partial x_3} &= -F_2^f \\ \frac{\partial}{\partial t} \rho_w(1-c)u_3^f + \frac{\partial}{\partial x_3} \rho_w(1-c)u_3^f u_3^f &= -\rho_w(1-c)g - \frac{\partial p^f}{\partial x_3} \\ &+ \frac{\partial \tau_{13}^f}{\partial x_1} + \frac{\partial \tau_{23}^f}{\partial x_2} + \frac{\partial \tau_{33}^f}{\partial x_3} + F_3^f \end{aligned} \quad (\text{A.23})$$

Averaging in time eq.(A.23), in which each term is substituted by the summation of its average plus its fluctuations, it results:

$$\begin{aligned} \frac{\partial}{\partial t} \rho_w(1-\bar{c}) + \frac{\partial}{\partial x_3} \rho_w(1-\bar{c})\overline{u_3^f} + \frac{\partial}{\partial x_3} \overline{\rho_w c' u_3^{f'}} &= 0 \\ \frac{\partial \tau_{31}^f}{\partial x_3} &= -F_1^f \\ \frac{\partial \tau_{32}^f}{\partial x_3} &= -F_2^f \\ \frac{\partial}{\partial t} \rho_w(1-\bar{c})\overline{u_3^f} + \frac{\partial}{\partial t} \overline{\rho_w c' u_3^{f'}} + \frac{\partial}{\partial x_3} \rho_w \left(\overline{u_3^f u_3^f} + \overline{u_3^{f'} u_3^{f'}} - \overline{c u_3^f u_3^f} - \overline{c u_3^{f'} u_3^{f'}} \right. \\ &\left. - 2\overline{u_3^f u_3^{f'} c'} - \overline{c' u_3^{f'} u_3^{f'}} \right) - \rho_w(1-\bar{c})g - \frac{\partial p^f}{\partial x_3} + \frac{\partial \tau_{13}^f}{\partial x_1} + \frac{\partial \tau_{23}^f}{\partial x_2} + \frac{\partial \tau_{33}^f}{\partial x_3} + F_3^f \end{aligned} \quad (\text{A.24})$$

The interaction forces in the three directions are:

$$\begin{aligned}
F_1^f &= -\bar{c} \frac{\partial \tau_{31}^f}{\partial x_3} \\
F_2^f &= -\bar{c} \frac{\partial \tau_{33}^f}{\partial x_3} \\
F_3^f &= \bar{c} \frac{\partial p^f}{\partial x_3} - \bar{c} \frac{\partial \tau_{13}^f}{\partial x_1} - \bar{c} \frac{\partial \tau_{23}^f}{\partial x_2} - \bar{c} \frac{\partial \tau_{33}^f}{\partial x_3} - \overline{D_3} - \overline{D'}
\end{aligned} \tag{A.25}$$

Substituting A.25 in A.24 the final system of equations is:

$$\begin{aligned}
\frac{\partial}{\partial t} \rho_w (1 - \bar{c}) + \frac{\partial}{\partial x_3} \rho_w (1 - \bar{c}) \overline{u_3^f} + \frac{\partial}{\partial x_3} \rho_w c' \overline{u_3^{f'}} &= 0 \\
\frac{\partial \tau_{31}^f}{\partial x_3} &= \bar{c} \frac{\partial \tau_{31}^f}{\partial x_3} \\
\frac{\partial \tau_{32}^f}{\partial x_3} &= \bar{c} \frac{\partial \tau_{32}^f}{\partial x_3} \\
\frac{\partial}{\partial t} \rho_w (1 - \bar{c}) \overline{u_3^f} + \frac{\partial}{\partial t} \rho_w c' \overline{u_3^{f'}} + \frac{\partial}{\partial x_3} \rho_w \left(\overline{u_3^f u_3^f} + \overline{u_3^{f'} u_3^{f'}} - \overline{c u_3^f u_3^f} - \overline{c u_3^{f'} u_3^{f'}} \right. \\
&\quad \left. - \overline{2 u_3^f u_3^{f'} c'} - \overline{c' u_3^{f'} u_3^{f'}} \right) = -\rho_w (1 - \bar{c}) g - (1 - \bar{c}) \frac{\partial p^f}{\partial x_3} \\
&\quad + (1 - \bar{c}) \left(\frac{\partial \tau_{13}^f}{\partial x_1} + \frac{\partial \tau_{23}^f}{\partial x_2} + \frac{\partial \tau_{33}^f}{\partial x_3} \right) - \overline{D_3} - \overline{D'}
\end{aligned} \tag{A.26}$$

Focus on the momentum equation in x_3 , eliminating the term that are negligible, it results:

$$0 = -\rho_w (1 - \bar{c}) g - (1 - \bar{c}) \frac{\partial p^f}{\partial x_3} + (1 - \bar{c}) \left(\frac{\partial \tau_{13}^f}{\partial x_1} + \frac{\partial \tau_{23}^f}{\partial x_2} \right) - \overline{D_3} \tag{A.27}$$

Finally the momentum equation is averaged on the section A and results:

$$0 = -\rho_w (1 - \bar{c}) g - (1 - \bar{c}) \frac{\partial p^f}{\partial x_3} + (1 - \bar{c}) + \frac{\tau_{r3}}{R_h} - \overline{D_3} \tag{A.28}$$

Appendix B

Decomposition of the drag force

In the case that the liquid phase is faster than the granular phase, i.e. $u_i^f > u_i^g$, the drag force is:

$$D = \frac{3}{4} C_D \frac{\rho_w}{d} c f(c) (u^f - u^g)^2 \quad (\text{B.1})$$

where: $C_D = \left(\frac{4.98}{\sqrt{Re}} + 0.63 \right)^2$ and $Re = \rho_w (1-c) (u^f - u^g) d / \mu_w$. By expanding each term of eq.(B.1), it reads as:

$$\begin{aligned} D &= \frac{3}{4} \left(\frac{4.8}{\sqrt{Re}} + 0.63 \right)^2 \frac{\rho_w}{d} c (1-c)^{-n} (u^f - u^g)^2 \\ &= \frac{3}{4} \left(\frac{23.04}{Re} + \frac{5.92}{\sqrt{Re}} + 0.397 \right) \frac{\rho_w}{d} c (1-c)^{-n} (u^f - u^g)^2 \\ &= \frac{3}{4} \left(\frac{23.04 \mu_w}{\rho_w d (1-c) (u^f - u^g)} + \frac{5.92 \sqrt{\mu_w}}{\sqrt{\rho_w d (1-c) (u^f - u^g)}} + 0.397 \right) \frac{\rho_w}{d} c \\ &\quad (1-c)^{-n} (u^f - u^g)^2 \end{aligned} \quad (\text{B.2})$$

Eq. (B.2) shows three different dependences on the relative velocities of the two-phase, and in the following each term is treated separately. In particular

$D = D_1 + D_2 + D_3$, where:

$$D_1 = 17.28 \frac{\mu_w}{d^2} c (1 - c)^{-n-1} (u^f - u^g) \quad (\text{B.3})$$

$$D_2 = 4.44 \frac{\sqrt{\mu_w} \sqrt{\rho_w}}{d^{1.5}} c (1 - c)^{-n-0.5} (u^f - u^g)^{1.5} \quad (\text{B.4})$$

$$D_3 = 0.297 \frac{\rho_w}{d} c (1 - c)^{-n} (u^f - u^g)^2 \quad (\text{B.5})$$

In order to obtain the average value of the drag force, each term D_1, D_2, D_3 is rewritten using the Reynolds decomposition and averaging the expressions. The average of the fluctuations of the first order are considered null.

B.1 Drag 1-Reynolds decomposition and average

The Reynolds decomposition is applied to the term of the drag force called 1:

$$D_1 = 17.28 \frac{\mu_w}{d^2} c (1 - c)^{-n-1} (u^f - u^g) \quad (\text{B.6})$$

Furthermore a simplification is introduced by changing the exponent of the term: $(1 - c)^{-n-1} = (1 - c)^{-m}$. Then, applying the Reynolds decomposition and expanding into a Taylor series and, finally, it results that:

$$\begin{aligned} (1 - c)^{-m} &= (1 - \bar{c} - c')^{-m} \simeq \frac{1}{(1 - \bar{c} - c')^m (1 - \bar{c} + c')^m} (1 - \bar{c} + c')^m \\ &\simeq \frac{(1 - \bar{c})^m - m(1 - \bar{c})^{m-1} c'}{[(1 - \bar{c})^2 - c'^2]^m} \simeq \frac{1}{(1 - \bar{c})^m} + m \frac{c'}{(1 - \bar{c})^{m+1}} \end{aligned} \quad (\text{B.7})$$

that is:

$$D_1 \simeq 17.28 \frac{\mu_w}{d^2} (\bar{c} + c') \left(\frac{1}{(1 - \bar{c})^m} + m \frac{c'}{(1 - \bar{c})^{m+1}} \right) (\overline{u^f} - \overline{u^g} + u'_f - u'_g)$$

$$\begin{aligned}
\simeq & 17.28 \frac{\mu_w}{d^2} \left\{ \frac{\bar{c}}{(1-\bar{c})^m} (\bar{u}^f - \bar{u}^g) + \frac{\bar{c}}{(1-\bar{c})^m} (u'_f - u'_g) \right. \\
& + \frac{c'}{(1-\bar{c})^m} (\bar{u}^f - \bar{u}^g) + \frac{c'}{(1-\bar{c})^m} (u'_f - u'_g) \\
& m \frac{\bar{c}c'}{(1-\bar{c})^{m+1}} (\bar{u}^f - \bar{u}^g) + m \frac{\bar{c}c'}{(1-\bar{c})^{m+1}} (u'_f - u'_g) \\
& \left. m \frac{c'c'}{(1-\bar{c})^{m+1}} (\bar{u}^f - \bar{u}^g) + m \frac{c'c'}{(1-\bar{c})^{m+1}} (u'_f - u'_g) \right\} \quad (\text{B.8})
\end{aligned}$$

by averaging and eliminating the correlations of the first order, it results:

$$\begin{aligned}
D_1 \simeq & 17.28 \frac{\mu_w}{d^2} \left\{ \frac{\bar{c}}{(1-\bar{c})^m} (\bar{u}^f - \bar{u}^g) + \frac{1}{(1-\bar{c})^m} \overline{c'(u'_f - u'_g)} \right. \\
& + m \frac{\bar{c}}{(1-\bar{c})^{m+1}} \overline{c'(u'_f - u'_g)} + m \frac{\bar{c}c'}{(1-\bar{c})^{m+1}} (\bar{u}^f - \bar{u}^g) \\
& \left. + m \frac{1}{(1-\bar{c})^{m+1}} \overline{c'c'(u'_f - u'_g)} \right\} \quad (\text{B.9})
\end{aligned}$$

So it is possible to collect the terms dependent on the average valuer of the velocity, which results:

$$D_1(\bar{c}, \bar{U}) = 17.28 \frac{\mu_w}{d^2} \frac{\bar{c}}{(1-\bar{c})^m} (\bar{u}^f - \bar{u}^g) \quad (\text{B.10})$$

while the residual component collecting is:

$$\begin{aligned}
D_{R-1} = & 17.28 \frac{\mu_w}{d^2} \left\{ \left[m \frac{\bar{c}}{(1-\bar{c})^{m+1}} + \frac{1}{(1-\bar{c})^m} \right] \overline{c'(u'_f - u'_g)} \right. \\
& \left. + \frac{m}{(1-\bar{c})^{m+1}} \bar{c}c'(\bar{u}^f - \bar{u}^g) + m \frac{1}{(1-\bar{c})^{m+1}} \overline{c'c'(u'_f - u'_g)} \right\} \quad (\text{B.11})
\end{aligned}$$

B.2 Drag 2-Reynolds decomposition and average

The Reynolds decomposition is applied to the term of the drag force called 2:

$$D_2 \simeq 4.44 \frac{\sqrt{\mu_w} \sqrt{\rho_w}}{d^{1.5}} (\bar{c} + c') \left(\frac{1}{(1 - \bar{c})^n} + n \frac{c'}{(1 - \bar{c})^{n+1}} \right) (\bar{u}^f - \bar{u}^g + u'_f - u'_g)^{1.5} \quad (\text{B.12})$$

A simplification is introduced changing the exponent of the term: $(1 - c)^{-n-0.5} = (1 - c)^{-r}$. Then, applying the Reynolds decomposition and expanding into a Taylor series and, finally, it results that:

$$\begin{aligned} (1 - c)^{-r} &= (1 - \bar{c} - c')^{-r} \simeq \frac{1}{(1 - \bar{c} - c')^r (1 - \bar{c} + c')^r} (1 - \bar{c} + c')^r \\ &= \frac{(1 - \bar{c})^r - r(1 - \bar{c})^{r-1} c'}{[(1 - \bar{c})^2 - c'^2]^r} \simeq \frac{1}{(1 - \bar{c})^r} + r \frac{c'}{(1 - \bar{c})^{r+1}} \end{aligned} \quad (\text{B.13})$$

Furthermore, it is assumed that:

$$(\bar{u}^f - \bar{u}^g + u'_f - u'_g)^{1.5} \simeq (\bar{u}^f - \bar{u}^g)^{1.5} + 1.5(\bar{u}^f - \bar{u}^g)^{0.5} (u'_f - u'_g) \quad (\text{B.14})$$

by averaging and eliminating the correlations of the first order, the second term of the drag is:

$$\begin{aligned} D_2 \simeq & 4.44 \frac{\sqrt{\mu_w} \sqrt{\rho_w}}{d^{1.5}} \left\{ \frac{\bar{c}}{(1 - \bar{c})^r} (\bar{u}^f - \bar{u}^g)^{1.5} \right. \\ & + \frac{1}{(1 - \bar{c})^r} [1.5(\bar{u}^f - \bar{u}^g)^{0.5} \overline{c'(u'_f - u'_g)}] + r \frac{\overline{c'c'}}{(1 - \bar{c})^{r+1}} (\bar{u}^f - \bar{u}^g)^{1.5} \\ & + r \frac{\bar{c}}{(1 - \bar{c})^{r+1}} [1.5(\bar{u}^f - \bar{u}^g)^{0.5} \overline{c'(u'_f - u'_g)}] \\ & \left. + r \frac{1}{(1 - \bar{c})^{r+1}} [1.5(\bar{u}^f - \bar{u}^g)^{0.5} \overline{c'c'(u'_f - u'_g)}] \right\} \end{aligned} \quad (\text{B.15})$$

So it is possible to collect the terms dependent on the average valuer of the velocity, which results:

$$D_2(\bar{c}, \bar{U}) = 4.44 \frac{\sqrt{\mu_w} \sqrt{\rho_w}}{d^{1.5}} \frac{\bar{c}}{(1 - \bar{c})^r} (\bar{u}^f - \bar{u}^g)^{1.5} \quad (\text{B.16})$$

and collect all the other terms in the residual drag, that is:

$$\begin{aligned} D_{R-2} = & 4.44 \frac{\sqrt{\mu_w} \sqrt{\rho_w}}{d^{1.5}} \left\{ \frac{1}{(1 - \bar{c})^r} [1.5(\bar{u}^f - \bar{u}^g)^{0.5} \overline{c'(u'_f - u'_g)}] + \right. \\ & + r \frac{\bar{c}'}{(1 - \bar{c})^{r+1}} (\bar{u}^f - \bar{u}^g)^{1.5} + r \frac{\bar{c}}{(1 - \bar{c})^{r+1}} [1.5(\bar{u}^f - \bar{u}^g)^{0.5} \overline{c'(u'_f - u'_g)}] \\ & \left. + r \frac{1}{(1 - \bar{c})^{r+1}} [1.5(\bar{u}^f - \bar{u}^g)^{0.5} \overline{c'c'(u'_f - u'_g)}] \right\} \quad (\text{B.17}) \end{aligned}$$

or collecting:

$$\begin{aligned} D_{R-2} = & 4.44 \frac{\sqrt{\mu_w} \sqrt{\rho_w}}{d^{1.5}} \left\{ r \frac{\bar{c}'}{(1 - \bar{c})^{r+1}} (\bar{u}^f - \bar{u}^g)^{1.5} \right. \\ & + \left(\frac{1}{(1 - \bar{c})^r} + r \frac{\bar{c}}{(1 - \bar{c})^{r+1}} \right) [1.5(\bar{u}^f - \bar{u}^g)^{0.5} \overline{c'(u'_f - u'_g)}] \\ & \left. + r \frac{1}{(1 - \bar{c})^{r+1}} [1.5(\bar{u}^f - \bar{u}^g)^{0.5} \overline{c'c'(u'_f - u'_g)}] \right\} \quad (\text{B.18}) \end{aligned}$$

B.3 Drag 3-Reynolds decompositions and average

The Reynolds decomposition is applied to the term of the drag force called 3, with the following simplification in applying the Reynolds decomposition and expanding into a Taylor series the voidage function, that is:

$$(1 - c)^{-n} = (1 - \bar{c} - c')^{-n} \simeq \frac{1}{(1 - \bar{c} - c')^n (1 - \bar{c} + c')^n}$$

$$= \frac{(1 - \bar{c})^n - n(1 - \bar{c})^{n-1}c'}{[(1 - \bar{c})^2 - c'^2]^n} \simeq \frac{1}{(1 - \bar{c})^n} + n \frac{c'}{(1 - \bar{c})^{n+1}} \quad (\text{B.19})$$

$$\begin{aligned} D_3 &\simeq 0.297 \frac{\rho_w}{d} (\bar{c} + c') \left(\frac{1}{(1 - \bar{c})^n} + n \frac{c'}{(1 - \bar{c})^{n+1}} \right) \\ &\quad [(\bar{u}^f - \bar{u}^g)^2 + (u'_f - u'_g)^2 - 2(\bar{u}^f - \bar{u}^g)(u'_f - u'_g)] \\ &= 0.297 \frac{\rho_w}{d} \left\{ \frac{\bar{c}}{(1 - \bar{c})^n} (\bar{u}^f - \bar{u}^g)^2 + \frac{\bar{c}}{(1 - \bar{c})^n} (u'_f - u'_g)^2 - \right. \\ &\quad - 2 \frac{\bar{c}}{(1 - \bar{c})^n} (\bar{u}^f - \bar{u}^g)(u'_f - u'_g) \\ &\quad + \frac{c'}{(1 - \bar{c})^n} (\bar{u}^f - \bar{u}^g)^2 + \frac{c'}{(1 - \bar{c})^n} (u'_f - u'_g)^2 \\ &\quad - 2 \frac{c'}{(1 - \bar{c})^n} (\bar{u}^f - \bar{u}^g)(u'_f - u'_g) \\ &\quad + n \frac{\bar{c}c'}{(1 - \bar{c})^{n+1}} (\bar{u}^f - \bar{u}^g)^2 + n \frac{\bar{c}c'}{(1 - \bar{c})^{n+1}} (u'_f - u'_g)^2 - \\ &\quad 2n \frac{\bar{c}c'}{(1 - \bar{c})^{n+1}} (\bar{u}^f - \bar{u}^g)(u'_f - u'_g) \\ &\quad + n \frac{c'c'}{(1 - \bar{c})^{n+1}} (\bar{u}^f - \bar{u}^g)^2 + n \frac{c'c'}{(1 - \bar{c})^{n+1}} (u'_f - u'_g)^2 - \\ &\quad \left. 2n \frac{c'c'}{(1 - \bar{c})^{n+1}} (\bar{u}^f - \bar{u}^g)(u'_f - u'_g) \right\} \quad (\text{B.20}) \end{aligned}$$

by averaging and eliminating the correlations of the first order:

$$\begin{aligned}
D_3(\bar{c}, \bar{U}) \simeq & 0.297 \frac{\rho_w}{d} \left\{ \frac{\bar{c}}{(1-\bar{c})^n} (\bar{u}^f - \bar{u}^g)^2 + \frac{\bar{c}}{(1-\bar{c})^n} \overline{(u'_f - u'_g)^2} \right. \\
& + \frac{1}{(1-\bar{c})^n} \overline{c'(u'_f - u'_g)^2} \\
& - 2 \frac{1}{(1-\bar{c})^n} (\bar{u}^f - \bar{u}^g) \overline{c'(u'_f - u'_g)} + n \frac{\bar{c}}{(1-\bar{c})^{n+1}} \overline{c'(u'_f - u'_g)^2} \\
& - 2n \frac{\bar{c}}{(1-\bar{c})^{n+1}} (\bar{u}^f - \bar{u}^g) \overline{c'(u'_f - u'_g)} + n \frac{\overline{c'c'}}{(1-\bar{c})^{n+1}} (\bar{u}^f - \bar{u}^g)^2 \\
& \left. + n \frac{1}{(1-\bar{c})^{n+1}} \overline{c'c'(u'_f - u'_g)^2} - 2n \frac{1}{(1-\bar{c})^{n+1}} (\bar{u}^f - \bar{u}^g) \overline{c'c'(u'_f - u'_g)} \right\}
\end{aligned} \tag{B.21}$$

It is possible to collect the terms dependent on the average valuer of the velocity, which results:

$$\overline{D_3} = 0.297 \frac{\rho_w}{d} \frac{\bar{c}}{(1-\bar{c})^n} (\bar{u}^f - \bar{u}^g)^2 \tag{B.22}$$

while the terms of the residual drag are:

$$\begin{aligned}
D_{R-3} = & 0.297 \frac{\rho_w}{d} \left\{ \frac{\bar{c}}{(1-\bar{c})^n} \overline{(u'_f - u'_g)^2} + \frac{1}{(1-\bar{c})^n} \overline{c'(u'_f - u'_g)^2} \right. \\
& - 2 \frac{1}{(1-\bar{c})^n} (\bar{u}^f - \bar{u}^g) \overline{c'(u'_f - u'_g)} + n \frac{\bar{c}}{(1-\bar{c})^{n+1}} \overline{c'(u'_f - u'_g)^2} \\
& - 2n \frac{\bar{c}}{(1-\bar{c})^{n+1}} (\bar{u}^f - \bar{u}^g) \overline{c'(u'_f - u'_g)} + n \frac{\overline{c'c'}}{(1-\bar{c})^{n+1}} (\bar{u}^f - \bar{u}^g)^2 \\
& + n \frac{1}{(1-\bar{c})^{n+1}} \overline{c'c'(u'_f - u'_g)^2} \\
& \left. - 2n \frac{1}{(1-\bar{c})^{n+1}} (\bar{u}^f - \bar{u}^g) \overline{c'c'(u'_f - u'_g)} \right\}
\end{aligned} \tag{B.23}$$

or collecting:

$$\begin{aligned}
D_{R-3} = & 0.297 \frac{\rho_w}{d} \left\{ \frac{\bar{c}}{(1-\bar{c})^n} \overline{(u'_f - u'_g)^2} \right. \\
& - 2 \left(\frac{1}{(1-\bar{c})^n} + n \frac{\bar{c}}{(1-\bar{c})^{n+1}} \right) (\bar{u}^f - \bar{u}^g) \overline{c'(u'_f - u'_g)} \\
& + n \frac{\overline{c'c'}}{(1-\bar{c})^{n+1}} (\bar{u}^f - \bar{u}^g)^2 + \left(\frac{1}{(1-\bar{c})^n} + n \frac{\bar{c}}{(1-\bar{c})^{n+1}} \right) \overline{c'(u'_f - u'_g)^2} \\
& \left. - 2n \frac{1}{(1-\bar{c})^{n+1}} (\bar{u}^f - \bar{u}^g) \overline{c'c'(u'_f - u'_g)} + n \frac{1}{(1-\bar{c})^{n+1}} \overline{c'c'(u'_f - u'_g)^2} \right\} \\
& \tag{B.24}
\end{aligned}$$

Appendix C

Equations of the diluted two phase flow in uniform flow conditions

In stationary condition the momentum conservation equations of a plane flow are:

$$x_1^f : 0 = -\rho_w(1-c)g \frac{\partial z}{\partial x_1} - \frac{\partial p^f}{\partial x_1} + \frac{\partial \tau_{21}^f}{\partial x_2} + F_1 \quad (\text{C.1})$$

$$x_2^f : 0 = -\rho_w(1-c)g \frac{\partial z}{\partial x_2} - \frac{\partial p^f}{\partial x_2} + \frac{\partial \tau_{12}^f}{\partial x_1} + F_2 \quad (\text{C.2})$$

$$x_1^s : 0 = -\rho_s c g \frac{\partial z}{\partial x_1} - \frac{\partial p^g}{\partial x_1} + \frac{\partial \tau_{21}^g}{\partial x_2} - F_1 \quad (\text{C.3})$$

$$x_2^s : 0 = -\rho_s c g \frac{\partial z}{\partial x_2} - \frac{\partial p^g}{\partial x_2} + \frac{\partial \tau_{12}^g}{\partial x_1} - F_2 \quad (\text{C.4})$$

The interaction forces are:

$$F_1 = c \frac{\partial p^f}{\partial x_1} - c \frac{\partial \tau_{21}^f}{\partial x_2} - D_1 \quad (\text{C.5})$$

$$F_2 = c \frac{\partial p^f}{\partial x_2} - c \frac{\partial \tau_{12}^f}{\partial x_1} - D_2 \quad (\text{C.6})$$

By substituting eq.(C.6) in eq.(C.4):

$$x_1^f : 0 = -\rho_w(1-c)g \frac{\partial z}{\partial x_1} - \frac{\partial p^f}{\partial x_1} + \frac{\partial \tau_{21}^f}{\partial x_2} + c \frac{\partial p^f}{\partial x_1} - c \frac{\partial \tau_{21}^f}{\partial x_2} - D_1 \quad (\text{C.7})$$

$$x_2^f : 0 = -\rho_w(1-c)g \frac{\partial z}{\partial x_2} - \frac{\partial p^f}{\partial x_2} + \frac{\partial \tau_{12}^f}{\partial x_1} + c \frac{\partial p^f}{\partial x_2} - c \frac{\partial \tau_{12}^f}{\partial x_1} - D_2 \quad (\text{C.8})$$

$$x_1^s : 0 = -\rho_s c g \frac{\partial z}{\partial x_1} - \frac{\partial p^g}{\partial x_1} + \frac{\partial \tau_{21}^g}{\partial x_2} - c \frac{\partial p^f}{\partial x_1} + c \frac{\partial \tau_{21}^f}{\partial x_2} + D_1 \quad (\text{C.9})$$

$$x_2^s : 0 = -\rho_s c g \frac{\partial z}{\partial x_2} - \frac{\partial p^g}{\partial x_2} + \frac{\partial \tau_{12}^g}{\partial x_1} - c \frac{\partial p^f}{\partial x_2} + c \frac{\partial \tau_{12}^f}{\partial x_1} + D_2 \quad (\text{C.10})$$

Furthermore, in uniform flow condition in the longitudinal direction x_1 , eq.(C.10) reduces to:

$$x_1^f : 0 = -\rho_w(1-c)g \frac{\partial z}{\partial x_1} + (1-c) \frac{\partial \tau_{21}^f}{\partial x_2} - D_1 \quad (\text{C.11})$$

$$x_2^f : 0 = -\rho_w(1-c)g \frac{\partial z}{\partial x_2} - (1-c) \frac{\partial p^f}{\partial x_2} - D_2 \quad (\text{C.12})$$

$$x_1^s : 0 = -\rho_s c g \frac{\partial z}{\partial x_1} + \frac{\partial \tau_{21}^g}{\partial x_2} + c \frac{\partial \tau_{21}^f}{\partial x_2} + D_1 \quad (\text{C.13})$$

$$x_2^s : 0 = -\rho_s c g \frac{\partial z}{\partial x_2} - \frac{\partial p^g}{\partial x_2} - c \frac{\partial p^f}{\partial x_2} + D_2 \quad (\text{C.14})$$

Notice that $D_2 = 0$ and the pressure of the liquid phase result to be hydrostatic:

$$x_2^f : \frac{\partial p^f}{\partial x_2} = -\rho_w g \frac{\partial z}{\partial x_2} \quad (\text{C.15})$$

The final system results:

$$x_1^f : \frac{\partial \tau_{21}^f}{\partial x_2} = \rho_w g \frac{\partial z}{\partial x_1} + \frac{1}{1-c} D_1 \quad (\text{C.16})$$

$$x_1^s : \frac{\partial \tau_{21}^g}{\partial x_2} = \rho_s c g \frac{\partial z}{\partial x_1} - c \left(\rho_w g \frac{\partial x_3}{\partial x_1} + \frac{1}{1-c} D_1 \right) - D_1 \quad (\text{C.17})$$

$$x_2^s : \frac{\partial p^g}{\partial x_2} = -c(\rho_s - \rho_w) g \frac{\partial z}{\partial x_2} \quad (\text{C.18})$$

and so:

$$x_1^f : \frac{\partial \tau_{21}^f}{\partial x_2} = \rho_w g \frac{\partial z}{\partial x_1} + \frac{1}{1-c} D_1 \quad (\text{C.19})$$

$$x_1^s : \frac{\partial \tau_{21}^g}{\partial x_2} = c(\rho_s - \rho_w) g \frac{\partial z}{\partial x_1} - \frac{1}{1-c} D_1 \quad (\text{C.20})$$

$$x_2^s : \frac{\partial p^g}{\partial x_2} = -c(\rho_s - \rho_w) g \frac{\partial z}{\partial x_2} \quad (\text{C.21})$$